Comparison of Monte Carlo methods for non-Markovian systems

Pro gradu-tutkielma
Turun yliopisto
Fysiikan ja tähtitieteen laitos
Fysiikka
2010
LuK Kimmo Luoma
Tarkastajat:
dos. Jyrki Piilo
prof. Kalle-Antti Suominen

TURUN YLIOPISTO
Fysiikan ja tähtitieteen laitos

LUOMA, KIMMO Ei-Markovisten Monte Carlo menetelmien vertailu

Pro gradu, 103 s., 18 liites.
Fysiikka
Toukokuu 2010

Suljettu kvanttisysteemi on täydellisesti eristetty muusta maailmankaikkeudesta. Tällaisen systeemin aikakehitys on unitaarista. Luonnollisesti tämä on vain hyödyllinen approksimaatio. Käytännössä kaikki kvanttisysteemit ovat avoimia systeemejä. Avoin systeemi on systeemi joka vuorovaikuttaa ympäristönsä kanssa. Tämä vuorovaikutus johtaa siihen että systeemin ja ympäristön tilat kietoutuvat toisiinsa ja aikakehitys ei ole enää unitaarista. Ei-unitaarinen aikakehitys aiheuttaa dissipaatiota ja dekoherenssia mikä johtaa siihen, että kvanttisysteemi menettää kvanttiominaisuutensa. Joissakin tapauksissa voidaan approksimoida, että avoin systeemi ei muista aikaisempaa tilaansa ja tällöin sanotaan, että se on Markovinen. Kun tätä approksimaatiota ei voida tehdä on systeemi ei-Markovinen. Ei-Markovisuus on ominaisuus jonka käsittely on hankalaa ja tunnetaan vain muutamia systeemejä, jotka voidaan ratkaista analyyttisesti. Tämän lisäksi myös niiden simuloiminen on vaikeaa, sillä yksinkertaiseen Markoviseen tapaukseen kehitetyt menetelmät eivät toimi.

Tässä työssä esitellään avointen kvanttisysteemien teoriaa Markovisille ja ei-Markovisille systeemeille, esitellään joitakin Monte Carlo-simulaatiomenetelmiä Markovisille systeemeille ja verrataan numeerisesti kolmen erilaisen ei-Markovisille systeemeille suunnitellun Monte Carlo menetelmän suorituskykyä. Menetelmät joita tutkitaan ovat **N**on-**M**arkovian **Q**uantum **J**ump (Phys. Rev. Lett. **100**, 180402), **D**oubled **H**ilbert **S**pace (Phys. Rev. A **59**, 1633) ja **T**ripled **H**ilbert **S**pace (Phys. Rev. A **70**, 012106) . Em. menetelmien suorituskykyä verrataan mittaamalla CPU-ajan kulutusta, tietokoneen muistin kulutusta ja menetelmien tarkkuutta suoritettaessa simulaatioita yksinkertaisilla kvanttioptisilla systeemeillä. Lisäksi tutkitaan millaisen fysikaalisen tulkinnan NMQJ, DHS ja THS menetelmät antavat ei-Markovisen systeemin dynamiikalle ja miten eri menetelmät kuvaavat systeemin muistia.

Numeerinen vertailu osoitti, että NMQJ on huomattavasti tehokkaampi kuin DHS ja THS mitattuna muistin ja CPU-ajan kulutuksella. Tarkkuudessa ei ollut suuria eroja, mutta simulaatiot antoivat viitteitä siitä, että NMQJ-menetelmän avulla on mahdollista saavuttaa haluttu tarkkuus laskennallisesti edullisemmilla parametrivalinnoilla kuin DHS- ja THS-menetelmillä. Simulaatioita tehdessä korostui, että NMQJ-menetelmä oli yksinkertaisempi käyttää kuin DHS ja THS johtuen siitä, että systeemin Hilbertin avaruutta ei tarvitse laajentaa. Samasta syystä NMQJ-menetelmä antaa myös selkeämmän fysikaalisen kuvan ei-Markovisesta muistista kuin DHS ja THS, sillä näissä menetelmissä ei-Markovisen muistin kuvaamiseen tarvitaan ylimääräisiä kvanttitiloja.

Asiasanat: kvanttimekaniikka, avoimet systeemit, ei-Markoviset systeemit, Markoviset systeemit, NMQJ-menetelmä, DHS-menetelmä, THS-menetelmä.

Contents

1 Introduction

In this thesis we benchmark three different non-Markovian Monte Carlo algorithms; Non-Markovian Quantum Jumps (NMQJ), Double Hilbert Space (DHS) and Triple Hilbert Space (THS) algorithms. We simulate simple quantum optical systems such as two state, ladder, Λ and V system with all three algorithms. Each method is applied as presented in the Refs. [23],[3] and [2].

There exists a large variety of different Monte Carlo methods for different purposes. In general Monte Carlo methods are based on a sampling of some probability distribution. It is best illustrated with an example of calculating a definite integral. We use the following notation: $X \sim \mathcal{U}_{[0,1]}$ means that random variable X is distributed uniformly in the interval $[0, 1]$. Suppose that we want to calculate an integral $\mathcal{I} = \int_0^1 \mathrm{d}x \, \sin(\pi x)$. Exact value is $\mathcal{I} = \frac{2}{\pi} \approx 0.63662$. With Monte Carlo method we first observe that $0 \leq \sin(\pi x) \leq 1$ in the integration interval. Rectangle (0,0),(0,1),(1,0),(1,1) has the area $A = 1$. We can then approximate $\mathcal{I}$ by first sampling pairs of random variables (R_1, R_2), such that $R_1, R_2 \sim \mathcal{U}_{[0,1]}$. $\mathcal{I}$ is approximated by the fraction of points under the curve $\sin(\pi x)$ to the total number of sampled points. For example with $M = 3000$ points (see Fig. 1.1) we get an estimate 0.634667 which is close to the exact result. This method is obviously easily generalized to other integrands and other distributions. There is error involved between the exact and numerical solutions. With Monte Carlo methods there is no error bounds but the error is estimated by the standard deviation and confidence intervals. In any case the accuracy is $\propto \frac{1}{\sqrt{M}}$, when the random variables involved are independent of each other [9].

This thesis is divided in four parts. In the first part (Sec. 2) we present the basic theory behind Markovian and local in time non-Markovian master equations. In the second part (Secs. 3-4) we present some Markovian Monte Carlo methods and physical interpretation for them. Then we present the three non-Markovian

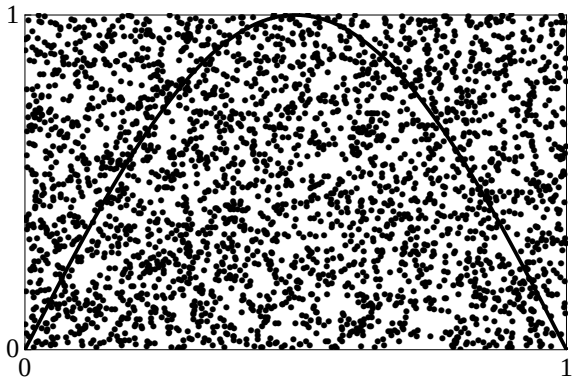

Figure 1.1: Evaluation of $\int_0^1 \mathrm{d}x\, \sin(\pi x)$ with Monte Carlo method. Random variables $R_1, R_2 \sim \mathcal{U}_{[0,1]}$. We sampled 3000 realizations $(r_1^i, r_2^i),\ i \in \{1, 2, \cdots, 3000\}$ from which we estimated the area under curve.

Monte Carlo methods and develop algorithms for them and discuss the physical interpretation of these methods and the problems involved. In the third part (Sec. 5) we derive a perturbative approximation for the local in time non-Markovian master equation and we present the "test" systems and construct the NMQJ, DHS and THS methods for them. In the fourth part (Secs. 6-7) we study the results of the simulations and conclude.

Simulations are done with C++ using `gsl` and `ATLAS` libraries, [10], [30]. Compiling is done with `g++` [16]. For profiling we used `gprof` [16] and memory profiling we used `valgrind` [27]. Planck's constant $\hbar = 1$ in this thesis.

2 Dynamics of open systems

Closed System A quantum system $\mathcal{S}$ in Hilbert space $\mathcal{H}_S$ is defined to be closed if it is not entangled to any other quantum system and there exists no interaction between $\mathcal{S}$ and any other quantum systems. This means that the system is independent of its environment both dynamically and statistically. System is described by state operator ρ which is a trace class operator with unit trace. Set of these operators is called $S(\mathcal{H}_S)$. State operators are also called as density operators and density matrices. We use these terms interchangeably.

Evolution of a closed system can be described by a dynamical group $\{V_t | t \in \mathbb{R}\}$ and the structure of the map V_t is given by the theorem of Wigner [31],[1]. It says that for every state operator $\rho \in S(\mathcal{H}_S)$: $\rho \to V_t(\rho) = U_t \rho U_t^\dagger \in S(\mathcal{H}_s)$, where $U_t \in \mathcal{U}(\mathcal{H}_S)$ (set of unitary operators in $\mathcal{H}_S$).

Stone's theorem gives us one-to-one correspondence between self-adjoint operators of Hilbert space $\mathcal{H}$ and one parameter unitary groups [29]. Unitary operators for every t are generated by some self-adjoint (Hermitian) operator H with mapping $U_t = e^{-itH}$. From now on H is called *Hamiltonian*.

For every element in a group there exists an inverse element. This means that the dynamics of a closed system is reversible. We define a state vector of system at $t = 0$ to be $\psi \in \mathcal{H}_S$ and at time t, $\psi(t) = U_t \psi = e^{-iHt}\psi$. This can be also solved from the Schrödinger equation

$$\frac{\mathrm{d}}{\mathrm{d}t}\psi(t) = -iH\psi(t).$$

If we have a situation, where the Hamiltonian is time dependent $H \to H(t)$,

$$U(t,s)\psi = \psi + \sum_{n=1}^{\infty}(-i)^n \int_s^t \int_s^{t_1} \cdots \int_s^{t_{n-1}} H(t_1)\cdots H(t_{n-1})\psi \mathrm{d}t_n \cdots \mathrm{d}t \qquad (2.1)$$

gives the evolution of a state vector ψ from time s to time t, $s \leq t$ and $(t \geq t_1 \geq t_2 \cdots \geq t_{n-1} \geq s)$. This time ordering is called chronological. For the density

matrix $\rho(t) = U_t \rho U_t^\dagger$ at time t the evolution is obtained from Liouville-von Neumann equation

$$\frac{\mathrm{d}}{\mathrm{d}t}\rho(t) = -i[H, \rho(t)],$$

when $\rho(t = 0) = \rho$.

Open System An Open system is a system that is not closed. This means that there exists some other system called $\mathcal{E}$ and the system $\mathcal{S}$ might be entangled with $\mathcal{E}$ and/or there exists some interaction between $\mathcal{S}$ and $\mathcal{E}$. The System $\mathcal{E}$ is called *environment* or *reservoir* from now on. Hilbert space of $\mathcal{S} + \mathcal{E}$ is $\mathcal{H}_{\mathcal{S}+\mathcal{E}} = \mathcal{H}_\mathcal{S} \otimes \mathcal{H}_\mathcal{E}$. The combined system $\mathcal{S} + \mathcal{E}$ is assumed to be a closed system. This means that the evolution of the combined system is generated by some Hamiltonian $H_{\mathcal{S}+\mathcal{E}}$ and it is reversible. We now know that if the state of the system is at $t = 0$ given by $\rho_{\mathcal{S}+\mathcal{E}}$, at time t it is evolved to $\rho_{\mathcal{S}+\mathcal{E}}(t) = U_t \rho_{\mathcal{S}+\mathcal{E}} U_t^\dagger$, where $U_t \in \mathcal{U}(\mathcal{H}_{\mathcal{S}+\mathcal{E}})$. At any given time t' the state of the system $\rho_\mathcal{S}(t)$ can be obtained by partial trace,

$$\rho_\mathcal{S}(t) = \mathrm{tr}_\mathcal{E}\{U_t \rho_{\mathcal{S}+\mathcal{E}} U_t^\dagger\}.$$

If the combined system is prepared initially ($t = 0$) to a factorized state $\rho_\mathcal{S} \otimes \rho_\mathcal{E}$ and the operator H is known we can then define a dynamical map: $\rho_\mathcal{S} \to \Lambda_t(\rho_\mathcal{S})$ by relation $\Lambda_t(\rho_\mathcal{S}) = \mathrm{tr}_\mathcal{E}\{U_t \rho_{\mathcal{S}+\mathcal{E}} U_t^\dagger\}$. It maps $S(\mathcal{H}_\mathcal{S}) \to S(\mathcal{H}_\mathcal{S})$. It can be shown that Λ_t is completely positive, convex-linear, trace preserving and contracting mapping [4]. Gorini et al. [15] and Lindblad [18] have shown that, if the dynamics of the open system is described by a dynamical semigroup then an exact form for generator ($\mathcal{L}$) can be obtained. It is useful to know that in ref. [18], it is assumed that the generator of the dynamical semi-group and Hamiltonian are bounded. This is not the case in physics usually but with certain modifications generators can be cast in correct form [4]. Because of the semi-group properties dynamics of the system is

not reversible. Generator of the dynamical semigroup is [4]

$$\begin{aligned}\frac{\mathrm{d}}{\mathrm{d}t}\rho(t) =& -i[H_{\mathcal{S}} + H_{\mathrm{LS}}, \rho_{\mathcal{S}}(t)] \\ &+ \sum_{\alpha,\omega} \Delta_\alpha(\omega)\left(S_\alpha(\omega)\rho_{\mathcal{S}}(t)S_\alpha^\dagger(\omega) - \frac{1}{2}\{S_\alpha^\dagger(\omega)S_\alpha(\omega), \rho_{\mathcal{S}}(t)\}\right) \\ &= \mathcal{L}\rho_{\mathcal{S}}(t). \end{aligned} \tag{2.2}$$

This is called the Lindblad equation. Operators S_α are called Lindblad or *jump* operators and Δ_α is called *decay rate*. H_{LS} is the *Lamb shift* Hamiltonian. This is a very important equation because it guarantees that $\rho_{\mathcal{S}}(t)$ is positive for all $t \geq 0$, $\mathrm{tr}_{\mathcal{S}}\{\rho_{\mathcal{S}}(t)\}$ is preserved and dynamical map generated by $\mathcal{L}$ is completely positive. If dynamics of a system are governed by the Lindblad equation, coherences of density matrix decrease. Information from the system is flowing to the environment and it can not be obtained back to the system.

For a non-Markovian system situation is different. The non-Markovian system may restore some of the coherence that it has lost earlier. This means that there is a two way information transfer between the system and the environment. In the next section we perform a *microscopic* derivation for the Markovian master equation in the Lindblad form. This gives us physical insight about the open system dynamics.

2.1 Markovian master equation

Hilbert space is $\mathcal{H} = \mathcal{H}_{\mathcal{S}} \otimes \mathcal{H}_{\mathcal{E}}$. There exists some interaction between $\mathcal{S}$ and $\mathcal{E}$. First approximation is that the system is weakly coupled to the environment and we can approximate that the combined density matrix for the system and the environment for all times is

$$\tilde{\rho}(t) \approx \tilde{\rho}_{\mathcal{S}}(t) \otimes \tilde{\rho}_{\mathcal{E}}, \tag{2.3}$$

$\tilde{\rho}(t) \in S(\mathcal{H}_{\mathcal{S}} \otimes \mathcal{H}_{\mathcal{E}})$. This is the *Born* or the *weak coupling* approximation. Tilde on arbitrary operator $\tilde{A}$ means that the operator is in the Schrödinger picture. Density

matrix for the environment is assumed to be constant for all t. Hamiltonian of the total system is

$$\tilde{H} = \tilde{H}_{\mathcal{S}} \otimes \tilde{I}_{\mathcal{E}} + \tilde{I}_{\mathcal{S}} \otimes \tilde{H}_{\mathcal{E}} + \tilde{H}_I. \tag{2.4}$$

Last term on the r.h.s. is the interaction Hamiltonian which couples the environment to the system. Dynamics of $\mathcal{S} + \mathcal{E}$ in the *interaction* picture can be solved from the following equation

$$\frac{\mathrm{d}}{\mathrm{d}t}\rho(t) = -i[H_I(t), \rho(t)], \tag{2.5}$$

where

$$H_I(t) = e^{i(\tilde{H}_{\mathcal{S}}+\tilde{H}_{\mathcal{E}})t}\tilde{H}_I e^{-i(\tilde{H}_{\mathcal{S}}+\tilde{H}_{\mathcal{E}})t}, \tag{2.6}$$

$$\rho(t) = e^{i(\tilde{H}_{\mathcal{S}}+\tilde{H}_{\mathcal{E}})t}\tilde{\rho}(t)e^{-i(\tilde{H}_{\mathcal{S}}+\tilde{H}_{\mathcal{E}})t}. \tag{2.7}$$

By integrating the Eq. (2.5) and inserting the result back to the Eq. (2.5), using the Born approximation, tracing over $\mathcal{E}$ and assuming that

$$\mathrm{tr}_{\mathcal{E}}\{H_I(t), \rho(0)\} = 0, \tag{2.8}$$

we get the following equation

$$\frac{\mathrm{d}}{\mathrm{d}t}\rho_{\mathcal{S}}(t) = -\int_0^t \mathrm{d}s\, \mathrm{tr}_{\mathcal{E}}\{[H_I(t), [H_I(s), \rho_{\mathcal{S}}(s) \otimes \rho_{\mathcal{E}}]]\}. \tag{2.9}$$

We see that the state of the system at time $t \geq 0$ depends on its state at earlier times. Next approximation is the *Markov* approximation. We simply replace $\rho_{\mathcal{S}}(s) \rightarrow \rho_{\mathcal{S}}(t)$. This means that the state of system at time t does not depend on state of the system at time $t' < t$. We arrive to

$$\frac{\mathrm{d}}{\mathrm{d}t}\rho_{\mathcal{S}}(t) = -\int_0^t \mathrm{d}s\, \mathrm{tr}_{\mathcal{E}}\{[H_I(t), [H_I(s), \rho_{\mathcal{S}}(t) \otimes \rho_{\mathcal{E}}]]\}. \tag{2.10}$$

This is sometimes called the Redfield equation. We can see that this equation is local in time, but this does not yet guarantee that dynamics is described by dynamical

semi-group, because the time evolution of ρ_S depends on the initial preparation at $t = 0$. Next we replace s with $t-s$ and change the upper integration limit to infinity. This is a part of the Markov approximation. The meaning of this approximation is to eliminate the dependence from the initial preparation. Changing the upper integration limit to infinity is valid when there exists a timescale $\tau_{\mathcal{E}}$, that when $s \gg \tau_{\mathcal{E}}$ the integrand disappears fast enough. That way the contribution $s \gg \tau_{\mathcal{E}}$ to the integral is negligible. The Markov approximation is valid if the system stays approximately constant in the time scale $\tau_{\mathcal{E}}$. This means that the relaxation time scale of the system τ_R is larger than $\tau_{\mathcal{E}}$. The form of the Markovian master equation (for $t \gg \tau_{\mathcal{E}}$) is

$$\frac{\mathrm{d}}{\mathrm{d}t}\rho_{\mathcal{S}}(t) = -\int_0^\infty \mathrm{d}s\, \mathrm{tr}_{\mathcal{E}}\{[H_I(t), [H_I(t-s), \rho_{\mathcal{S}}(t) \otimes \rho_{\mathcal{E}}]]\}. \tag{2.11}$$

Equation (2.11) does not necessarily define generator of dynamical semi-group. To guarantee that we need to perform the *secular* approximation. Most general form of the interaction is

$$\tilde{H}_I = \sum_\alpha \tilde{S}_\alpha \otimes \tilde{E}_\alpha. \tag{2.12}$$

$\tilde{S}_\alpha,\ \tilde{E}_\alpha$ are self-adjoint operators. We can express the system operators $\tilde{S}_\alpha$ with the help of spectral decomposition of the system Hamiltonian $\tilde{H}_{\mathcal{S}} = \sum_\epsilon \epsilon \Pi(\epsilon)$, where $\Pi(\epsilon)$ is projection to the eigenspace corresponding to the eigenvalue ϵ of $\tilde{H}_{\mathcal{S}}$.

$$\begin{aligned} \tilde{S}_\alpha(\omega) &= \sum_{\epsilon'-\epsilon=\omega} \Pi(\epsilon)\tilde{S}_\alpha\Pi(\epsilon'), \\ \tilde{S}_\alpha &= \sum_\omega \tilde{S}_\alpha(\omega). \end{aligned} \tag{2.13}$$

In the interaction picture we get the following equation

$$\begin{aligned} H_I(t) &= \sum_{\alpha,\omega} e^{i\tilde{H}_{\mathcal{S}}t}\tilde{S}_\alpha(\omega)e^{-i\tilde{H}_{\mathcal{S}}t} \otimes e^{i\tilde{H}_{\mathcal{E}}t}\tilde{E}_\alpha e^{-i\tilde{H}_{\mathcal{E}}t} \\ &= \sum_{\alpha,\omega} e^{-i\omega t} S_\alpha(\omega) \otimes E_\alpha(t) \\ &= \sum_{\alpha,\omega} e^{+i\omega t} S_\alpha^\dagger(\omega) \otimes E_\alpha^\dagger(t), \end{aligned} \tag{2.14}$$

where have used the spectral decomposition of $\tilde{H}_S$. The assumption (2.8) now reads $\mathrm{tr}_{\mathcal{E}}\{E_\alpha(t)\rho_{\mathcal{E}}\} = 0$, which says that the density matrix of the environment is prepared in a way that the mean value of operators $E_\alpha(t)$ vanishes. This is exactly the case when one considers the quantized electromagnetic field and the environment is described by the number states [13]. Inserting the Eq. (2.14) to the Eq. (2.11) and after some calculation we find

$$\begin{aligned}\frac{\mathrm{d}}{\mathrm{d}t}\rho_{\mathcal{S}}(t) = &\sum_{\alpha,\beta,\omega,\omega'}\int_0^\infty \mathrm{d}s\,\mathrm{tr}_{\mathcal{E}}\{E_\alpha^\dagger(t)E_\beta(t-s)\rho_{\mathcal{E}}\}e^{i\omega s}\\ &\times e^{it(\omega-\omega')}\Big(S_\beta(\omega')\rho_{\mathcal{S}}(t)S_\alpha^\dagger(\omega) - S_\alpha^\dagger(\omega)S_\beta(\omega')\rho_{\mathcal{S}}(t)\Big) + \mathrm{h.c.}\\ = &\sum_{\alpha,\beta,\omega,\omega'}\Gamma_{\alpha\beta}(\omega)e^{it(\omega-\omega')}\Big(S_\beta(\omega')\rho_{\mathcal{S}}(t)S_\alpha^\dagger(\omega) - S_\alpha^\dagger(\omega)S_\beta(\omega')\rho_{\mathcal{S}}(t)\Big) + \mathrm{h.c.},\end{aligned} \tag{2.15}$$

where h.c. stands for hermitian conjugate. Typical time scale of the system $\tau_{\mathcal{S}}$ is given by $|\omega-\omega'|^{-1}$, where $\omega \neq \omega'$. If $\tau_{\mathcal{S}}$ is smaller than τ_R (time scale for relaxation) then terms $e^{i(\omega-\omega')t}$ oscillate very rapidly in the time scale τ_R. Thus we can neglect them because their average value is approximately zero [4],[13]. We are then left with

$$\frac{\mathrm{d}}{\mathrm{d}t}\rho_{\mathcal{S}}(t) = \sum_{\alpha,\beta,\omega}\Gamma_{\alpha\beta}(\omega)\Big(S_\beta(\omega)\rho_{\mathcal{S}}(t)S_\alpha^\dagger(\omega) - S_\alpha^\dagger(\omega)S_\beta(\omega)\rho_{\mathcal{S}}(t)\Big) + \mathrm{h.c.} \tag{2.16}$$

We assume that $[H_{\mathcal{E}}, \rho_{\mathcal{E}}] = 0$. We thus have a stationary process [17] which implies that the reservoir correlation functions are homogeneous in time, $\mathrm{tr}_{\mathcal{E}}\{E_\alpha^\dagger(t)E_\beta(t-s)\} = \mathrm{tr}_{\mathcal{E}}\{E_\alpha^\dagger(s)E_\beta(0)\}$. We can define the following matrices

$$\Gamma_{\alpha,\beta}(\omega) = \frac{1}{2}\Delta_{\alpha\beta}(\omega) + i\lambda_{\alpha\beta}(\omega),$$

$$\Delta_{\alpha\beta}(\omega) = \Gamma_{\alpha\beta}(\omega) + \Gamma_{\beta\alpha}^*(\omega) = \int_\infty^\infty \mathrm{d}s\, e^{i\omega s}\mathrm{tr}_{\mathcal{E}}\{E_\alpha^\dagger(s)E_\beta(0)\}, \tag{2.17}$$

$$\lambda_{\alpha\beta}(\omega) = \frac{1}{2i}(\Gamma_{\alpha\beta}(\omega) - \Gamma_{\beta\alpha}^*(\omega)). \tag{2.18}$$

With these definitions we arrive to the following equation

$$\begin{aligned}\frac{\mathrm{d}}{\mathrm{d}t}\rho_{\mathcal{S}}(t) =& -i[\sum_{\omega,\alpha,\beta}\lambda_{\alpha\beta}(\omega)S^{\dagger}_{\alpha}(\omega)S_{\beta}(\omega),\rho_{\mathcal{S}}(t)] \\ &+\sum_{\omega,\alpha,\beta}\Delta_{\alpha\beta}(\omega)\Big(S_{\beta}(\omega)\rho_{\mathcal{S}}(t)S^{\dagger}_{\alpha}(\omega)-\frac{1}{2}\{S^{\dagger}_{\alpha}(\omega)S_{\beta}(\omega),\rho_{\mathcal{S}}(t)\}\Big) \\ =& -i[H_{LS},\rho_{\mathcal{S}}(t)]+\mathcal{D}(\rho_{\mathcal{S}}(t)). \end{aligned} \tag{2.19}$$

The Lamb shift Hamiltonian H_{LS} commutes with the system Hamiltonian $H_{\mathcal{S}}$. We can immediately see that in the case when $\alpha = \beta$ the equation is in the Lindblad form. In the general case if matrix $\Delta_{\alpha\beta}$ is positive we can diagonalize it and put the equation in the Lindblad form. Positivity of matrix $\Delta_{\alpha\beta}$ follows from the positivity of the homogeneous correlation functions $\mathrm{tr}_{\mathcal{E}}\{E^{\dagger}_{\alpha}(s)E_{\beta}(0)\}$ and from the Bochner's theorem which states that the Fourier transform of positive function is positive [26]. When we have the equation in the Lindblad form Δ_{α} is called decay rate. We can transform this interaction picture master equation into the Schrödinger picture by replacing $H_{LS} \rightarrow H_{\mathcal{S}} + H_{LS}$ [4]. If we have a situation where the Hamiltonian of the open system is time dependent, we can have time dependent generator of the dynamical semi-group, if for each fixed $t_i \geq 0$ $\mathcal{L}_{t_i}$ generates a dynamical semi-group. If the reservoir has structure (spectrum of the reservoir is not flat) we have a situation where the decay rates become time dependent. If the decay rates stay positive for all t the system is Markovian.

2.2 Non-Markovian master equation

In the last section we arrived to the Markovian master equation after a number of approximations, which gave us a (time dependent) generator of the dynamical semi-group. Physical idea behind those approximations was to coarse grain the time scale of the dynamics in a way that memory effects are not resolved. Memory effects emerge when decay rate(s) turns from positive to negative. During those negative periods information flows from the environment back to the system.

In this section we will derive local in time non-Markovian master equation with time-convolutionless (TCL) method [4], [28]. We have a system $\mathcal{S}$ that is interacting with the environment $\mathcal{E}$. Hilbert space of the system and the environment is $\mathcal{H}_{\mathcal{S}\otimes\mathcal{E}}$. Hamiltonian for the system and the environment is

$$H = H_0 + \alpha H_I, \tag{2.20}$$

where α is a dimensionless expansion parameter. H_I is the interaction part of the Hamiltonian. Let us assume that density matrix ρ describes the system and the environment. In the interaction picture the time evolution of ρ is governed by

$$\frac{\partial}{\partial t}\rho(t) = -i\alpha[H_I(t), \rho(t)] = \alpha\mathcal{L}(t)\rho(t). \tag{2.21}$$

Time dependent generator $\mathcal{L}(t)$ is not necessarily in the Lindblad form. We define following projection super operators that operate in the space of density matrices of $\mathcal{S}+\mathcal{E}$

$$\rho \to \mathcal{P}\rho = \mathrm{tr}_{\mathcal{E}}\{\rho\} \otimes \rho_{\mathcal{E}} = \rho_{\mathcal{S}} \otimes \rho_{\mathcal{E}}, \tag{2.22}$$

$$\rho \to \mathcal{Q}\rho = \rho - \mathcal{P}\rho, \tag{2.23}$$

where $\rho_{\mathcal{E}}$ is some fixed density matrix describing the environment. We assume that $\rho_{\mathcal{E}}$ is time independent. This means that the interaction between the system and the environment has an effect only on the system. We say that $\mathcal{P}$ projects to the relevant part of the total system and $\mathcal{Q}$ to the irrelevant part. These operators have following properties

$$\mathcal{Q} + \mathcal{P} = I, \tag{2.24}$$

$$\mathcal{P}^2 = \mathcal{P}, \tag{2.25}$$

$$\mathcal{Q}^2 = \mathcal{Q}, \tag{2.26}$$

$$\mathcal{P}\mathcal{Q} = \mathcal{Q}\mathcal{P} = 0. \tag{2.27}$$

We assume that the odd moments respect to the interaction Hamiltonian vanish in environmental state. This leads to the following equation

$$\mathcal{P}\mathcal{L}(t_1)\mathcal{L}(t_2)\cdots\mathcal{L}(t_{2n+1})\mathcal{P} = 0, \tag{2.28}$$

where $n = 0, 1, 2, \cdots$. This is not a necessary assumption for the method to work but it simplifies calculations. With the help of the operators $\mathcal{P}$ and $\mathcal{Q}$ we can derive an equation of motion for the relevant part of the density operator. We first operate on Eq. (2.21) with $\mathcal{P}$ and $\mathcal{Q}$ and get

$$\frac{\partial}{\partial t}\mathcal{P}\rho(t) = \alpha\mathcal{P}\mathcal{L}(t)\rho(t) = \alpha\mathcal{P}\mathcal{L}(t)\mathcal{P}\rho(t) + \alpha\mathcal{P}\mathcal{L}(t)\mathcal{Q}\rho(t), \tag{2.29}$$

$$\frac{\partial}{\partial t}\mathcal{Q}\rho(t) = \alpha\mathcal{Q}\mathcal{L}(t)\rho(t) = \alpha\mathcal{Q}\mathcal{L}(t)\mathcal{P}\rho(t) + \alpha\mathcal{Q}\mathcal{L}(t)\mathcal{Q}\rho(t). \tag{2.30}$$

We can solve equation (2.30) and obtain

$$\mathcal{Q}\rho(t) = \mathcal{G}(t,0)\mathcal{Q}\rho(0) + \alpha\int_0^t \mathrm{d}s\,\mathcal{G}(t,s)\mathcal{Q}\mathcal{L}(s)\rho(s). \tag{2.31}$$

Here the generator is

$$\mathcal{G}(s,t) = I + \sum_{n=1}^{\infty}(-\alpha)^n\int_s^t\int_s^{t_1}\cdots\int_s^{t_{n-1}}\mathcal{Q}\mathcal{L}(t_1)\cdots\mathcal{Q}\mathcal{L}(t_n)\mathrm{d}t_n\cdots\mathrm{d}t, \tag{2.32}$$

and the time intervals are ordered as $(t \geq t_1 \geq t_2 \geq \cdots t_n \geq s)$. We want to eliminate the dependence of the past state of the system and create an equation that is local in time. We define a *backward* propagator $G(t,s)$ for the combined system. It operates on density matrix at time t and propagates it backward to the earlier time s. Formally we write

$$G(t,s) = I + \sum_{n=1}^{\infty}\alpha^n\int_s^t\int_s^{t_1}\cdots\int_s^{t_{n-1}}\mathcal{L}(t_1)\cdots\mathcal{L}(t_n)\mathrm{d}t_n\cdots\mathrm{d}t, \tag{2.33}$$

where the time intervals are ordered as $(s \leq t_1 \leq t_2 \cdots \leq t_n \leq t)$. This is called an anti-chronological time ordering. With this definition we can express the density matrix at time $s \leq t$ as

$$\rho(s) = G(t,s)(\mathcal{P}+\mathcal{Q})\rho(t). \tag{2.34}$$

Inserting the Eq. (2.34) to the Eq. (2.31) we obtain for the irrelevant part

$$\mathcal{Q}\rho(t) = \mathcal{G}(t,0)\mathcal{Q}\rho(0) + \alpha \int_0^t \mathrm{d}s\, \mathcal{G}(t,s)\mathcal{Q}\mathcal{L}(s)\mathcal{P}G(t,s)(\mathcal{P}+\mathcal{Q})\rho(t). \tag{2.35}$$

Let us introduce a new super operator

$$\Sigma(t) = \alpha \int_0^t \mathrm{d}s\, \mathcal{G}(t,s)\mathcal{Q}\mathcal{L}(s)\mathcal{P}G(t,s), \tag{2.36}$$

and we get for the irrelevant part

$$[1-\Sigma(t)]\mathcal{Q}\rho(t) = \mathcal{G}(t,0)\mathcal{Q}\rho(0) + \Sigma(t)\mathcal{P}\rho(t). \tag{2.37}$$

Because $\Sigma(0) = 0$ and $\Sigma(t)|_{\alpha=0} = 0$ the operator $[1-\Sigma(t)]$ may be inverted for not too large couplings and for all couplings if the time interval is small. Thus we get for the irrelevant part

$$\mathcal{Q}\rho(t) = [1-\Sigma(t)]^{-1}\Sigma(t)\mathcal{P}\rho(t) + [1-\Sigma(t)]^{-1}\mathcal{G}(t,0)\mathcal{Q}\rho(0). \tag{2.38}$$

Inserting the previous equation into the Eq. (2.29) we obtain the following exact time convolutionless master equation

$$\frac{\partial}{\partial t}\mathcal{P}\rho(t) = \mathcal{K}(t)\mathcal{P}\rho(t) + \mathcal{I}(t)\mathcal{Q}\rho(0), \tag{2.39}$$

with a generator that is local in time, i.e., it depends only on the present state of the system

$$\mathcal{K}(t) = \alpha\mathcal{P}\mathcal{L}(t)[1-\Sigma(t)]^{-1}\mathcal{P}, \tag{2.40}$$

and the time local inhomogeneity

$$\mathcal{I}(t) = \alpha\mathcal{P}\mathcal{L}(t)[1-\Sigma(t)]^{-1}\mathcal{G}(t,0)\mathcal{Q}. \tag{2.41}$$

This equation of motion is exact, local in time, and extremely complicated. It is useful because by expanding $\mathcal{K}(t)$ and $\mathcal{I}(t)$ in powers of α one can systematically create approximations. This is obviously possible only if the operator $[1-\Sigma(t)]$ is

invertible. We want to consider only to second order in α. Let us assume that the operator $\Sigma(t)$ can be expanded to geometric series

$$[1 - \Sigma(t)]^{-1} = \sum_{n=0}^{\infty} [\Sigma(t)]^n. \tag{2.42}$$

Inserting this into the Eq. (2.40) we obtain

$$\mathcal{K}(t) = \alpha \sum_{n=0}^{\infty} \mathcal{P}\mathcal{L}(t)[\Sigma(t)]^n \mathcal{P} = \sum_{n=1}^{\infty} \alpha^n \mathcal{K}_n(t). \tag{2.43}$$

Expanding also the operator

$$\Sigma(t) = \sum_{n=1}^{\infty} \alpha^n \Sigma_n(t), \tag{2.44}$$

and inserting it into the Eq. (2.43) and collecting all equal powers of α, we obtain in the second order

$$\mathcal{K}_1(t) = \mathcal{P}\mathcal{L}(t)\mathcal{P}, \tag{2.45}$$

$$\mathcal{K}_2(t) = \mathcal{P}\mathcal{L}(t)\Sigma_1(t)\mathcal{P}. \tag{2.46}$$

Using the assumption (2.28) we see that $\mathcal{K}_1(t) = 0$. Using the Eqs. (2.32), (2.33) and (2.36) to $\mathcal{K}_2(t)$ and considering only to order of α^2 we arrive to the following

$$\mathcal{K}_2(t) = \int_0^t \mathrm{d}s\, \mathcal{P}\mathcal{L}(t)\mathcal{L}(s)\mathcal{P}. \tag{2.47}$$

Applying this to the Eq. (2.39) and taking the partial trace over the environmental degrees of freedom we obtain

$$\frac{\partial}{\partial t}\rho_{\mathcal{S}}(t) = -\alpha^2 \int_0^t \mathrm{d}s\, \mathrm{tr}_{\mathcal{E}}\{[H_I(t), [H_I(s), \rho_{\mathcal{S}}(t) \otimes \rho_{\mathcal{E}}]]\}. \tag{2.48}$$

This is the Redfield equation which we obtained earlier before Markov approximation. Occasionally this level of approximation is called TCL2. With this equation it is possible to describe non-Markovian phenomena. In the next section we go back to the Markovian systems and discuss about simulation methods designed for them.

3 Markovian Monte Carlo methods

In this chapter we introduce three different unravelings for the Markovian master equation. Two of them are jump type and one is diffusion type unraveling. Density matrix can be expressed as

$$\rho = \sum_{m=0}^{K-1} w_m |\psi_m\rangle\langle\psi_m|, \tag{3.1}$$

where w_a are positive weights, $\sum_{m=0}^{K-1} w_m = 1$. This can be seen as a statistical ensemble of pure states. Representation is not unique and in fact there are infinite number of ways to express the same density matrix as a convex combination of pure states.

In this thesis we study situations where the initial state of the system is a pure state. In the Monte Carlo methods studied in this thesis one constructs a statistical ensemble of M members which are initially identical pure states of the form

$$|\phi(t_0)\rangle = \sum_{m=0}^{D-1} c_m(t_0)|\varphi_m\rangle. \tag{3.2}$$

Vectors $|\varphi_m\rangle$ form an orthonormal basis in the Hilbert space of the system and D is the dimension of the Hilbert space. Then the states in the ensemble are evolved *independently*. We thus create independent trajectories. Time evolution of the density matrix is obtained as an ensemble average over all of the trajectories. If one wants to simulate the dynamics of a mixed state, which can not be given as a state vector, we construct a distribution from different initial state vectors $|\phi_i(t_0)\rangle$ and choose our initial states from that distribution.

For Monte Carlo methods in general there are no exact error boundaries because of the probabilistic nature of this type of methods. Some estimates for accuracy can be obtained from the standard deviation that can be estimated. Fortunately we do not have to rely only on this information in this thesis. We can measure the error directly, because it is simple to solve the dynamics with direct numerical integration

in all cases studied here. Then we can simply compare the numerically integrated and the simulated solutions.

3.1 MCWF

Monte Carlo Wave Function approach has been developed by Mølmer et al., Refs. [20],[19],[21]. This method applies to a small system coupled to a large reservoir in the regime of the Markov approximation. By a small system we mean that the system has much smaller number of degrees of freedom than the environment. For example a two state atom coupled to the modes of the quantized EM field.

The density matrix is treated as an ensemble of state vectors. We consider only pure initial states and hence initially all the state vectors in the ensemble are the same. Dynamics are then solved by evolving each of the state vectors in the ensemble independently and calculating the ensemble average. One ensemble member experiences deterministic evolution interrupted by jumps at random times. We discuss the physical meaning of this process in Sec. 3.4.

Starting point of this method is the Markovian master equation (please note that we have absorbed decay rates into the operators C_m)

$$\dot{\rho}(t) = i[\rho(t), H_S] - \frac{1}{2}\sum_m \left(\{\rho(t), C_m^\dagger C_m\} - 2C_m \rho(t) C_m^\dagger \right), \tag{3.3}$$

where $\{\cdot,\cdot\}$ is an anti-commutator. Let us assume that one member of the ensemble is in state $|\phi(t)\rangle$ and $||\phi(t)|| = 1$. Evolution of the state vector over a small time interval δt has two steps.

Step 1. We first calculate the deterministic state vector $|\phi^{(1)}(t+\delta t)\rangle$. It is obtained by evolving $|\phi(t)\rangle$ over a small time step with the non-Hermitian Hamiltonian:

$$H = H_s - \frac{i}{2}\sum_m C_m^\dagger C_m. \tag{3.4}$$

We get for the first order in small enough δt:

$$|\phi^{(1)}(t+\delta t)\rangle = (1 - iH\delta t)|\phi(t)\rangle. \tag{3.5}$$

We have $||\phi^{(1)}(t+\delta)||^2 = 1-\delta p$, where $\delta p = \sum_m \delta p_m$ and $\delta p_m = \delta t \langle\phi(t)|C_m^\dagger C_m|\phi(t)\rangle$. We need to adjust δt in such a way that the calculation is valid in first order. That means $\delta p \ll 1$.

Step 2. In this step we have possibility of a jump. We have a probability of δp for a jump and probability $1-\delta p$ for the deterministic evolution. We draw a random number $\epsilon \sim \mathcal{U}_{[0,1]}$ and if $\epsilon > \delta p$, deterministic evolution takes place and

$$|\phi(t+\delta t)\rangle = \frac{|\phi^{(1)}(t+\delta t)\rangle}{||\phi^{(1)}(t+\delta t)||}. \tag{3.6}$$

If $\delta p > \epsilon$, we have a jump. This means that the state $|\phi(t)\rangle$ experiences instantaneous transition

$$|\phi(t)\rangle \to |\phi(t+\delta t)\rangle = \frac{C_m|\phi(t)\rangle}{||C_m\phi(t)||}. \tag{3.7}$$

If we have many operators C_m we choose one according to probability $P_m = \delta p_m/\delta p$. Few remarks. The probability of a jump is calculated at the same time as the deterministic evolution. Jumps are rare occasions compared to deterministic evolution because we have $\delta p \ll 1$.

3.2 Quantum Trajectories

Quantum trajectories (QT) method was developed by Carmichael and Zoller [33],[6]. It has some similarities with the MCWF method. Both of them generate realizations with continuous deterministic parts interrupted by discontinuous jumps. Formalism between these methods looks very different but the main difference is in the determination of the jumps. In the MCWF method we have seen that for each time step δt we have two possible scenarios for the state vector; jump or deterministic evolution.

We decide the path of the state vector for each instance of time by choosing a random number and comparing the jump and no-jump probabilities in a way described earlier. In QT we do this differently. We define the so called waiting time function from which we can determine the times of the jumps.

Definition 1: The waiting time function tells us that if a jump has happened at time t_0 with probability $p_0 = 1$ to the state x_0 we have the next jump at time t_1 away from x_0 with a probability $p_1 < 1$. This is the definition found in the Ref. [7]. This can be defined also in another way.

Definition 2: If a jump has happened at time t_0 to the state x_0, the waiting time function $F(t_0|t_0; x_0) = 0$ and the probability for a jump at time $t_1 > t_0$ away from x_0 with a condition that a jump happened at time t_0 is $F(t_1|t_0; x_0) = p_1$, with $0 < p_1 \leq 1$. This definition is from the Ref. [4].

We use here the definition 2. Generally $F(\tau|t_0; x_0)$ increases monotonically (for Markovian systems) with τ, and there are essentially two different types of behavior for $F(\tau|t_0; x_0)$:

i) $\lim_{\tau\to\infty} F(\tau|t_0; x_0) = 1$, which means that the system will eventually jump when enough time is passed.

ii) $\lim_{\tau\to\infty} F(\tau|t_0; x_0) = 1 - q$. This means that there is a probability $0 < q \leq 1$ for a situation where the system does not jump away from the state x_0. q is called a defect.

We can simulate the Markovian master equation (3.3) with this method in the following way. We define the non-Hermitian Hamiltonian in the same way as in the MCWF method, $H = H_s - \frac{i}{2}\sum_m C_m^\dagger C_m$. First we assume that the system has arrived to the state $|\psi(0)\rangle$ at time t_0 through a jump and $||\psi(0)|| = 1$. The waiting time function is given by [4]

$$F(\tau|t_0; \psi(0)) = 1 - ||e^{-iH\tau}\psi(0)||. \tag{3.8}$$

As in the MCWF method the probability for a jump is proportional to the decrease of the norm. Also notice that $q = \lim_{\tau\to\infty} ||e^{-iH\tau}\psi(0)||$. The non-normalized state vector is $|\psi(\tau)\rangle = e^{-iH\tau}|\psi(0)\rangle$. The steps of the algorithm are

1) Draw a random number $\epsilon \sim \mathcal{U}_{[0,1]}$ at t_0.

2) Solve equation $||\psi(\tau)||^2 = ||e^{-iH\tau}|\psi(0)\rangle||^2 = \epsilon$, for τ.

3) State vector evolves deterministically in time interval $s \in [t_0, \tau]$,

$$|\psi(t_0 + s)\rangle = \frac{|e^{-iHs}\psi(0)\rangle}{||e^{-iHs}\psi(0)||}. \tag{3.9}$$

4) Jump happens at time τ. Jumps are the same form as in MCWF method and their probabilities are the same. Go to step 1.

Advantages of this method over MCWF is that less random numbers are generated. Depending on the random number generator algorithm this might become problem in MCWF. If the need for random numbers is smaller than the period of random number generator this is not a problem. Disadvantage is that in simulations we must take into account a possibility of having a defect.

3.3 Quantum State Diffusion

Originally the Quantum State Diffusion was developed when several authors became interested in alternative versions of quantum mechanics. The method is based on a stochastic differential equation and under certain symmetry conditions it is possible derive a unique diffusion model which is called the Quantum State Diffusion model [25].

The diffusion expansion can be performed to a given Markovian master equation if the size of the transitions among the states becomes arbitrarily small and if at the same time the number of transitions in a given interval becomes arbitrarily large [4]. If we consider this with the MCWF description in mind, this means that we

must have much larger jump probability but state transitions must be very small. In fact QSD model can be obtained in many ways: from MCWF using the invariance of the Markovian master equation under certain transformations and defining new jump operators that give large jump probability and small change in state vector if jump happens [19]. Another approach with more mathematical detail is in the Ref. [4]. We present here a formulation from the original paper by Gisin [14], where the evolution of a single state vector over a small time interval is given as stochastic differential equation in Itô form.

Starting point is the Markovian master equation (3.3). We are assuming that the system is initially at a pure state $|\psi\rangle$ and we formulate a stochastic differential equation for the variations $|d\psi\rangle$ of state vector $|\psi\rangle$ in a time interval dt. The variations are governed by

$$|d\psi\rangle = |v\rangle d\mathrm{t} + \sum_m |u_m\rangle d\xi_m, \tag{3.10}$$

where $|v\rangle d\mathrm{t}$ is the drift term and stochastic fluctuations are given as a sum over independent complex valued Wiener processes $d\xi_m$. States $|u_m\rangle$ are orthogonal to $|\psi\rangle$ in order to preserve the normalization. With the methods presented in the Ref. [14] we can obtain a unique form for the vectors $|v\rangle$ and $|u_m\rangle$ in the Eq. (3.10) when the dynamics of the density matrix are governed by the Eq. (3.3). We get

$$\begin{aligned} |d\psi\rangle = &- iH_S|\psi\rangle dt + \sum_m \left(\langle C_m^\dagger \rangle_\psi C_m - \frac{1}{2} C_m^\dagger C_m - \frac{1}{2} \langle C_m \rangle_\psi \langle C_m^\dagger \rangle_\psi \right) |\psi\rangle \\ &+ \sum_m \frac{1}{\sqrt{2}} \left(C_m - \langle C_m \rangle_\psi \right) |\psi\rangle d\xi_m. \end{aligned} \tag{3.11}$$

This equation preserves normalization of the state vector on average, but for numerical studies it is simpler to use modified version of the previous equation which does not preserve the normalization. In practice the drift part of the equation is solved as a finite difference equation and a random component is added directly to the solution. Physical interpretation of this process is discussed in the Sec. 3.4.

3.4 Measurement scheme interpretation for Markovian systems

In the previous chapter we have seen three different types of simulation methods for the Markovian master equation. They treat the open system as an ensemble of stochastic state vectors, but Quantum Trajectories (QT) and MCWF type unravelings introduced discrete jumps between different states at random times and QSD adds a random element for every time step of the evolution of the state vector. In physical interpretations the environment of the system is thought to be monitored continuously and simulation generates measurement records. Obviously simulations can not give exact picture of the measurement records because we have to use discretized time intervals and finite statistical ensembles in the simulations. In this chapter we begin by describing the measurement process involved in the jump type unraveling of the master equation and use the understanding gained to describe the measurement scheme involved in the QSD.

Jump-type process Interpretation presented here applies to the both QT and MCWF method, because those methods produce trajectories that have the same properties. In the jump type unraveling single realization or trajectory corresponds to a one possible outcome of a process where the environment of the system is monitored continuously [19]. We know that if we see a photon in the environment it must have been emitted by the system and therefore the system has jumped (downward transition + emission). We assume that our detectors are perfect and every photon is measured. We thus propagate in parallel a conditional state vector and a detection record. The state vector is conditioned to a detection and no detection of a photon in the environment [6].

The decrease of the norm when the system does not jump has a relevant physical meaning. Let us take an example: two state model decaying spontaneously without

driving between energy levels. We have one jump operator σ_-. Let us assume that we evolve state vector $|\psi(t_0)\rangle = c_e(t_0)|e\rangle + c_g(t_0)|g\rangle$, $\{|c_g(t_0)|^2, |c_e(t_0)|^2\} \neq 0$, $c_g(t), c_e(t) \in \mathbb{C} \, \forall \, t \in \mathbb{R}$, $||\psi(t_0)|| = 1$ over one time step $t_0 \rightarrow t_0 + \delta t$ and that we have a nonzero decay rate value and the system does not jump. Following things happen:

i) $||\psi(t_0)|| > ||\psi(t_0 + \delta t)||$ and

ii) $|\psi(t_0 + \delta t)\rangle \rightarrow \frac{|\psi(t_0+\delta t)\rangle}{||\psi(t_0+\delta t)||}$.

First item i). Because the evolution is generated by the non-Hermitian Hamiltonian (3.4), we know that the excited state amplitude has become smaller but the ground state amplitude has not changed. Now because of ii) we see that ground state amplitude is increased compared to the excited state amplitude after the normalization. Jump probability is proportional to the probability of the excited state and therefore after no-jump evolution we have a smaller probability to jump in the next interval. This means that there exists a possibility that the system may go to the ground state without emitting any photons. If the probability a jump would not decrease we would then eventually have a jump and that would be wrong. If we have initially system in the state $|e\rangle$ then the system has non-zero jump probability if the decay rate is not zero and eventually system jumps and emits a photon. Individual trajectories give us insight about the physical process that take place when the system evolves and we gain understanding about the physical mechanisms involved in the process. This also applies to more complex systems with the addition that we have more than one state that can jump.

The fact that the decomposition of the density matrix is not unique and that two different statistical ensembles can generate the same expectation values gives

rise to different measurement schemes. Let us express the Eq. (3.3) in a form

$$\begin{aligned}\dot{\rho}(t) =& i[\rho(t), H_S] - \frac{1}{2}\sum_m \left(\{\rho(t), D_m^\dagger D_m\} - 2D_m \rho(t) D_m^\dagger \right) \\ =& \mathcal{L}\rho, \end{aligned} \tag{3.12}$$

where the operators D_m are different from the original operators C_m. Different schemes appear when we have

$$U\mathcal{L}\rho U^\dagger = \mathcal{L}U\rho U^\dagger,$$

for some unitary operator U. This means that we must have

$$D_m = U^\dagger C_m U. \tag{3.13}$$

Operators D_m give a totally different picture from the system than the operators C_m because the jump channels and probabilities are different. Non-Hermitian Hamiltonian is unaffected by the transformation. This helps to understand what it means physically that every density matrix can be expressed in infinite number of different ways as a convex combination: the MCWF and QT methods relate different U:s to a different type of measurement scheme which may look very different but the information content is the same in the expectation value sense. This also implies that we are not only simulating the state vector but the state vector conditioned on a specific detection record [6].

Diffusion type process Although we have spoken about measurements we have not defined any specific measurement schemes in the previous paragraph. The fact that the unraveling of the Markovian master equation is not unique gives us a possibility to introduce new Lindblad operators $D_{m,\epsilon}$ and the process given by these operators can be formulated as a QSD-process with physical interpretation as homodyne photo detection [19]. Choosing yet a different set of operators and after a limiting process we can obtain Eq. (3.11), which can be interpreted as heterodyne

photo detection. In the Ref. [32] a laser excited two-level atom is studied with different homodyne and heterodyne detection schemes, and very different distributions of state vectors appear. Since we know that the expectation value for operator $\hat{A}$ is independent of the detection scheme, this means that the second moments of different distributions must be the same [21].

The heterodyne detection scheme is more appealing because it connects with the QSD-process presented in this thesis and it was originally derived by Gisin and Percival from more general considerations. Their idea was to introduce dynamical localization into an eigenstate whereas in the jump methods the localization is discontinuous. Usually one thinks that the destruction of superposition in open quantum system is due to the environment induced decoherence, which results from tracing over the environment that has become entangled with the system. In QSD superposition is destroyed by the random nature of the evolution. It is therefore very interesting that there exists a connection between these two rather different viewpoints. It is worth to mention that the diffusion type processes in quantum mechanics are not originally introduced in the context of measurement but as an alternative version of quantum mechanics which would explain why macroscopic systems are not usually found in the superposition states [4],[25].

4 Non-Markovian Monte Carlo methods

4.1 NMQJ

We begin by presenting the local in time non-Markovian master equation in the following form [23],[24]:

$$\dot{\rho}(t) = -\imath[H_S, \rho(t)] + \sum_{j_+} \Delta_{j_+}(t)\left[C_{j_+}\rho(t)C_{j_+}^\dagger - \frac{1}{2}\{\rho(t), C_{j_+}^\dagger C_{j_+}\}\right] - \sum_{j_-} |\Delta_{j_-}(t)|\left[C_{j_-}\rho(t)C_{j_-}^\dagger - \frac{1}{2}\{\rho(t), C_{j_-}^\dagger C_{j_-}\}\right]. \tag{4.1}$$

We present the method in a form where the operators $C_{j\pm}$ are independent of time. We have defined the positive and negative decay channels separately with the indices j_+ and j_- respectively. For all $t \in \mathbb{R}$ and j_+, j_- we have assumed that $\Delta_{j_+}(t) \geq 0$ and $\Delta_{j_-}(t) \leq 0$. Also notice that the decay rates are pulled out from the operators $C_{j\pm}$ in contrast to MCWF. First idea of this method can be obtained from the fact that, if $\forall\, t, j_- : \Delta_{j_-}(t) = 0$ the NMQJ method reduces to the MCWF method because positive part of the Eq. (4.1) is operationally in the Lindblad form for each fixed $t \in \mathbb{R}$. In this method the density operator $\rho(t)$ is expressed in the following form [23]:

$$\rho(t) = \sum_{\beta=0}^{M_{\text{eff}}} \frac{M_\beta(t)}{M} |\psi_\beta(t)\rangle\langle\psi_\beta(t)|, \tag{4.2}$$

where β indexes all different contributions to the density operator. Number M_{eff} depends on the type of the system where NMQJ method is applied to. $\frac{M_\beta(t)}{M}$ is a weight factor in front of the contribution $|\psi_\beta(t)\rangle\langle\psi_\beta(t)|$. M is the size of the statistical ensemble we use and $M_\beta(t)$ is the number of state vectors in the state $|\psi_\beta\rangle$ at time t. In general there are many possible jump paths that contribute to the specific $M_\beta(t)$ and the behavior of these integers is system dependent. From now on in this thesis we use $M_0(t)$ for the number of the ensemble members at time t that are in the deterministically evolving initial state.

NMQJ is a non-Markovian piecewise deterministic process. Deterministic parts are solutions to the equation

$$\frac{\partial}{\partial t}|\psi_0(t)\rangle = -\imath\hat{H}(t)|\psi_0(t)\rangle, \tag{4.3}$$

where $\hat{H}(t)$ is the non-Hermitian Hamiltonian

$$\hat{H}(t) = H_s - \frac{\imath}{2}\sum_{j_+}\Delta_{j+}(t)C_{j_+}^\dagger C_{j_+} - \frac{\imath}{2}\sum_{j_-}\Delta_{j-}(t)C_{j_-}^\dagger C_{j_-}. \tag{4.4}$$

For solving the deterministic evolution we have to discretize the Eq. (4.3). Because $\hat{H}(t)$ is non-Hermitian it does not preserve the norm of the state vector. After each time step δt we normalize our state vector. Solution to the discretized version of the Eq. (4.3) over one time step is

$$|\psi_0(t+\delta t)\rangle = e^{-i\hat{H}(t)\delta t}|\psi_0(t)\rangle,$$

where $\hat{H}(t)$ means that we evaluate the non-Hermitian Hamiltonian at time t. For a small enough δt we can use series expansion and truncate it to the first order in δt: $|\psi_0(t+\delta t)\rangle \approx (1 - i\delta t\hat{H}(t))|\psi_0(t)\rangle$.

In the non-deterministic parts we can have jumps to positive and negative channels. Jump probability to an arbitrary positive channel j_+ from an arbitrary state $|\psi_\beta(t)\rangle$ at time $t \in \mathbb{R}$ is

$$P^{j_+}_{\beta\to\beta'}(t) = \Delta_{j_+}(t)\delta t\langle\psi_\beta(t)|C_{j_+}^\dagger C_{j_+}|\psi_\beta(t)\rangle \tag{4.5}$$

and this induces transitions of the form

$$|\psi_{\beta'}(t+\delta t)\rangle \to \frac{C_{j_+}|\psi_\beta(t)\rangle}{||C_{j_+}|\psi_\beta(t)\rangle||} \tag{4.6}$$

and

$$\{M_\beta(t+\delta t), M_{\beta'}(t+\delta t)\} = \{M_\beta(t) - 1, M_{\beta'}(t) + 1\} \tag{4.7}$$

We see here that one must choose δt so that $P^{j_+}_{\beta\to\beta'}(t) \ll 1$.

For a jump via negative channel j_- from the state $|\psi_{\beta'}(t)\rangle$ to the state $|\psi_\beta(t)\rangle$ and its associated probability to be well defined, we have the following conditions:

i) Condition on state: $|\psi_{\beta'}(t)\rangle \equiv \frac{C_{j_-}|\psi_\beta(t)\rangle}{||C_{j_-}|\psi_\beta(t)\rangle||}$.

ii) Condition on probability: $M_{\beta'}(t) \neq 0$.

Reasons for the conditions (i,ii) is that the non-Markovian jump probability via channel j_- from the state $|\psi_{\beta'}(t)\rangle$ to the state $|\psi_\beta(t)\rangle$ is

$$P^{j_-}_{\beta'\to\beta}(t) = \frac{M_\beta(t)}{M_{\beta'}(t)}|\Delta_{j_-}(t)|\delta t\langle\psi_\beta(t)|C^\dagger_{j_-}C_{j_-}|\psi_\beta(t)\rangle, \tag{4.8}$$

and the corresponding state transition is

$$|\psi_{\beta'}(t+\delta t)\rangle \leftarrow \frac{C_{j_-}|\psi_\beta(t)\rangle}{||C_{j_-}|\psi_\beta(t)\rangle||} \tag{4.9}$$

and

$$\{M_\beta(t+\delta t), M_{\beta'}(t+\delta t)\} = \{M_\beta(t)-1, M_{\beta'}(t)+1\}. \tag{4.10}$$

With these definitions we get a correct process that unravels the Eq. (4.1). The proof is in the Ref. [23]. We note that when $\Delta_{j_-}(t) = 0 \;\forall\; j_-$, we have $1 - |||\psi_\beta(t+\delta t)\rangle|| = \sum_{j_+} P^{j_+}_\beta(t)$ [20]. This means that in the situation when all the decay channels are positive we can get the total jump probability from the decrease of the norm of the deterministic state. This is computationally very efficient because jumps are rare events compared to deterministic evolution and we will have to calculate jump probabilities explicitly only when jump happens.

Algorithm We are now in a position to introduce algorithm to simulate local-in-time non-Markovian master equation (4.1). We want to monitor our system in the time interval $[t_0, T]$. First we discretize the interval $[t_0, T]$ into N sub-intervals of δt in length. We a have statistical ensemble of M state vectors. Initially we have $M_0(t_0) = M, M_{\beta\neq 0}(t_0) = 0$. We present our algorithm for evolution over one time step $[t_0 + n\delta t, t_0 + (n+1)\delta t] = [t_n, t_{n+1}]$. We have the system in some state $|\Psi_0(t_n)\rangle$, which has evolved deterministically from the initial state of the system at time t_0.

We have reserved index $\beta = 0$ for the deterministic state. It might be in one of the eigenstates or in superposition state and $|\langle\Psi_0(t_n)|\Psi_0(t_n)\rangle|^2 = 1$. Let us assume that the effective ensemble size is M_{eff}. For example in the two level system $M_{\text{eff}} = 2$ and it includes the deterministically evolving initial state and the ground state.

1. Copy numbers $M_\beta(t_n)$ to $M_\beta(t_{n+1})$ $\forall$ β.

2. Evolve the state vector $|\Psi_0(t_n)\rangle \rightarrow |\Theta(t_{n+1})\rangle$ and all the vectors in the effective ensemble. Normalize the evolved vectors.

3. Calculate the total jump probability using Eqs. (4.8) and (4.5). Then we have $P_{\text{tot}}(t_n) = \sum_{P^+_{\beta'\rightarrow\beta}(t_n)\neq 0} P^+_{\beta'\rightarrow\beta}(t_n) + \sum_{P^-_{\beta'''\rightarrow\beta''}(t_n)\neq 0} P^-_{\beta'''\rightarrow\beta''}(t_n)$.

4. For those jump channels (positive or negative) that have a non-zero jump probability number $M_\beta(t_n)$ tells how many states have possibility to jump and thus how many uniformly distributed random numbers $\epsilon \sim \mathcal{U}_{[0,1]}$ we need (per channel). Then decide how many jumps take place and update the numbers $M_\beta(t_{n+1})$ correspondingly.

5. Calculate the estimate for $\hat{\rho}(t_{n+1})$. Calculate the estimate for standard deviation $\hat{\sigma}(t_{n+1})$.

In the step 2 in all the cases studied in this thesis we have only one state that evolves in time, the deterministic initial state, and all the other states stay constant. Notice that in the step 4 we go through only the part of the statistical ensemble at time t_n which has a non-zero jump probability and decide which members in that part jump at the time t_n. All the information we need for estimating the density matrix and the standard deviation is in the numbers M_β and in the states that belong to M_{eff}.

4.2 DHS

This section is based on the Ref. [3]. DHS method uses auxiliary states to describe the non-Markovian dynamics. The method uses Hilbert space $\tilde{\mathcal{H}} = \mathcal{H}_S \oplus \mathcal{H}_S$. We present this method in a form which is applicable to a local in time non-Markovian master equation in the form

$$\dot{\rho}(t) = -\imath[H_S, \rho(t)] + \sum_j \Delta_j(t)\left[C_j\rho(t)C_j^\dagger - \frac{1}{2}\{\rho(t), C_j^\dagger C_j\}\right]. \tag{4.11}$$

One can see that this is the same equation as Eq. (4.1) when we allow the decay rates to take positive and negative values. Let us introduce a stochastic state vector in $\tilde{\mathcal{H}}$:

$$\theta(t) = \begin{pmatrix} \phi(t) \\ \psi(t) \end{pmatrix}, \tag{4.12}$$

with the following condition $||\theta(t_0)|| \equiv 1$, where $t_0 \in \mathbb{R}$ is the initial time. We can also express the stochastic state vector in the following form $\theta(t) = \phi(t) \oplus \psi(t)$. Time evolution of $\theta(t)$ is determined by the following stochastic differential equation

$$\begin{aligned} d\theta(t) = &- iG(\theta, t)\mathrm{d}t \\ &+ \sum_i \left(\frac{||\theta(t)||}{||J_i(t)\theta(t)||}J_i(t)\theta(t) - \theta(t)\right)dN_i(t), \end{aligned} \tag{4.13}$$

where $\mathrm{d}N_i(t)$ is a differential of a Poisson process with a mean

$$\langle dN_i(t)\rangle = \frac{||J_i(t)\theta(t)||^2}{||\theta(t)||^2}dt. \tag{4.14}$$

The differentials of Poisson process satisfy also the following relation

$$dN_i(t)dN_j(t) = \delta_{ij}dN_i(t), \tag{4.15}$$

which means intuitively that the state vector can jump only once at time t. The functional $G(\theta, t)$ is the generator of the deterministic evolution of the state vectors. Therefore the deterministic pieces of the evolution are solutions to

$$i\frac{\partial}{\partial t}\theta(t) = G(\theta, t). \tag{4.16}$$

One can see that $G(\theta,t)$ has the same type of role as $\hat{H}(t)$ in the NMQJ method. The explicit form of $G(\theta,t)$ is

$$G(\theta,t) = i\left(F(t) + \frac{1}{2}\sum_i \frac{||J_i(t)\theta(t)||^2}{||\theta(t)||^2}\right)\theta(t), \tag{4.17}$$

where the operators $F(t)$ and $J_i(t)$ are:

$$F(t) = \begin{pmatrix} -iH_S - \frac{1}{2}\sum_j \Delta_j(t)C_j^\dagger C_j & 0 \\ 0 & -iH_S - \frac{1}{2}\sum_j \Delta_j(t)C_j^\dagger C_j \end{pmatrix},$$
$$J_i(t) = \sqrt{|\Delta_i(t)|}\begin{pmatrix} \mathrm{sgn}(\Delta_i(t))C_i & 0 \\ 0 & C_i \end{pmatrix}. \tag{4.18}$$

Jumps are of the form

$$\theta(t) \to \frac{||\theta(t)||}{||J_i(t)\theta(t)||}J_i(t)\theta(t) = \frac{||\theta(t)||}{||J_i(t)\theta(t)||}\sqrt{|\Delta_i(t)|}\begin{pmatrix} \mathrm{sgn}(\Delta_i(t)C_i\phi(t) \\ C_i\psi(t) \end{pmatrix}. \tag{4.19}$$

From the previous equation we can see that the state vector that jumps takes the norm of the source state to the destination state. That is different than in the NMQJ method, where the state vector is normalized to unity after a jump. The reduced density matrix of the system is defined as

$$\rho(t) = \int D\theta D\theta^\star |\phi\rangle\langle\psi|\tilde{P}[\theta,t], \tag{4.20}$$

where $\tilde{P}[\theta,t]$ is a probability density functional in the Hilbert space $\tilde{\mathcal{H}}$.

We can examine the square of the norm of the deterministically evolving state vector. We have

$$\begin{aligned}\frac{\partial}{\partial t}||\theta(t)||^2 =& \langle\frac{\partial\theta(t)}{\partial t}|\theta(t)\rangle + \langle\theta(t)|\frac{\partial\theta(t)}{\partial t}\rangle \\ =& \overbrace{\langle\theta(t)|(F(t)^\dagger + F(t))\theta(t)\rangle + \sum_j ||J_i(t)\theta(t)||^2}^{(4.16),(4.17)} \\ =& \underbrace{2\sum_j |\Delta_j(t)|(||C_j\phi(t)||^2 + ||C_j\psi(t)||^2)}_{(4.18)}\end{aligned} \tag{4.21}$$

We can put this into a more suggestive form

$$\frac{\partial}{\partial t}||\theta(t)||^2 = 2P_J^-(t), \tag{4.22}$$

where $P_J^-(t)$ is the cumulative jump probability to the negative channels. This is obviously zero if all the channels are positive. This result applies also in the cases where we have positive and negative decay channels at the same time. We can calculate that by splitting the operators $J_i(t)$ into positive and negative parts $J_{i+}(t)$ and $J_{i-}(t)$. We get then a result that the positive contribution cancels out and the negative contribution remains.

From this simple consideration we conclude that as in the NMQJ method we can solve the deterministic evolution of the state vector with the same type of non-Hermitian Hamiltonian as in NMQJ only for those times when all the decay channels are positive. We have chosen not to do so in our simulations. We discretize the Eq. (4.17) in time intervals δt and calculate the deterministic evolution as in the NMQJ method (first order in δt). This is not the most efficient way because we have to calculate the jump probabilities for every time step to all the channels and this comes ineffective when the summation in the Eq. (4.17) is long. On the other hand this method is simpler to use in practice because one can apply it in every time step regardless of the signs of the decay channels.

Idea of the simulations is to create independent realizations of the time evolution of the stochastic state vector in $\tilde{\mathcal{H}}$ and with the statistical ensemble created to estimate the r.h.s. of the Eq. (4.20). The correct estimator is

$$\hat{\rho}(t) = \frac{1}{M}\sum_k |\phi_k(t)\rangle\langle\psi_k(t)|. \tag{4.23}$$

We can see from the Eq. (4.19) that if at time t', $\Delta_\beta(t') < 0$ a stochastic vector $\theta_i(t')$ jumps to the state $|\chi_\beta\rangle$, its contribution to the ensemble average of the population of the state $|\chi_\beta\rangle$ is $-||\theta_i(t')||$. Thus when the negative decay channels are open we have two "opposite" processes going on. We have the increase of the norm of the

deterministically evolving stochastic vector and on the other hand we have negative contribution to the ensemble average. These two processes are unphysical, but on average they compensate each other and we can get physical results out from the Eq. (4.23).

Algorithm We define the parameters M and N the same way as in the Sec. 4.1. Let us index the ensemble members with $j \in \{1, 2, ..., M\}$. We have the system in some state $\theta_j(t_0)$ in $\mathcal{H} \oplus \mathcal{H}$ and $||\theta_j(t_0)|| = 1$. We implement this method so that at every time step $t_n = t_0 + n\delta t$ we use the following algorithm to all M ensemble members $\theta_j(t_n)$ and evolve them to the next time step t_{n+1}. This way we must calculate all the necessary operators only once at every time step.

1. Calculate $P_k(t_n)\ \forall\ k$ using the Eq. (4.14). This is the probability to jump to the channel k at time t_n.

2. Calculate $P_{\text{tot}}(t_n) = \sum_k P_k(t_n)$.

3. Draw a random number $\epsilon_j \sim \mathcal{U}_{[0,1]}$.

   - If $\epsilon_j < P_{\text{tot}}(t_n)$, a jump takes place. Use the linear search algorithm to decide the jump channel. Update $\theta_j(t_n) \rightarrow \theta_j(t_{n+1})$ by using the Eq. (4.19).
   - If $\epsilon_j > P_{\text{tot}}(t_n)$, the deterministic evolution takes place. Update $\theta_j(t_n) \rightarrow \theta_j(t_{n+1})$ by using the Eq. (4.16).

4. Calculate the ensemble member $\rho_j(t) = |\phi_j(t)\rangle\langle\psi_j(t)|$.

After going through all the states in the ensemble at time t_n, calculate the estimates for $\hat{\rho}(t_{n+1})$ and $\hat{\sigma}(t_{n+1})$. Applying this to the N different δt-intervals we have the estimates for the whole interval $[t_0, T]$. An important difference in respect to the NMQJ is that we must evolve all the M state vectors in DHS and, at the most, M_{eff} state vectors in NMQJ in one δt-interval.

4.3 THS

This section is based on the Ref. [2]. THS method is based on enlarging the state space of the physical system appropriately. In particular, if the Hilbert space of the system is $\mathcal{H}$, then the new Hilbert space required by THS is $\tilde{\mathcal{H}} = \mathcal{H} \otimes \mathbb{C}_3 \simeq \mathcal{H} \oplus \mathcal{H} \oplus \mathcal{H}$. We begin from the Eq. (4.11) which is a local in time non-Markovian master equation. The basic idea behind this method is to construct a Markovian master equation with a time dependent Lindblad generator in $S(\tilde{\mathcal{H}})$ from which we can extract the non-Markovian dynamics.

Let us define the density matrix in $S(\tilde{\mathcal{H}})$ to be $W(t)$. The Markovian master equation with the time dependent Lindblad generator is then

$$\begin{aligned}\frac{d}{dt}W(t) =& -i[\tilde{H}_S(t), W(t)] \\ &+ \sum_{k,\alpha}\left(J_{k,\alpha}(t)W(t)J_{k,\alpha}(t)^\dagger - \frac{1}{2}\{J_{k,\alpha}(t)^\dagger W(t) J_{k,\alpha}(t)\}\right).\end{aligned} \tag{4.24}$$

As it is shown in the Ref. [2], with the correct operators $J_{k,\alpha}(t)$, the following Stochastic Schrödinger Equation (SSE) for a stochastic vector $\Phi \in \tilde{\mathcal{H}}$

$$d\Phi(t) = -iG(\Phi, t)dt + \sum_{k,\alpha}\left(\frac{J_{k,\alpha}(t)\Phi(t)}{||J_{k,\alpha}(t)\Phi(t)||} - \Phi(t)\right)dN_{k,\alpha}(t) \tag{4.25}$$

gives $W(t)$ as an expectation value

$$W(t) = E[\Phi(t)\Phi^\dagger(t)], \tag{4.26}$$

in respect to the ensemble. In general the previous SSE unravels the Markovian master equation with time dependent Lindblad generator [4],[25]. $G(\Phi, t)$ is the generator of the deterministic part of evolution which is governed by the following equation

$$\frac{\partial}{\partial t}\Phi(t) = -iG(\Phi, t). \tag{4.27}$$

The explicit form of the generator $G(\Phi, t)$ is

$$G(\Phi, t) = \left(\hat{H}(t) + \frac{i}{2}\sum_{k,\alpha}||J_{k,\alpha}(t)\Phi(t)||^2\right)\Phi(t), \tag{4.28}$$

where $\hat{H}(t)$ is the standard non-Hermitian Hamiltonian

$$\hat{H}(t) = \tilde{H}_S - \frac{i}{2}\sum_{k,\alpha} J^\dagger_{k,\alpha}(t)J_{k,\alpha}(t). \tag{4.29}$$

$dN_{k,\alpha}(t)$:s are the differentials of the Poisson process. The Eq. (4.15) holds for them (with obvious addition) but the expectation value is different because the stochastic differential equation is not the same. We have now

$$\langle dN_{k,\alpha}(t)\rangle = ||J_{k,\alpha}(t)\Phi(t)||^2 dt. \tag{4.30}$$

One advantage of this method is that the Eq. (4.28) can be solved with the MCWF approach. This gives us the deterministic evolution over single time step and the total jump probability simultaneously. Because the non-Markovian dynamics are embedded in the Markovian dynamics in THS, this is valid even when decay rates are negative. The operators $J_{k,\alpha}(t)$ for a fixed k are defined as

$$J_{k,0}(t) = \sqrt{\frac{|\Delta_k(t)|}{2}}C_k \otimes |1\rangle\langle 1| + \sqrt{\frac{|\Delta_k(t)|}{2}}\mathrm{sgn}(\Delta_k(t))C_k \otimes |2\rangle\langle 2|, \tag{4.31}$$

$$J_{k,1}(t) = \sqrt{\frac{|\Delta_k(t)|}{2}}\mathrm{sgn}(\Delta_k(t))C_k \otimes |1\rangle\langle 1| + \sqrt{\frac{|\Delta_k(t)|}{2}}C_k \otimes |1\rangle\langle 1|, \tag{4.32}$$

$$J_{k,2}(t) = \Omega_k(t) \otimes |3\rangle\langle 1|, \tag{4.33}$$

$$J_{k,3}(t) = \Omega_k(t) \otimes |3\rangle\langle 2|. \tag{4.34}$$

The vectors $|1\rangle$, $|2\rangle$ and $|3\rangle$ form an orthonormal basis in $\mathbb{C}_3$. The jumps follow the MCWF prescription

$$\Phi(t) \to \frac{J_i(t)\Phi(t)}{||J_i(t)\Phi(t)||}. \tag{4.35}$$

The system Hamiltonian in $\tilde{\mathcal{H}}$ is

$$\tilde{H}_S = H_S \otimes I. \tag{4.36}$$

The non-Hermitian Hamiltonian is defined in the standard way

$$\hat{H}(t) = \tilde{H}_{\mathcal{S}} \otimes I - \frac{i}{2}\sum_k \sum_{j=0}^{3} J_{k,j}(t)^\dagger J_{k,j}(t). \tag{4.37}$$

We see now that for one physical decay channel k, the THS method needs four additional jump channels. With the previous definitions we get the original density matrix $\rho(t)$ out from $W(t)$ with the following operation

$$\rho(t) = \frac{\langle 1|W(t)|2\rangle}{\mathrm{tr}\langle 1|W(t)|2\rangle}, \tag{4.38}$$

with an initial condition that

$$W(t_0) \equiv \rho(t_0) \otimes |\chi\rangle\langle\chi|,$$

where $|\chi\rangle = \frac{1}{\sqrt{2}}(|1\rangle + |2\rangle)$. In the simulations the deterministic initial state is thus

$$\Phi = |\psi_0\rangle \otimes |\chi\rangle.$$

From the Eq. (4.38) we see that the non-Markovian dynamics are embedded in the certain coherences of the density matrix $W(t)$. We can therefore implement the system Hamiltonian as $\tilde{H}_{\mathcal{S}} = H_{\mathcal{S}} \otimes (|1\rangle\langle 1| + |2\rangle\langle 2|)$ in the simulations.

There is one restriction for this method to be valid. We need that the operators $\sqrt{\frac{|\Delta_k(t)|}{2}}\mathrm{sgn}(\Delta_k(t))C_k$ and $\sqrt{\frac{|\Delta_k(t)|}{2}}C_k$ are bounded because we have to solve $\Omega_k(t)$ from the equation

$$\Omega_k^\dagger\Omega_k(t) = a_k(t)I - |\Delta_k(t)|[1 - \mathrm{sgn}(\Delta_k(t))]C^\dagger C. \tag{4.39}$$

$\Omega_k^\dagger\Omega_k(t)$ is a positive operator and for the r.h.s of the Eq. (4.39) to be positive, we choose $a_k(t)$ to be the largest eigenvalue of the operator $|\Delta_k(t)|[1-\mathrm{sgn}(\Delta_k(t))]C_k^\dagger C_k$. The form of the operator $\Omega_k(t)$ is not unique, because there are multiple solutions to the Eq. (4.39). Proof of this method is in the Ref. [2].

Algorithm We use the same definitions for N and M as in the Sec. 4.1. We have some initial state $\Phi(t_0) = |\Psi(t_0)\rangle \otimes \frac{1}{\sqrt{2}}(|1\rangle + |2\rangle)$, where $|\Psi(t_0)\rangle \in \mathcal{H}$. We will use the following algorithm at every time step $t_n = t_0 + n\delta t$ to a member $\Phi_j(t_n),\ j \in \{1, 2, ..., M\}$ of the ensemble. This way we need to calculate the necessary operators only once at every time step.

1. Evolve $\Phi_j(t_n) \rightarrow \Phi_j(t_{n+1})$ using the Eq. (4.27). Calculate $P_{\text{tot}}(t_n) = 1 - ||\Phi_j(t_{n+1})||$.

2. Draw a random number $\epsilon_j \sim \mathcal{U}_{[0,1]}$.

3. - If $\epsilon_j > P_{\text{tot}}(t)$, the deterministic evolution will follow. Normalize $\Phi_j(t_{n+1})$.
   - If $\epsilon_j \leq P_{\text{tot}}(t)$, an instantaneous jump happens. Calculate the jump operators $J_{\alpha,k}(t)\ \forall\, \alpha, k$ using the Eq. (4.31). Apply the linear search to decide which channel the system jumps. Use the Eq. (4.35) to make the instantaneous jump.

4. Calculate the ensemble member $\rho_j(t_{n+1})$ by using the Eq. (4.38).

After we have calculated the evolution for all j at time t_{n+1} we calculate the estimates for $\hat{\rho}(t_{n+1})$ and $\hat{\sigma}(t_{n+1})$. When we repeat this for the N different δt-intervals we have estimates for the whole interval $[t_0, T]$.

4.4 Physical interpretation and insights for non-Markovian systems

In the previous chapter we have introduced the three different Monte Carlo methods for solving the non-Markovian local in time master equation. In NMQJ the realizations generated depend on each other and one can see how the memory of the system affects the dynamics. THS on the other hand is a method where the non-Markovian dynamics are embedded in the Markovian dynamics of a larger system and thus we can simulate the time dependent Lindblad type Markovian master equation. This makes it much harder to gain physical understanding from the non-Markovian system because the system that we simulate has no memory. DHS method is in between these two methods in a sense that the master equation that we simulate is local in time non-Markovian (it does not even have to be operatorially in Lindblad form) but

the realizations are independent of each other. The way that the non-Markovianity is introduced in DHS is more similar to THS than NMQJ because the jumps during the negative decay rate give negative contribution to the ensemble average.

Let us consider a two state atom as an example. In NMQJ description the memory of one ensemble member is carried by the other ensemble members. When a non-Markovian jump for a given member occurs, this ensemble member returns back to the deterministic initial state. This is the state that the given member would have if a prior positive decay rate jump had not taken place. The non-Markovian jump thus restores the earlier superposition and this means that the information lost earlier must be present in the environment when the decay rate turns negative. If we think of the measurement scheme involved in the MCWF method, we monitor the environment continuously and if we observe a photon in the environment, a measurement destroys the photon. This means that the information is not present in the environment anymore and thus the non-Markovian dynamics gets distorted [23].

In the two level example oscillations in the excited state probability are due virtual processes [4], [2], [3]. The virtual processes can not be measured directly but they affect the dynamics. In NMQJ the physical insight is that it describes the oscillations in excited state probability as destruction and restoration of quantum superposition instead of a virtual exchange of photons between the system and the environment. Photon exchange cannot increase coherence and thus the difference between physical pictures given by MCWF and NMQJ arises. All the possible paths contribute to the dynamics of the system, but if we measure one of these paths the non-Markovian memory gets distorted.

In the DHS method we simulate master equations that are not in Lindblad form and therefore we do not have a measurement scheme. From this method it is hard to gain physical understanding because the ensemble members can have norm larger

than unity and some ensemble members give negative population contributions in the ensemble average. On average these two unphysical realizations cancel each other and the end result is physical.

The THS method has a measurement scheme interpretation because we simulate a Markovian master equation. The enlarged system in $\mathcal{H}_1 \oplus \mathcal{H}_2 \oplus \mathcal{H}_3$ is monitored continuously and evolution of a state vector is conditioned on detection or no-detection of photon in the environment. We stress that the measurement scheme exists for the enlarged system. Therefore in order to actually do experiments we would need a very complex system where we would have the non-Markovian part ($\mathcal{H}_1 \oplus \mathcal{H}_2$) and the sink ($\mathcal{H}_3$). Therefore this method does not give as much physical insight to non-Markovian system as NMQJ, because we do not simulate a non-Markovian system.

NMQJ suggests that we can not measure the environment of the system and THS tells that there is a measurement scheme for a non-Markovian system that is a sub-system of a larger Markovian system. Gambetta and Wiseman have concluded that solutions to the non-Markovian SSE at different times can not be linked to form a trajectory [11] and they have proposed that the non-Markovian stochastic Schrödinger equation could be interpreted as a hidden variable theory [12], which is one interpretation for the lack of measurement scheme.

5 Methods and systems

In this section we derive the general form for the local in time non-Markovian master equation in TCL2 approximation for a multi level atom in quantized electromagnetic field. We also construct the NMQJ, DHS and THS processes in detail for the two state, Λ, V and three level ladder systems, see Fig. 5.1. As we construct the process for the two-state system we discuss the differences of the physical pictures given by these three methods in detail.

Local in time non-Markovian master equation Perturbative approximation to second order in the TCL method in the interaction picture yielded the Redfield equation

$$\frac{\mathrm{d}}{\mathrm{d}t}\rho_{\mathcal{S}}(t) = -\,\alpha^2 \int_0^t \mathrm{d}s\, \mathrm{tr}_{\mathcal{E}}\{[H_I(t),[H_I(s),\rho_{\mathcal{S}}(t)\otimes\rho_{\mathcal{E}}]]\}. \tag{5.1}$$

We know from the Sec. 2.1 that we must have made the assumption that environment is in the initial state where the expectation value of the environment part of the interaction vanishes for all times. This suggests that the environmental correlation functions are homogeneous. The system Hamiltonian is $H_{\mathcal{S}} = \sum_k \hbar\omega_k|k\rangle\langle k| = \sum_k \epsilon_k|k\rangle\langle k|$, the environment Hamiltonian is $H_{\mathcal{E}} = \sum_{\mathbf{k}\lambda} \hbar\nu_{\mathbf{k}} a^\dagger_{\mathbf{k}\lambda} a_{\mathbf{k}\lambda}$ and the interaction Hamiltonian is $H_I = -\mathbf{D}\otimes\mathbf{E}$. $\mathbf{D}$ is the dipole operator and $\mathbf{E} = i\sum_{\mathbf{k}\lambda} \hat{\mathbf{e}}_{\mathbf{k}\lambda}\alpha_{\mathbf{k}}(a_{\mathbf{k}\lambda} - a^\dagger_{\mathbf{k}\lambda})$ is the quantized electromagnetic field [17]. Operators $a_{\mathbf{k}\lambda}$, $a^\dagger_{\mathbf{k}\lambda}$ are the annihilation and creation operators of the field mode, $\nu_{\mathbf{k}}$ is the frequency of the field mode, $\mathbf{k}$ is a wave vector, $\lambda = \{1,2\}$ gives the polarization, $\hat{\mathbf{e}}_{\mathbf{k}\lambda}$ is a unit vector and $\alpha_{\mathbf{k}}$ gives the strength of the field mode. Next step is to perform the secular approximation. Using the Eq. (2.13) and defining the Lindblad operators to be dimensionless we arrive to

$$S(\omega) = \sum_{\epsilon_i-\epsilon_j=\omega} d_{ji}|j\rangle\langle i|, \tag{5.2}$$

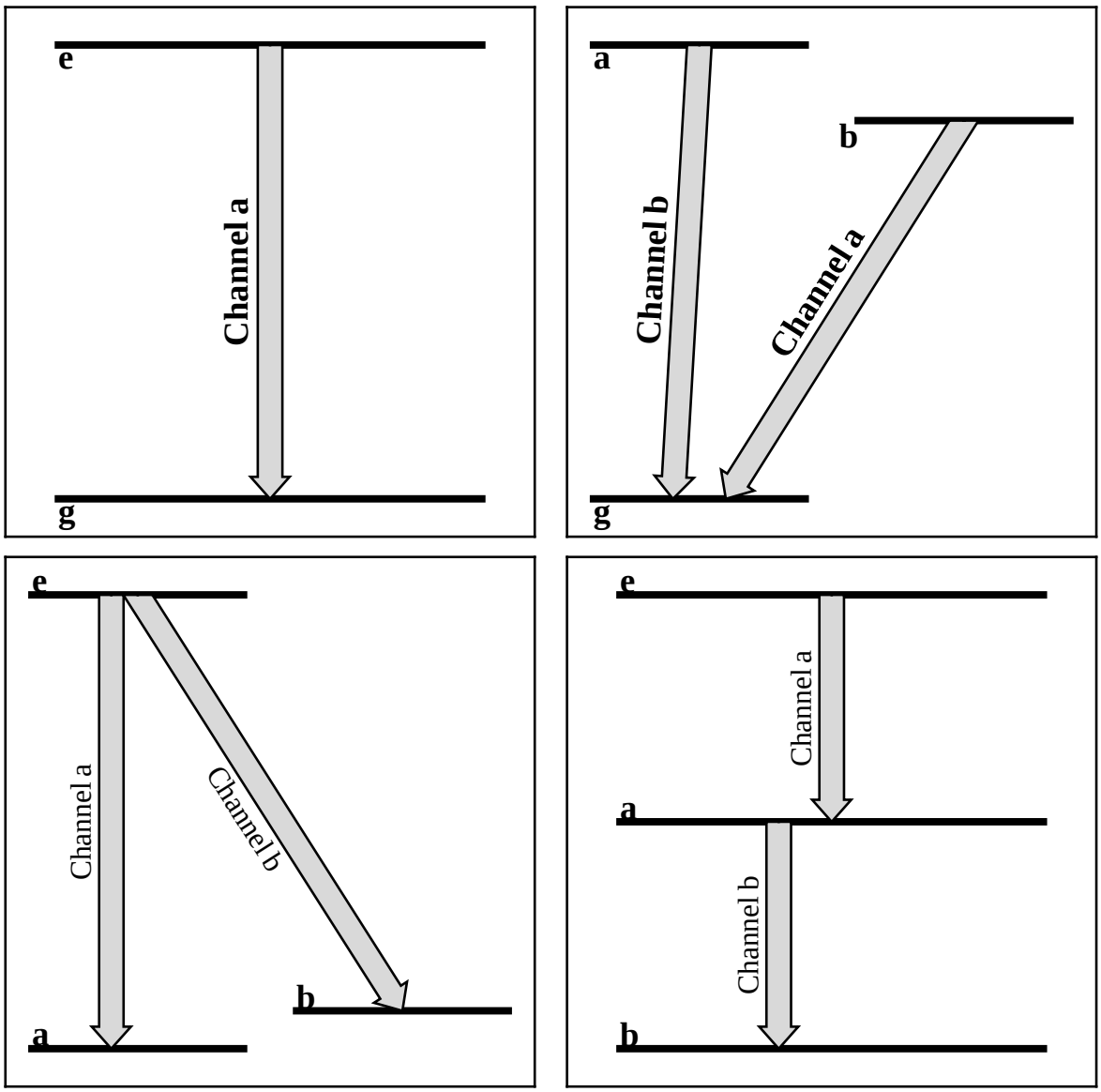

Figure 5.1: Level schemes for the two state, V, Λ and ladder systems. Arrows show the possible routes for system to decay.

where $d_{ji} = \frac{\langle j|(-\mathbf{D})|i\rangle}{D}$ and D scales d_{ji} to be dimensionless. Next we use the Eq. (2.15) and neglect terms that $\omega \neq \omega'$ and obtain

$$\frac{\mathrm{d}}{\mathrm{d}t}\rho_{\mathcal{S}}(t) = \sum_{\omega} \int_0^t \mathrm{d}s\, \mathrm{tr}_{\mathcal{E}}\{E^\dagger(t)E(s)\rho_{\mathcal{E}}\}e^{i\omega(t-s)} \times \Big(S(\omega)\rho_{\mathcal{S}}(t)S^\dagger(\omega) - S^\dagger(\omega)S(\omega)\rho_{\mathcal{S}}(t) \Big) + \mathrm{h.c.} \tag{5.3}$$

The quantized EM field at time t is expressed as

$$\mathbf{E}(t) = -\,i \sum_{\mathbf{k}\lambda} \hat{\mathbf{e}}_{\mathbf{k}\lambda}\alpha_{\mathbf{k}} \Big(a_{\mathbf{k}\lambda}e^{-i\nu_k t} - a^\dagger_{\mathbf{k}\lambda}e^{i\nu_k t} \Big). \tag{5.4}$$

After this point we must specify the initial state of the environment. We assume that the environment is in zero temperature and all the modes are empty. It is easy to calculate the integral of the field correlation functions

$$\Gamma(\omega) = \int_0^t \mathrm{d}s\, \mathrm{tr}_{\mathcal{E}}\{E^\dagger(t)E(s)\rho_{\mathcal{E}}\}e^{i\omega(t-s)} = \sum_{\mathbf{k}} \alpha^2_{\mathbf{k}} \int_0^t \mathrm{d}s\, e^{-i(\nu_k-\omega)s}$$

and passing to the continuum limit $\sum_{\mathbf{k}} \alpha^2_{\mathbf{k}} \to \int \mathrm{d}\nu\, J(\nu)$ we obtain the following expressions for the decay rate and the Lamb shift

$$\Delta_\omega(t) = 2 \int_0^t \mathrm{d}s \int_0^\infty \mathrm{d}\nu\, J(\nu) \cos\left((\nu-\omega)s\right), \tag{5.5}$$

$$\lambda_\omega(t) = \int_0^t \mathrm{d}s \int_0^\infty \mathrm{d}\nu\, J(\nu) \sin\left((\omega-\nu)s\right). \tag{5.6}$$

Spectral density of the EM field inside an imperfect cavity is well approximated by the Lorentzian distribution (see Fig. 5.2).

$$J(\nu) = \frac{\alpha^2}{2\pi} \frac{\gamma\Gamma^2}{(\nu-\omega_{\mathrm{cav}})^2 + (\Gamma/2)^2}. \tag{5.7}$$

Γ is the width of the distribution, α is coupling constant, ν is the frequency of the field, ω_{cav} is the resonance frequency of the cavity and $\gamma = 1[\nu]$ and it scales the dimension of $J(\nu)$ to the units of frequency. In the simulations we fix the time scale with the inverse of the spectral width; $[t] = 1/\Gamma$. Another important parameter in the simulations is the detuning $\delta_\omega = \omega_{\mathrm{cav}} - \omega$, where ω is the transition frequency

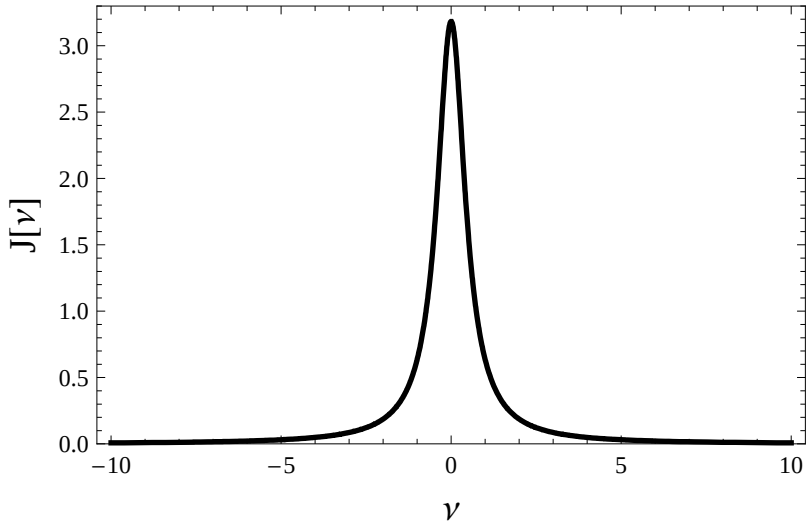

Figure 5.2: Lorentzian reservoir. Full width with the half height is Γ. x-axis gives the frequency of the field ν and y-axis gives the spectral density $J(\nu)$. Only the modes near the cavity resonance frequency are supported and thus only a few energy levels only contribute to the dynamics.

of the atom. We define for the dipole matrix elements $d_{ji} = 1,\ i \neq j$. If $\omega_{\text{cav}} \gg \Gamma$ decay rates converge to their stable Markovian values approximately at $\tau_{\text{M}} \approx 10\,\Gamma^{-1}$. The time scale of the reservoir correlation functions $\tau_{\mathcal{E}}$ is connected to width of the spectral density, $\tau_{\mathcal{E}} = \Gamma^{-1}$. The coupling constant is defined as $\alpha^2 = \tau_{\mathcal{E}}/\tau_{\mathcal{S}}$ [4]. In the simulations we use $\alpha^2 = 5$ for the two state system and $\alpha^2 = 2$ for all the other systems. Let us define the following shorthand notation

$$D_j(t) = \int_0^t \mathrm{d}s\ \Delta_j(s). \tag{5.8}$$

Formal solutions for the populations can be expressed using $D_j(t)$. In all the cases studied we have assumed that $\lambda_j(t) = 0\ \forall j$. $\lambda_j(t)$ term causes renormalization of the system Hamiltonian H_S, but with the parameter values used $\lambda(t)$ does not affect quantitatively to the dynamics. We use j to index the different physical decay channels. All master equations and formal solutions for different systems are from the Ref. [23].

5.1 Two state system

Hilbert space is $\mathcal{H} = \mathbb{C}_2$. Local in time non-Markovian master equation for the two state system, solutions for the populations and the Lindblad operators are

$$\dot{\rho} = \Delta(t)\sigma_-\rho(t)\sigma_+ - \frac{1}{2}\Delta(t)\{\rho(t), \sigma_+\sigma_-\}, \tag{5.9}$$

$$\rho_{ee} = e^{-D_1(t)}\rho_{ee}(0), \tag{5.10}$$

$$\rho_{gg} = (1 - e^{-D_1(t)})\rho_{ee}(0) + \rho_{gg}(0), \tag{5.11}$$

$$C_1 = \sigma_- = |g\rangle\langle e|. \tag{5.12}$$

As an example we present a solution for the two state system using direct numerical integration and the NMQJ, DHS and THS methods with the following parameters: $[t] = 1/\Gamma$, $\delta t = 0.01\Gamma^{-1}$, $M = 10^5$, $\alpha^2 = 5$, $\delta_1 = 5\Gamma$, $T = 10\Gamma$. The decay rate with these parameters is plotted in the Fig. 5.3. The initial state of the system is chosen to be $|\psi_0(0)\rangle = \frac{3|e\rangle+2|g\rangle}{\sqrt{13}}$. The populations are in the Fig. 5.4.

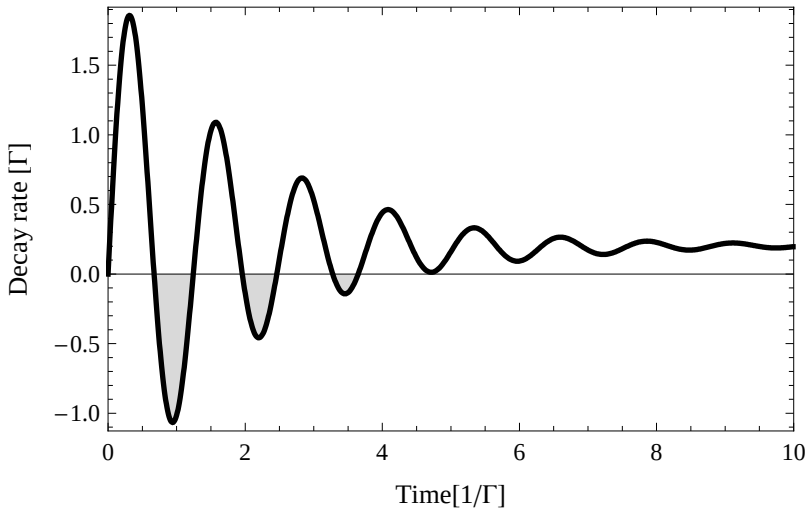

Figure 5.3: The decay rate for the two state system. Parameters defined as in the Sec. 5.1, $\alpha^2 = 5$ and $\delta_1 = 5\,\Gamma$. In the light gray regions the decay rate is negative. The Markovian time scale is $\tau_{\mathrm{M}} \approx 10\Gamma^{-1}$.

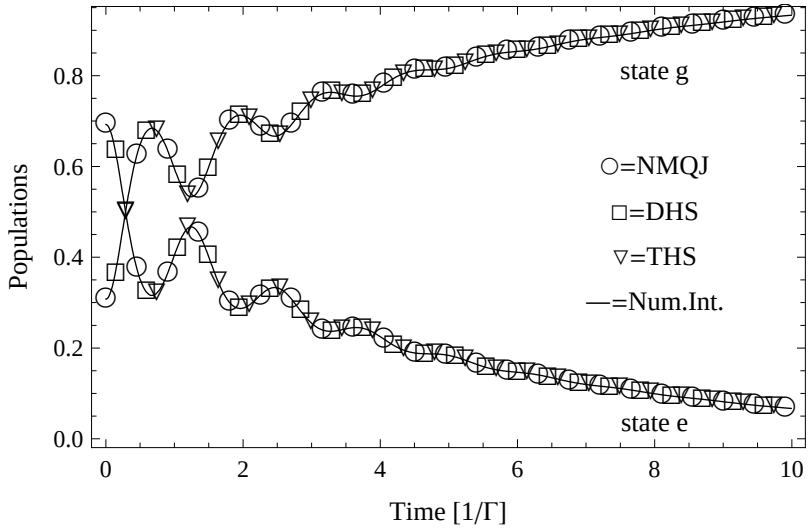

Figure 5.4: Numerically integrated solution and simulated solutions with the NMQJ, DHS and THS methods for the two state system. The parameters are defined in the Sec. 5.1. Agreement of the curves is very good. In further sections we make quantitative analysis of the accuracy of the different methods.

5.1.1 NMQJ

We do not need to expand the Hilbert space for the NMQJ method to work, so it is $\mathbb{C}_2$. We have $M_{\text{eff}} = 2$. Construction of the NMQJ process is simple. There is only one jump channel present and with these parameter values there are three regions where the decay rate is negative. Lindblad operator C_a, Eq. (5.9), acts like $|\phi\rangle \rightarrow C_a|\phi\rangle = \frac{c_e(t)}{|c_e(t)|}|g\rangle$, where $c_e(t) \in \mathbb{C}$ is the complex amplitude of the excited state. Because the effective ensemble size is 2 we have $M_0(t)$ and $M_1(t)$ which measure the number of the deterministically evolved state vectors and the number of the state vectors that have performed a jump, respectively. Eq. (4.4) gives us the non-Hermitian Hamiltonian, $\hat{H}(t) = -\frac{i}{2}\Delta_a(t)|e\rangle\langle e|$. We can see that for the case when $\Delta_a(t) > 0$ the non-Hermitian Hamiltonian decreases the excited state amplitude and when $\Delta_a(t) < 0$ it increases the excited state amplitude. For the jumps there are two cases (see Fig. 5.5):

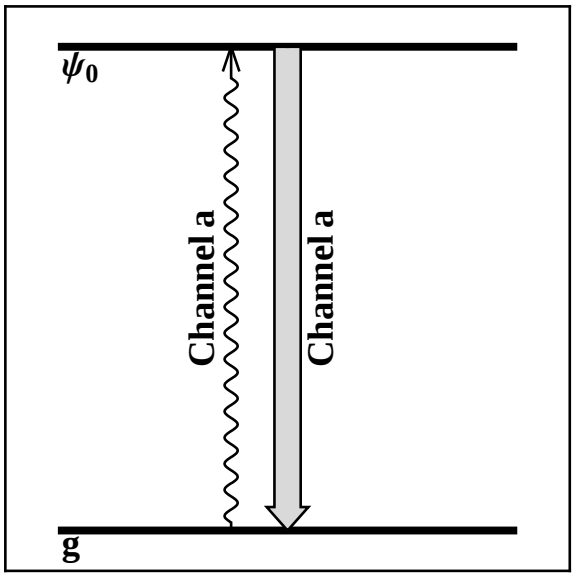

Figure 5.5: The effective ensemble for the two state system and the NMQJ method. $|\psi_0\rangle$ is the deterministic initial state and $|g\rangle$ is the ground state. The thick arrow shows jumps during the positive decay rate and the squiggly arrow shows the direction of non-Markovian jumps.

- When $\Delta_a(t) \geq 0$ and one ensemble member jumps, we update the numbers $\{M_0(t),\ M_1(t)\} \to \{M_0(t) - 1,\ M_1(t) + 1\}$.

- When $\Delta_a(t) < 0$ and one ensemble member performs a non-Markovian jump, we update the numbers $\{M_0(t),\ M_1(t)\} \to \{M_0(t) + 1,\ M_1(t) - 1\}$.

5.1.2 DHS

Hilbert space for the DHS method is $\mathcal{H}_1 \oplus \mathcal{H}_2$, where $\mathcal{H}_1 = \mathcal{H}_2 = \mathbb{C}_2$. We have one decay channel as in NMQJ. From the Eq. (5.9) and Ref. [3] we conclude that the operators $F(t)$ and $J_1(t)$ are:

$$\begin{aligned} F(t) =& -\frac{1}{2}\Delta_1(t)|e\rangle\langle e| \otimes (|1\rangle\langle 1| + |2\rangle\langle 2|), \\ J_1(t) =& C_1(t) \otimes |1\rangle\langle 1| + D_1(t) \otimes |2\rangle\langle 2|, \end{aligned} \tag{5.13}$$

where $C_1(t) = \sqrt{|\Delta_1(t)|}\mathrm{sgn}(\Delta_1(t))|g\rangle\langle e|$ and $D_1(t) = \sqrt{|\Delta_1(t)|}|g\rangle\langle e|$. One can see that the Hilbert spaces $\mathcal{H}_1$ and $\mathcal{H}_2$ are not coupled (Fig. 5.6). If we assume that the decay rate is positive for interval $t \in [0, \tau_0]$, then the DHS and NMQJ methods evolve state vectors similarly. When the decay rate after ($t > \tau_0$) turns negative, the state vector in $\mathcal{H}_1$ gets a minus sign in front if it jumps. In the NMQJ method the possibility for reverse jump emerges during the negative decay rates. In DHS memory effects emerge because of the minus sign during the negative decay rate periods. This gives negative contributions to the ensemble average. That then decreases the population of the ground state and thus effectively a larger part of the ensemble is in the deterministic state which contributes to the coherences. We can see from the Eqs. (4.17), (4.22) that the norm of the deterministically evolved states increases during the negative decay rate. This is necessary in order to preserve the normalization of the ensemble average in this method. In NMQJ we increase the coherence more directly by restoring the lost superposition state.

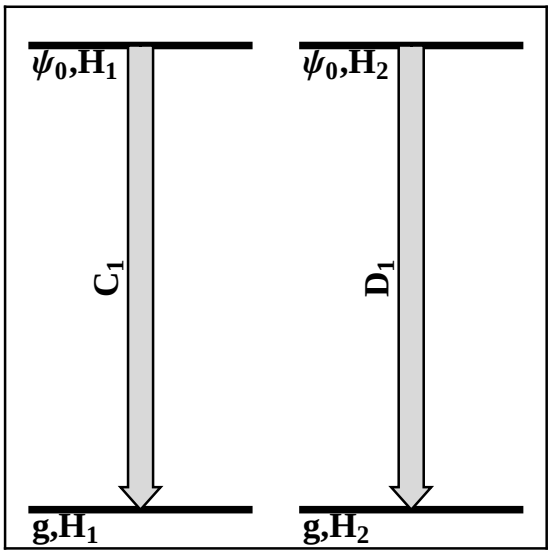

Figure 5.6: DHS method in the two state system. $|\psi_0\rangle, \mathcal{H}_1$ is the deterministic state and $|g\rangle, \mathcal{H}_1$ is the ground state. $\mathcal{H}_2$ respectively. Only difference in the dynamics of the states in $\mathcal{H}_1$ and $\mathcal{H}_2$ is in the jump operator. During the negative decay rate the part of the state vector in $\mathcal{H}_1$ that jumps gets minus sign in front.

5.1.3 THS

Hilbert space for the THS method is $\mathcal{H}_1 \oplus \mathcal{H}_2 \oplus \mathcal{H}_3$, where $\mathcal{H}_1 = \mathcal{H}_2 = \mathcal{H}_3 = \mathbb{C}_2$. This method is more complex than the NMQJ and DHS methods by construction because even though we have one physical decay channel in the Eq. (5.9), this method needs four decay channels for the correct description of the non-Markovian dynamics. The non-Hermitian Hamiltonian is:

$$H(t) = -\frac{i}{2}(a(t)|g\rangle\langle g| + |\Delta_1(t)||e\rangle\langle e|) \otimes (|1\rangle\langle 1| + |2\rangle\langle 2|). \tag{5.14}$$

We can clearly see the effect of the operator. Jump operators are:

$$J_0(t) = \sqrt{\frac{|\Delta_1(t)|}{2}}|g\rangle\langle e| \otimes (|1\rangle\langle 1| + \mathrm{sgn}\Delta_1(t)|2\rangle\langle 2|), \tag{5.15}$$

$$J_1(t) = \sqrt{\frac{|\Delta_1(t)|}{2}}|g\rangle\langle e| \otimes (|2\rangle\langle 2| + \mathrm{sgn}\Delta_1(t)|1\rangle\langle 1|), \tag{5.16}$$

$$J_2(t) = \sqrt{a(t)}|e\rangle\langle g| \otimes |3\rangle\langle 1|, \qquad J_3(t) = \sqrt{a(t)}|e\rangle\langle g| \otimes |3\rangle\langle 2|. \tag{5.17}$$

where $a(t) = |\Delta_1(t)| - \Delta_1(t)$. Calculation of $a(t)$ for this case is in the Ref. [2]. We can see that $a(t) = 0$, when $\Delta_1(t) < 0$ and thus the jump channels 2 and 3 are closed for the positive decay rate and also that $H(t)$ leaves the ground state invariant. This means that for the positive decay the deterministic evolution decreases the population in the ground state for the ensemble members in $\mathcal{H}_1 \oplus \mathcal{H}_2$. For the positive decay rate $J_0(t)$ and $J_1(t)$ induce transitions to the ground state for the vectors in $\mathcal{H}_1 \oplus \mathcal{H}_2$. When the decay rate turns negative, the deterministic evolution starts to increase the population of the ground state and the jump channels 2 and 3 open. We have now four cases (Fig. 5.7):

- Jump to channel 0: $\mathcal{H}_3$ stays invariant, but vectors in the subspace $\mathcal{H}_1 \oplus \mathcal{H}_2$ go to the ground state with additional minus sign in front of the component in $\mathcal{H}_2$.

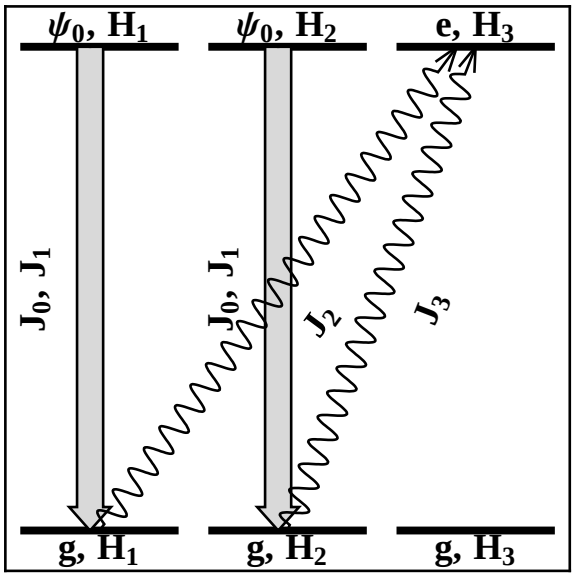

Figure 5.7: The THS method in the two state system. $|\psi_0\rangle$ is the deterministic initial state in $\mathcal{H}_1 \oplus \mathcal{H}_2$ and $|g\rangle$ is the ground state in $\mathcal{H}_1 \oplus \mathcal{H}_2$. Thick arrow shows direction of the jumps during the positive and negative decay rate and squiggly arrow shows the directions of the jumps that can take place only when the decay rate is negative. The operators J_0 and J_1 operate to the state vector in $\mathcal{H}_1 \oplus \mathcal{H}_2$ and induce transitions to the ground state, but the operators J_2 and J_3 send the ground state amplitude (scaled with $a(t)$) of the stochastic vector in $\mathcal{H}_1 \oplus \mathcal{H}_2$ to $|e\rangle_{\mathcal{H}_3}$. Notice that J_0 and J_1 introduce additional minus signs when the decay rate is negative.

- Jump to channel 1: Same as channel 0 but now the minus sign goes in front of the component in $\mathcal{H}_1$.

- Jump to channel 2: Vector leaves from $\mathcal{H}_1 \oplus \mathcal{H}_2$ and the amplitude of the state $|g\rangle_{\mathcal{H}_1}$ goes to $|e\rangle_{\mathcal{H}_3}$.

- Jump to channel 3: Vector leaves from $\mathcal{H}_1 \oplus \mathcal{H}_2$ and the amplitude of the state $|g\rangle_{\mathcal{H}_2}$ goes to $|e\rangle_{\mathcal{H}_3}$.

We see that state vectors that jump during the negative decay rate leave the subspace $\mathcal{H}_1 \oplus \mathcal{H}_2$ and go to $\mathcal{H}_3$ and also that transitions to the ground state in $\mathcal{H}_1 \oplus \mathcal{H}_2$ take place. Jumps back to $\mathcal{H}_1 \oplus \mathcal{H}_2$ from $\mathcal{H}_3$ are not possible by construction. Only states that have negative contribution to the ensemble average are the ones that have jumped to $|g\rangle_{\mathcal{H}_1 \oplus \mathcal{H}_2}$ during the negative decay rate but have not jumped to $\mathcal{H}_3$ during that same period or some other period of the negative decay rate. Another consequence is that the ensemble becomes effectively smaller because we lose states to $\mathcal{H}_3$. This is compensated in the method and we can see that from the Eq. (4.38) which can be expressed as

$$\rho(t) = \frac{E(|\phi_1(t)\rangle\langle\phi_2(t)|)}{E(\langle\phi_1(t)|\phi_2(t)\rangle)},$$

where $\phi_1(t), \phi_2(t)$ are the amplitudes of the stochastic state vector in $\mathcal{H}_1$ and $\mathcal{H}_2$ respectively and E stands for the ensemble average. As in NMQJ and DHS; jumps during negative decay rate increase the weight of the deterministically evolving state vectors. In THS there are two factors contributing to it and compared to DHS all the stochastic vectors have unit norm regardless of the sign of the decay rate. In the Sec. 4.3 we mentioned that there are multiple solutions to the Eq. (4.39). Another solution is $\Omega(t) = \sqrt{a(t)}|g\rangle\langle g|$ which gives a different picture of the dynamics.

5.2 V system

We use the following notation, $|g\rangle$ is the ground state and $|a\rangle$ and $|b\rangle$ are the excited states. Local in time master equation, Lindblad operators and formal solutions for the populations are from the Ref. [23]. The local in time master equation is

$$\begin{aligned}\dot{\rho}(t) = &+\Delta_a(t)\left[|g\rangle\langle a|\rho(t)|a\rangle\langle g| - \frac{1}{2}\{\rho(t), |a\rangle\langle a|\}\right] \\ &+\Delta_b(t)\left[|g\rangle\langle b|\rho(t)|b\rangle\langle g| - \frac{1}{2}\{\rho(t), |b\rangle\langle b|\}\right].\end{aligned} \tag{5.18}$$

The Lindblad operators are

$$C_a = |g\rangle\langle a|, \qquad C_b = |g\rangle\langle b|, \tag{5.19}$$

and the solutions for the populations are

$$\rho_{aa}(t) = e^{-D_a(t)}\rho_{aa}(0), \tag{5.20}$$

$$\rho_{bb}(t) = e^{-D_b(t)}\rho_{bb}(0), \tag{5.21}$$

$$\rho_{gg}(t) = (1 - e^{-D_a(t)})\rho_{aa}(0) + (1 - e^{-D_b(t)})\rho_{bb}(0) + \rho_{gg}(0). \tag{5.22}$$

As an example we plot the populations and the decay rate with the following parameters: $[t] = 1/\Gamma,\ \delta t = 0.01\Gamma^{-1},\ M = 10^5,\ \alpha^2 = 2,\ \delta_a = 3\Gamma,\ \delta_b = 5\Gamma,\ T = 10\Gamma$. The initial state of the system is chosen to be $|\psi_0(0)\rangle = \frac{|g\rangle+|a\rangle+|b\rangle}{\sqrt{3}}$. The populations and the decay rates with the chosen parameter values are plotted in the Figs. 5.8 and 5.9.

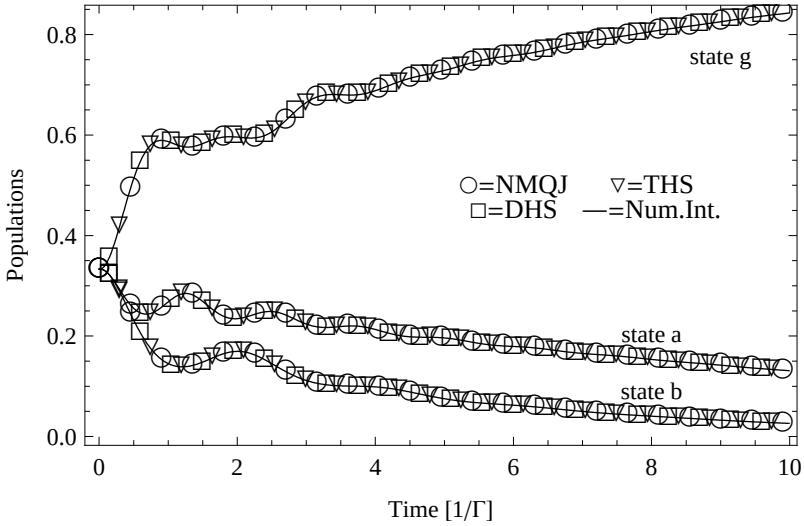

Figure 5.8: Numerically integrated solution and simulated solutions with the NMQJ, DHS and THS methods the for V system. Parameters are defined in the Sec. 5.2. Agreement of the curves is good. In further sections we make quantitative analysis about the accuracy of the different methods.

5.2.1 NMQJ

Hilbert space is $\mathcal{H} = \mathbb{C}_3$. We have two physical decay channels in the Eq. (5.18) and three different states in our system. NMQJ formulation consists effectively of

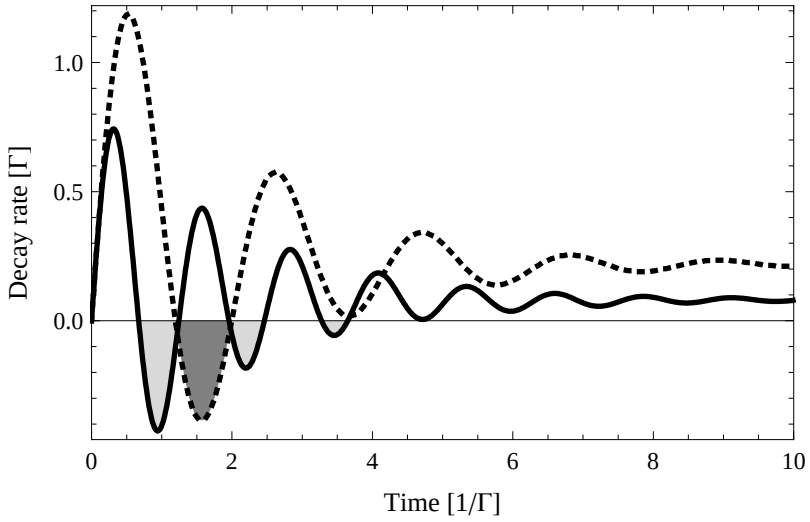

Figure 5.9: Decay rates for V-system. Parameter values are the same as in Sec. 5.2, $\alpha^2 = 2$ and $\delta_1 = 3\,\Gamma$ and $\delta_2 = 5\,\Gamma$. Solid line is the decay rate for channel a and in the light gray regions it is negative. Dotted line is the decay rate for channel b and in the gray region it is negative. Markovian time scale is $\tau_{\mathrm{M}} \approx 10\,\Gamma^{-1}$.

only two states, because the both Lindblad operators (5.18) act like $C_1|\psi_0\rangle \to |g\rangle$ and $C_2|\psi_0\rangle \to |g\rangle$ (Fig. 5.10). For the description of the memory effects we need again $M_0(t)$ and $M_1(t)$ and they are defined the same way as in the Sec. 5.1.1. The non-Hermitian Hamiltonian $\hat{H}(t)$ is

$$\hat{H}(t) = -\frac{i}{2}(\Delta_a(t)|a\rangle\langle a| + \Delta_b(t)|b\rangle\langle b|). \tag{5.23}$$

The two different decay rates and channels a and b give us four different situations:

- $\Delta_a(t), \Delta_b(t) \geq 0$: The deterministic evolution drives the system to the ground state. Jumps only from the deterministic state to the ground state.

- $\Delta_a(t), \Delta_b(t) < 0$: The deterministic evolution increases the population in the states $|a\rangle$ and $|b\rangle$. Only non-Markovian jumps from the ground state back to the deterministic state.

- $\Delta_a(t) \geq 0 \wedge \Delta_b(t) < 0$: The deterministic evolution decreases the population

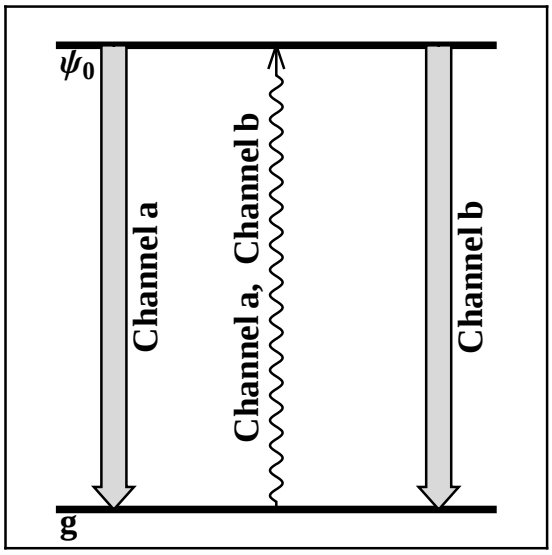

Figure 5.10: Effective ensemble of the NMQJ method in the V-system. $|\psi_0\rangle$ is the deterministic initial state and $|g\rangle$ is the ground state. Thick arrows show jumps during the positive decay rate and squiggly arrow shows the direction of non-Markovian jumps. Both decay channels take the system away from the state $|\psi_0\rangle$ to the ground state during the positive decay rates and during the negative decay rates they take system back to the state $|\psi_0\rangle$.

in the state $|a\rangle$ and increases the population in the state $|b\rangle$. Jumps from the deterministic state to the ground state via channel a and non-Markovian jumps from the ground state back to the deterministic state via channel b.

- $\Delta_a(t) < 0 \wedge \Delta_b(t) \geq 0$: Same as the previous situation except that indices a and b are interchanged.

5.2.2 DHS

Hilbert space is $\mathcal{H}_1 \oplus \mathcal{H}_2$, where $\mathcal{H}_1 = \mathcal{H}_2 = \mathbb{C}_3$. We have two decay channels a and b and thus we need two operators $J_\alpha(t)$, $\alpha \in \{a, b\}$. Level geometry also affects the

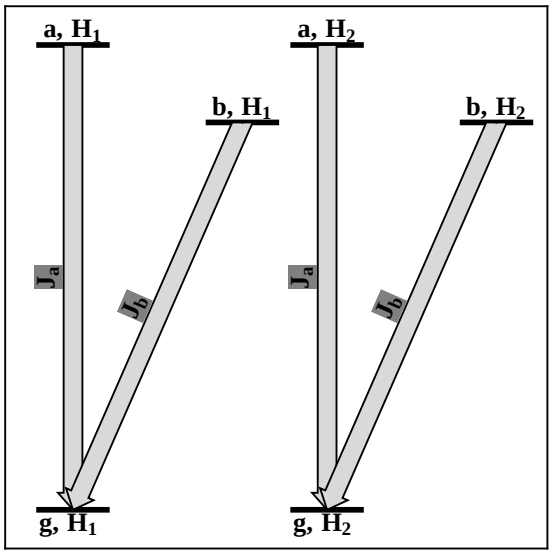

Figure 5.11: DHS method in the V-system. Let us define a state $|\psi_0(t)\rangle = c_g(t)|g\rangle + c_a(t)|a\rangle + c_b(t)|b\rangle$. State $\theta(t) = \frac{1}{\sqrt{2}}(|\psi_0(t)\rangle \oplus |\psi_0(t)\rangle)$ is the deterministic initial state in $\mathcal{H}_1 \oplus \mathcal{H}_2$ and $|g\rangle$ is the ground state. Thick arrow shows jumps during the positive and negative decay rate. Operator J_α take the state vector to the ground state, if it has non-zero amplitude in the excited state $|\alpha\rangle$, where $\alpha = \{a, b\}$. Notice that J_a and J_b introduce additional minus signs when the decay rate is negative. We have jumps only from the excited states to the ground state.

evolution generator $F(t)$:

$$F(t) = -\frac{1}{2}\Big(\Delta_a(t)|a\rangle\langle a| + \Delta_b(t)|b\rangle\langle b|\Big) \otimes \Big(|1\rangle\langle 1| + |2\rangle\langle 2|)\Big), \tag{5.24}$$

Explicit form of the jump operators is:

$$J_a(t) = \sqrt{|\Delta_a(t)|}(|g\rangle\langle a|) \otimes \Big(\mathrm{sgn}(\Delta_a(t))|1\rangle\langle 1| + |2\rangle\langle 2|\Big), \tag{5.25}$$

$$J_b(t) = \sqrt{|\Delta_b(t)|}(|g\rangle\langle b|) \otimes \Big(\mathrm{sgn}(\Delta_b(t))|1\rangle\langle 1| + |2\rangle\langle 2|\Big). \tag{5.26}$$

The deterministic evolution is practically the same as in the NMQJ method for the V system but it takes place in doubled Hilbert space. Effect of the jump operators

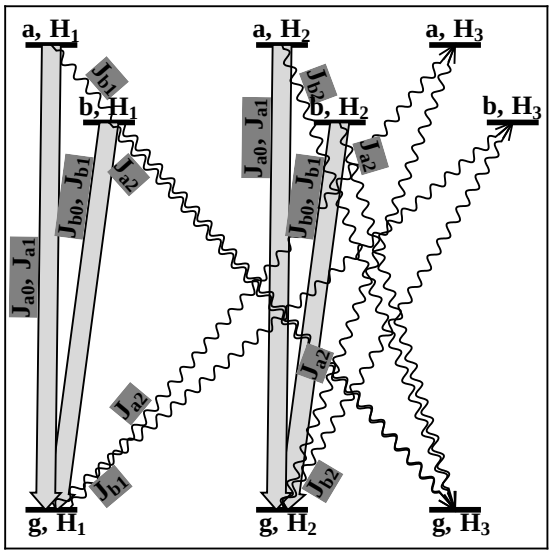

Figure 5.12: THS method in the V-system. The deterministic initial state is $\Psi_0(t) = (c_g(t)|g\rangle + c_a(t)|a\rangle + c_b(t)|b\rangle) \otimes \frac{1}{\sqrt{2}}(|1\rangle + |2\rangle)$. Thick arrow shows possible jumps when the decay rates a and b are positive or negative. Squiggly arrow shows possible jumps when the decay rates are negative. Essential part is that the squiggly arrows take stochastic vector from $\mathcal{H}_1 \oplus \mathcal{H}_2$ to $\mathcal{H}_3$. Populations of the physical system can be calculated without the information how the states $|g\rangle$, $|a\rangle$ and $|b\rangle$ are populated in $\mathcal{H}_3$.

is the same for both channels, as is illustrated in the Fig. 5.11. If the channel α is positive, the stochastic state vector in $\mathcal{H}_1 \oplus \mathcal{H}_2$ may jump to the ground state. If channel α is negative, the stochastic vector in $\mathcal{H}_1 \oplus \mathcal{H}_2$ may jump to the ground state, but J_α gives minus sign in front of the component in $\mathcal{H}_1$.

5.2.3 THS

Hilbert space for the process is $\mathcal{H} \oplus \mathcal{H} \oplus \mathcal{H}$, where $\mathcal{H} = \mathbb{C}_3$. We have two decay channels in Eq. (5.18) and therefore we have eight jump channels for the THS

method in this case. The non-Hermitian Hamiltonian reads:

$$\hat{H}(t) = -\frac{\imath}{2}\Big((a(t)+b(t))|g\rangle\langle g| + (|\Delta_a(t)|+b(t))|a\rangle\langle a| + (|\Delta_b(t)|+a(t))|b\rangle\langle b|\Big) \otimes \Big(|1\rangle\langle 1| + |2\rangle\langle 2|\Big). \quad (5.27)$$

Jump operators $J_{a0}(t),\ J_{a1}(t),\ J_{a2}(t),\ J_{a3}(t)\ J_{b0}(t),\ J_{b1}(t),\ J_{b2}(t),\ J_{b3}(t)$ are:

$$J_{a0}(t) = \sqrt{\frac{|\Delta_a(t)|}{2}}|g\rangle\langle a| \otimes \Big(|1\rangle\langle 1| + \mathrm{sgn}(\Delta_a(t))|2\rangle\langle 2|\Big), \quad (5.28)$$

$$J_{a1}(t) = \sqrt{\frac{|\Delta_a(t)|}{2}}|g\rangle\langle a| \otimes \Big(|2\rangle\langle 2| + \mathrm{sgn}(\Delta_a(t))|1\rangle\langle 1|\Big), \quad (5.29)$$

$$J_{a2}(t) = \Omega_a(t) \otimes |3\rangle\langle 1|, \qquad J_{a3}(t) = \Omega_a(t) \otimes |3\rangle\langle 2|, \quad (5.30)$$

$$J_{b0}(t) = \sqrt{\frac{|\Delta_b(t)|}{2}}|g\rangle\langle b| \otimes \Big(|1\rangle\langle 1| + \mathrm{sgn}(\Delta_b(t))|2\rangle\langle 2|\Big), \quad (5.31)$$

$$J_{b1}(t) = \sqrt{\frac{|\Delta_b(t)|}{2}}|g\rangle\langle b| \otimes \Big(|2\rangle\langle 2| + \mathrm{sgn}(\Delta_b(t))|1\rangle\langle 1|\Big), \quad (5.32)$$

$$J_{b2}(t) = \Omega_b(t) \otimes |3\rangle\langle 1|, \qquad J_{b3}(t) = \Omega_b(t) \otimes |3\rangle\langle 2|, \quad (5.33)$$

where $\Omega_a(t) = \sqrt{a(t)}\Big(|a\rangle\langle g| + |g\rangle\langle b|\Big)$, $\Omega_b(t) = \sqrt{b(t)}\Big(|b\rangle\langle g| + |g\rangle\langle a|\Big)$, $a(t) = |\Delta_a(t)| - \Delta_a(t)$ and $b(t) = |\Delta_b(t)| - \Delta_b(t)$. The form of the non-Hermitian Hamiltonian shows us that when the channels a and b are positive the population is increased in the state $|g\rangle$. When one or both channels turn negative, the population in the ground states starts to decrease during the deterministic evolution. Jump channels J_{a2}, J_{a3} are closed if $\Delta_a(t) \geq 0$ and jump channels J_{b2}, J_{b3} are closed if $\Delta_b(t) \geq 0$. Jumps to the positive channels are analogous to the two state system case. Jumps to the channels $J_{\alpha 2}$ and $J_{\alpha 3}$, $\alpha = \{a, b\}$ are different. State vector leaves the Hilbert space $\mathcal{H}_1 \oplus \mathcal{H}_2$ and goes to $\mathcal{H}_3$. The population from the state $|g\rangle$ goes to $|\alpha\rangle$ and

the population from the state $|\beta \neq \alpha\rangle$ goes to $|g\rangle$. For a graphical presentation see Fig. 5.12. The form of the operators $\Omega_\alpha(t)$ and thus $J_{\alpha 2}$ and $J_{\alpha 3}$ is not unique because we have multiple solutions to Eq. (4.39). Different solutions give different distribution of the populations in $\mathcal{H}_3$ but that does not affect the non-Markovian dynamics.

5.3 Λ system

We have one excited state and two states with smaller energy. We use the following notation: $|e\rangle$ is the excited state and $|a\rangle$ and $|b\rangle$ are the lower energy states. Local in time master equation, Lindblad operators and solutions for the populations are from the Ref. [23]. The local in time master equation is:

$$\begin{aligned}\dot{\rho}(t) = \Delta_a(t)\left[|a\rangle\langle e|\rho(t)|e\rangle\langle a| - \frac{1}{2}\{\rho(t), |e\rangle\langle e|\}\right] \\ +\Delta_b(t)\left[|b\rangle\langle e|\rho(t)|e\rangle\langle b| - \frac{1}{2}\{\rho(t), |e\rangle\langle e|\}\right].\end{aligned} \tag{5.34}$$

The solutions for the populations are:

$$\rho_{ee}(t) = e^{-(D_a(t)+D_b(t))}\rho_{ee}(0), \tag{5.35}$$

$$\rho_{aa}(t) = \int_o^t \mathrm{d}s\ e^{-(D_a(s)+D_b(s))}\rho_{ee}(0) + \rho_{aa}(0), \tag{5.36}$$

$$\rho_{bb}(t) = \int_o^t \mathrm{d}s\ e^{-(D_a(s)+D_b(s))}\rho_{ee}(0) + \rho_{bb}(0). \tag{5.37}$$

The Lindblad operators are:

$$C_a = |a\rangle\langle e|, \qquad C_b = |b\rangle\langle e|. \tag{5.38}$$

As an example we plot the populations and the decay rates with the following parameter values: $[t] = 1/\Gamma$, $\delta t = 0.01\Gamma^{-1}$, $M = 10^5$, $\alpha^2 = 2$, $\delta_a = 3\Gamma$, $\delta_b = 5\Gamma$, $T = 10\Gamma$. The initial state of the system is chosen to be $|\psi_0(0)\rangle = \frac{4|e\rangle+2|a\rangle+|b\rangle}{\sqrt{21}}$. Populations and decay rates with parameter values chosen are plotted in the Figs. 5.13 and 5.14. With these parameter values we see that at the time interval $t \approx$

$[1/\Gamma, 2/\Gamma]$ there is a plateau in the population $\rho_{ee}(t)$ because the decay rates $\Delta_a(t)$ and $\Delta_b(t)$ have different signs and they counteract each other.

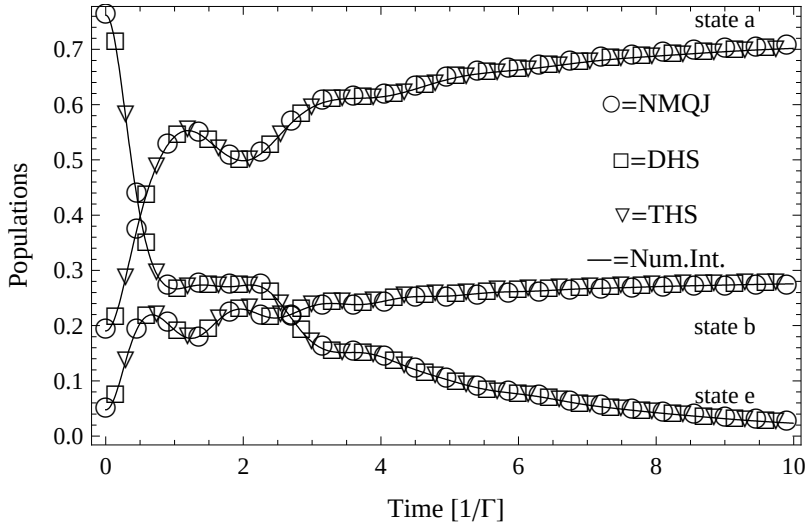

Figure 5.13: Numerically integrated and simulated solutions (with the NMQJ, DHS and THS methods) for the populations of the Λ system. Parameter values are defined in the Sec. 5.3. Agreement of the curves is good. Quantitative information about the accuracy is in the Sec. (6.1).

5.3.1 NMQJ

Hilbert space for the NMQJ method in this case is $\mathcal{H} = \mathbb{C}_3$. $M_{\text{eff}} = 3$, if we have initially some population in the excited state because the initial state can now decay to the two different states $|a\rangle$ and $|b\rangle$. The non-Hermitian Hamiltonian is

$$\hat{H}(t) = -\frac{\imath}{2}\Big(\Delta_a(t) + \Delta_b(t)\Big)|e\rangle\langle e|. \tag{5.39}$$

The two different decay rates give four possible situations (their graphical presentation is in the Fig. 5.15)

- $\Delta_a(t), \Delta_b(t) \geq 0$: The deterministic evolution drives the system to the lower energy states. The deterministic initial state can jump to $|a\rangle$ or $|b\rangle$ where no further decay can happen.

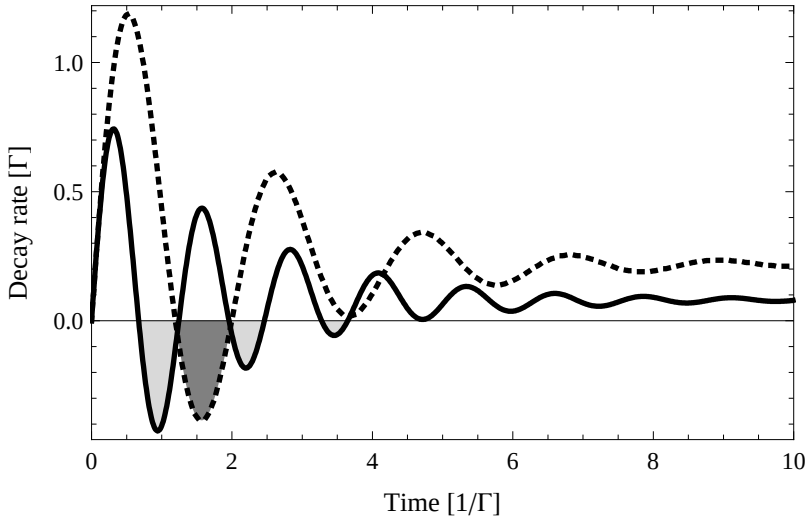

Figure 5.14: Decay rates for the Λ system. Parameters values are the as in the Sec. 5.3, $\alpha^2 = 2$ and $\delta_a = 3\,\Gamma$ and $\delta_b = 5\,\Gamma$. Solid line is the decay rate for channel a and in the light gray regions it is negative. Dotted line is the decay rate for channel b and in the gray region it is negative. Markovian time scale is $\tau_{\mathrm{M}} \approx 10\,\Gamma^{-1}$.

- $\Delta_a(t), \Delta_b(t) < 0$: The deterministic evolution increases the population in the excited state. If the system has jumped to the state $|a\rangle$ or $|b\rangle$ we can now have a reverse jump back to the initial state from the state $|a\rangle$ or $|b\rangle$.

- $\Delta_a(t) \geq 0 \wedge \Delta_b(t) < 0$: The system can now jump from the deterministic initial state to the state $|a\rangle$ or the system can make a reverse jump from the state $|b\rangle$ to the deterministic initial state.

- $\Delta_a(t) < 0 \wedge \Delta_b(t) \geq 0$: Same as the previous situation except the indices a and b interchanged.

5.3.2 DHS

We have $\mathcal{H} = \mathbb{C}_3 \oplus \mathbb{C}_3 = \mathcal{H}_1 \oplus \mathcal{H}_2$. We have one jump operator for each physical decay channel and operator $F(t)$ that handles the deterministic evolution. The

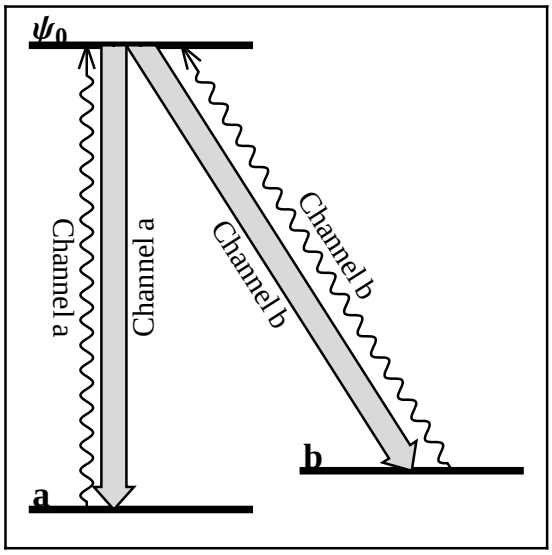

Figure 5.15: Effective ensemble of the NMQJ method in Λ system. $|\psi_0\rangle$ is the deterministic initial state and $|a\rangle$ and $|b\rangle$ are the lower energy states. Thick arrow shows jumps during the positive decay rate and squiggly arrow shows the direction of the non-Markovian jumps. Both decay channels take the system away from $|\psi_0\rangle$ to different lower energy states during the positive decay rate. During the negative decay rate they take system back to $|\psi_0\rangle$ from the lower energy states.

operator $F(t)$ is

$$F(t) = -\frac{1}{2}\Big(\Delta_a(t) + \Delta_b(t)\Big)|e\rangle\langle e| \otimes \Big(|1\rangle\langle 1| + |2\rangle\langle 2|\Big), \tag{5.40}$$

explicit form of the jump operators $J_a(t)$ and $J_b(t)$ is

$$J_a(t) = \sqrt{|\Delta_a(t)|}|a\rangle\langle e| \otimes \Big(\mathrm{sgn}(\Delta_a(t))|1\rangle\langle 1| + |2\rangle\langle 2|\Big), \tag{5.41}$$

$$J_b(t) = \sqrt{|\Delta_b(t)|}|b\rangle\langle e| \otimes \Big(\mathrm{sgn}(\Delta_b(t))|1\rangle\langle 1| + |2\rangle\langle 2|\Big). \tag{5.42}$$

Dynamics are similar to the NMQJ when both decay rates are positive, but the jumps during the negative decay rate in channel a or b gives a minus sign in front of the component of the stochastic vector in $\mathcal{H}_1$. For a graphical presentation, see the Fig. 5.16.

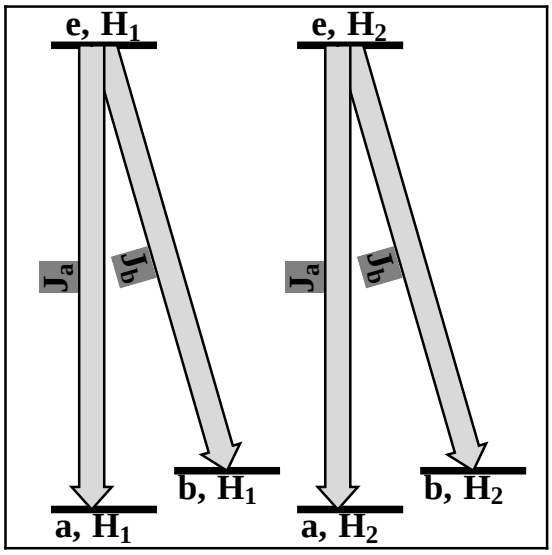

Figure 5.16: DHS method in the Λ system. Let us define the state $|\psi_0(t)\rangle = c_g(t)|e\rangle + c_a(t)|a\rangle + c_b(t)|b\rangle$. The state $\theta(t) = \frac{1}{\sqrt{2}}(|\psi_0(t)\rangle \oplus |\psi_0(t)\rangle)$ is the deterministic initial state in $\mathcal{H}_1 \oplus \mathcal{H}_2$ and $|a\rangle$ and $|b\rangle$ are the lower energy states. Thick arrow shows jumps during the positive and negative decay rate. Operators J_a and J_b take the stochastic vector from the excited state or deterministic initial state (if $|c_e(t)|^2 \neq 0$) to the lower energy states. Notice that the operators J_a and J_b introduce an additional minus sign when one or both decay rates are negative. We have jumps only from the excited state to the lower energy states.

5.3.3 THS

Hilbert space is now $\mathcal{H} = \mathbb{C}_3 \oplus \mathbb{C}_3 \oplus \mathbb{C}_3 = \mathcal{H}_1 \oplus \mathcal{H}_2 \oplus \mathcal{H}_3$. We have eight decay channels. The non-Hermitian Hamiltonian reads

$$\begin{aligned}\hat{H}(t) = &-\frac{\imath}{2}\Bigg((a(t)+b(t))(|a\rangle\langle a| + |b\rangle\langle b|) \\ &+ (|\Delta_a(t)| + |\Delta_b(t)|)|e\rangle\langle e|\Bigg) \otimes \Big(|1\rangle\langle 1| + |2\rangle\langle 2|\Big).\end{aligned} \tag{5.43}$$

Jump operators $J_{a0}(t),\ J_{a1}(t),\ J_{a2}(t),\ J_{a3}(t),\ J_{b0}(t),\ J_{b1}(t),\ J_{b2}(t),\ J_{b3}(t)$ are

$$J_{a0}(t) = \sqrt{\frac{|\Delta_a(t)|}{2}}|a\rangle\langle e| \otimes \Big(|1\rangle\langle 1| + \mathrm{sgn}(\Delta_a(t))|2\rangle\langle 2|\Big), \tag{5.44}$$

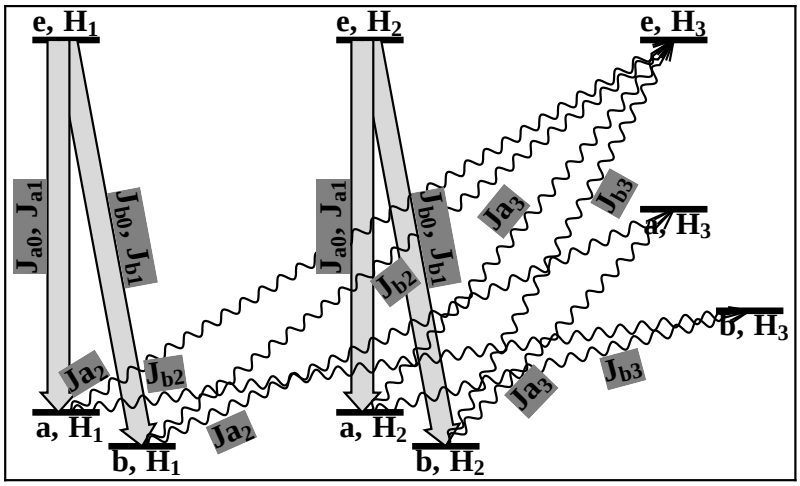

Figure 5.17: THS method in the Λ system. Systems in $\mathcal{H}_1$, $\mathcal{H}_2$ and $\mathcal{H}_3$ are identical, but they are drawn in different scale in order to simplify the figure. Let us define the state $|\psi_0(t)\rangle = c_g(t)|e\rangle + c_a(t)|a\rangle + c_b(t)|b\rangle$. The state $\Psi(t) = |\psi_0(t)\rangle \otimes \frac{1}{\sqrt{2}}(|1\rangle + |2\rangle)$ is the deterministic initial state in $\mathcal{H}_1 \oplus \mathcal{H}_2$ and $|a\rangle$ and $|b\rangle$ are the lower energy states. Thick arrow shows possible jumps during the positive and negative decay rate. Squiggly arrow shows possible jumps during the negative decay rate. Operators J_{a0}, J_{a1} and J_{b0}, J_{b1} take the stochastic vector from the deterministic state to the lower energy states and keep it in $\mathcal{H}_1 \oplus \mathcal{H}_2$. $J_{a2}, J_{a3}, J_{b2}, J_{b3}$ take the stochastic vector from one of the lower energy states or from the initial state (if any $\{|c_a(t)|^2, |c_b(t)|^2\} \neq 0$) in $\mathcal{H}_1 \oplus \mathcal{H}_2$ to $\mathcal{H}_3$. Notice that J_a and J_b introduce an additional minus sign when the decay rate is negative.

$$J_{a1}(t) = \sqrt{\frac{|\Delta_a(t)|}{2}}|a\rangle\langle e| \otimes \Big(|2\rangle\langle 2| + \mathrm{sgn}(\Delta_a(t))|1\rangle\langle 1|\Big), \tag{5.45}$$

$$J_{a2}(t) = \Omega_a(t) \otimes |3\rangle\langle 1|, \qquad J_{a3}(t) = \Omega_a(t) \otimes |3\rangle\langle 2|, \tag{5.46}$$

$$J_{b0}(t) = \sqrt{\frac{|\Delta_b(t)|}{2}}|b\rangle\langle e| \otimes \Big(|1\rangle\langle 1| + \mathrm{sgn}(\Delta_b(t))|2\rangle\langle 2|\Big), \tag{5.47}$$

$$J_{b1}(t) = \sqrt{\frac{|\Delta_b(t)|}{2}}|b\rangle\langle e| \otimes \Big(|2\rangle\langle 2| + \mathrm{sgn}(\Delta_b(t))|1\rangle\langle 1|\Big), \tag{5.48}$$

$$J_{b2}(t) = \Omega_b(t) \otimes |3\rangle\langle 1|, \qquad J_{b3}(t) = \Omega_b(t) \otimes |3\rangle\langle 2|, \tag{5.49}$$

where $\Omega_a(t) = \sqrt{a(t)}\Big(|e\rangle\langle a| + |a\rangle\langle b|\Big)$, $\Omega_b(t) = \sqrt{b(t)}\Big(|b\rangle\langle a| + |e\rangle\langle b|\Big)$, $a(t) = |\Delta_a(t)| - \Delta_a(t)$ and $b(t) = |\Delta_b(t)| - \Delta_b(t)$. A graphical presentation of the action of the operators $J_{\alpha,i}$ is in the Fig. 5.17. As before the definition of $J_{\alpha,i}(t)$, $\alpha = \{a, b\}$, $i = \{2, 3\}$ is not unique. The essential part is that the jump probability depends on the population in the states $|a\rangle_{\mathcal{H}_1\oplus\mathcal{H}_2}$ and $|b\rangle_{\mathcal{H}_1\oplus\mathcal{H}_2}$ and and that it takes the state vectors from $\mathcal{H}_1 \oplus \mathcal{H}_2$ to $\mathcal{H}_3$.

5.4 Three level ladder system

We have a three level system that forms a short cascade. State of the highest energy is $|e\rangle$, $|a\rangle$ is the intermediate state and the ground state is $|b\rangle$. Local in time non-Markovian master equation, solutions for the populations and Lindblad operators are from the Ref. [23]. The local in time non-Markovian master equation for this system is

$$\begin{aligned}\dot{\rho}(t) =& \Delta_a(t)\Big[|a\rangle\langle e|\rho(t)|e\rangle\langle a| - \frac{1}{2}\{\rho(t), |e\rangle\langle e|\}\Big] \\ &+ \Delta_b(t)\Big[|b\rangle\langle a|\rho(t)|a\rangle\langle b| - \frac{1}{2}\{\rho(t), |a\rangle\langle a|\}\Big].\end{aligned} \tag{5.50}$$

The solutions for the populations are

$$\rho_{ee}(t) = e^{-D_a(t)}\rho_{ee}(0), \tag{5.51}$$

$$\rho_{aa}(t) = e^{-D_b(t)}\int_0^t \mathrm{d}s\, \Delta_a(s)e^{-D_a(s)+D_b(s)}\rho_{ee}(0) + e^{-D_b(t)}\rho_{aa}(0), \tag{5.52}$$

$$\begin{aligned}\rho_{bb}(t) =& \Big[1 - e^{-D_a(t)} - e^{-D_b(t)}\int_0^t \mathrm{d}s\, \Delta_a(s)e^{-D_a(s)+D_b(s)}\Big]\rho_{ee}(0) \\ &+ \Big[1 - e^{-D_b(t)}\Big]\rho_{aa}(0) + \rho_{bb}(0).\end{aligned} \tag{5.53}$$

and the Lindblad operators are

$$C_a = |a\rangle\langle e|, \qquad C_b = |b\rangle\langle a|. \tag{5.54}$$

From the Lindblad operators we see that the system can perform jumps from the states $|e\rangle \rightarrow |a\rangle$ and $|a\rangle \rightarrow |b\rangle$. As an example we plot the time evolution of the populations and the decay rates with the following parameter values: $[t] = 1/\Gamma$, $\delta t = 0.01\Gamma^{-1}$, $M = 10^5$, $\alpha^2 = 2$, $\delta_a = 3\Gamma$, $\delta_b = 5\Gamma$, $T = 10\Gamma$. The initial state of the system is chosen to be $|\psi_0(0)\rangle = \frac{4|e\rangle+2|a\rangle+|b\rangle}{\sqrt{21}}$. Plot of the populations and the decay rates with the parameter values chosen are in the Figs. 5.18 and 5.19. With these parameter values decay to the ground state of the system is slower than in other cases and the intermediate state $|a\rangle$ stays populated longer.

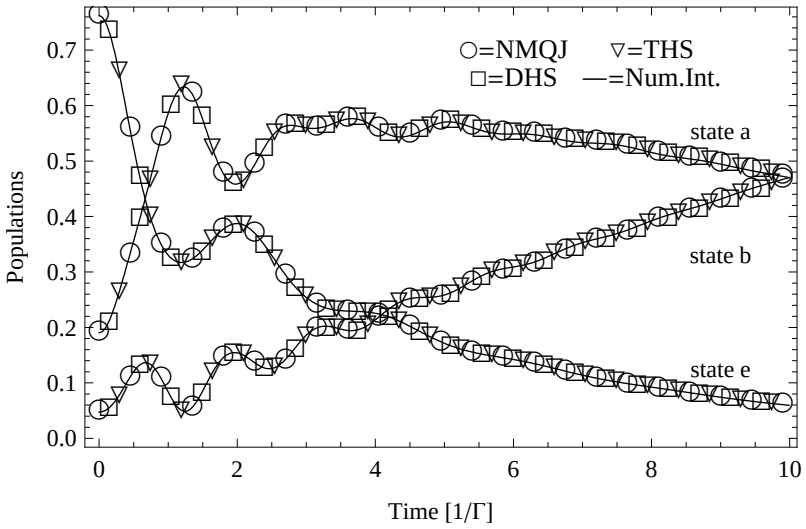

Figure 5.18: Populations for the ladder system with numerical integration and with the NMQJ, DHS and THS methods. Parameters are defined in the Sec. (5.4). Agreement of curves is good.

5.4.1 NMQJ

Hilbert space is $\mathbb{C}_3$. If we have an initial state that has non-zero population in the state $|e\rangle$ then $M_{\text{eff}} = 3$. The non-Hermitian Hamiltonian reads:

$$\hat{H}(t) = -\frac{\imath}{2}\Big(\Delta_a(t)|a\rangle\langle a| + \Delta_b(t)|b\rangle\langle b|\Big). \tag{5.55}$$

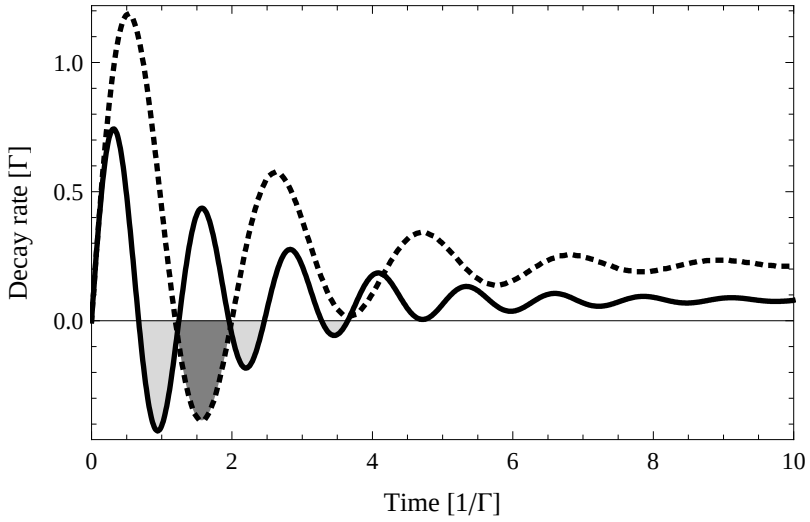

Figure 5.19: Decay rates for the ladder system. Parameters are values are the same as in the Sec. (5.4), $\alpha^2 = 2$ and $\delta_a = 3\,\Gamma$ and $\delta_b = 5\,\Gamma$. Solid line is the decay rate for the channel a and in the light gray regions it is negative. Dotted line is the decay rate for the channel b and in the gray region it is negative. Markovian time scale is $\tau_{\mathrm{M}} \approx 10\,\Gamma^{-1}$.

Two different decay rates give four possible situations. The Fig. 5.20 illustrates the situation. We have assumed that the initial state is a superposition of the states $|a\rangle$ and $|e\rangle$. This way we can obtain some new phenomena compared to earlier situations. If we include the ground state to the superposition the following applies also then.

- $\Delta_a(t), \Delta_b(t) \geq 0$: The deterministic evolution drives the system to the lower energy states. Possible jump paths from the initial states are $|\psi_0\rangle \to |a\rangle \to |b\rangle$ or $|\psi_0\rangle \to |b\rangle$.

- $\Delta_a(t), \Delta_b(t) < 0$: The deterministic evolution increases the population in the states $|e\rangle$ and $|a\rangle$. Non-Markovian jumps can occur from the state $|a\rangle \to |\psi_0\rangle$ via channel a and from the state $|b\rangle \to |\psi_0\rangle$ or $|b\rangle \to |a\rangle$ via channel b. This is new compared to the earlier systems, because there are two possible target

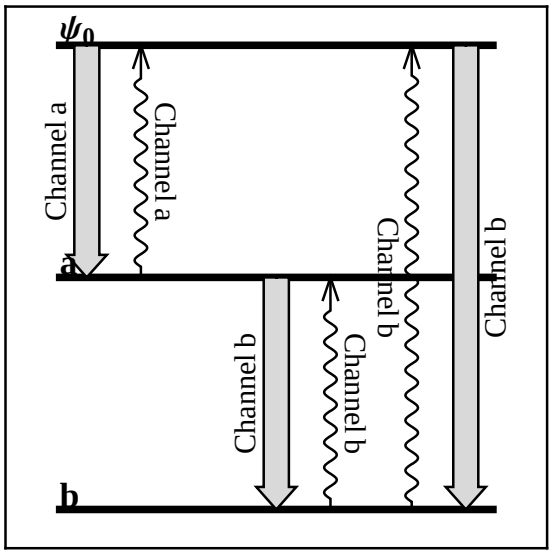

Figure 5.20: Effective ensemble of the NMQJ method in the ladder system. $|\psi_0\rangle$ is the deterministic initial state, $|a\rangle$ is the intermediate state and $|b\rangle$ is the ground state. Thick arrow shows jumps during the positive decay rate and squiggly arrow shows the direction of the non-Markovian jumps.

states for the non-Markovian jump away from state $|b\rangle$.

- $\Delta_a(t) \geq 0 \wedge \Delta_b(t) < 0$: The system can jump from $|\psi_0\rangle \rightarrow |a\rangle$ via channel a. Non-Markovian jumps can take place from $|b\rangle \rightarrow |a\rangle$ and $|b\rangle \rightarrow |\psi_0\rangle$. In this case the population in the state $|a\rangle$ can increase heavily.

- $\Delta_a(t) < 0 \wedge \Delta_b(t) \geq 0$: It is possible for the system to jump from $|\psi_0\rangle \rightarrow |b\rangle$ and $|a\rangle \rightarrow |b\rangle$ via channel b. Non-Markovian jumps may occur from $|a\rangle \rightarrow |\psi_0\rangle$.

5.4.2 DHS

Hilbert space is $\mathcal{H} = \mathbb{C}_3 \oplus \mathbb{C}_3 = \mathcal{H}_1 \oplus \mathcal{H}_2$. We need the same three operators as before to solve a three-state system, but the structure of operators is different. Operator $F(t)$ is

$$F(t) = -\frac{1}{2}\Big(\Delta_a(t)|a\rangle\langle a| + \Delta_b(t)|b\rangle\langle b|\Big) \otimes \Big(|1\rangle\langle 1| + |2\rangle\langle 2|\Big). \tag{5.56}$$

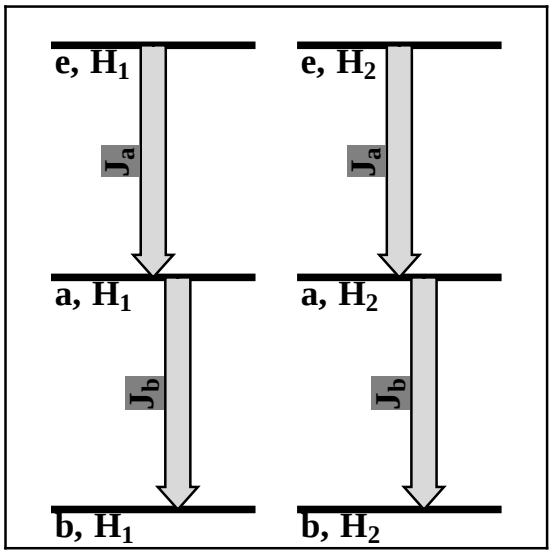

Figure 5.21: DHS method in the ladder system. Let us define the state $|\psi_0(t)\rangle = c_e(t)|e\rangle + c_a(t)|a\rangle + c_b(t)|b\rangle$. The state $\theta(t) = \frac{1}{\sqrt{2}}(|\phi_0(t)\rangle \oplus |\phi_0(t)\rangle)$ is the deterministic initial state in $\mathcal{H}_1 \oplus \mathcal{H}_2$ and $|a\rangle$ and $|b\rangle$ are the lower energy states. Thick arrow shows the possible jumps during the positive and negative decay rate. Notice that J_a and J_b introduce an additional minus sign when the decay rate is negative. We have jumps only from the excited states to the lower energy states.

The jump operators $J_a(t)$ and $J_b(t)$ are

$$J_a(t) = \sqrt{|\Delta_a(t)|}|a\rangle\langle e| \otimes \Big(\mathrm{sgn}(\Delta_a(t))|1\rangle\langle 1| + |2\rangle\langle 2|\Big), \tag{5.57}$$

$$J_b(t) = \sqrt{|\Delta_b(t)|}|b\rangle\langle a| \otimes \Big(\mathrm{sgn}(\Delta_b(t))|1\rangle\langle 1| + |2\rangle\langle 2|\Big), \tag{5.58}$$

Jumps happen only from the higher energy states to the lower energy states. During the negative decay rate periods the norm of deterministically evolving ensemble member increases. See the Fig. 5.21 for a graphical presentation of the action of the jump operators.

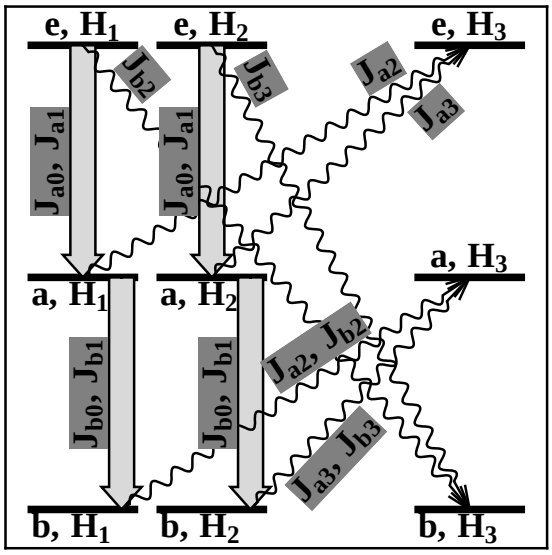

Figure 5.22: THS method in the ladder system. Let us define the state $|\psi_0(t)\rangle = c_g(t)|e\rangle + c_a(t)|a\rangle + c_b(t)|b\rangle$. The state $\Phi(t) = |\psi_0(t)\rangle \otimes \frac{1}{\sqrt{2}}(|1\rangle + |2\rangle)$ is the deterministic initial state in $\mathcal{H}_1 \oplus \mathcal{H}_2$ and $|a\rangle$ and $|b\rangle$ are the lower energy states. Thick arrow shows possible jumps during the positive and negative decay rates. Squiggly arrow shows possible jumps only during the negative decay rate. During the negative decay rates operators J_{a0}, J_{a1}, J_{b0}, J_{b1} introduce a relative minus sign between the components of the stochastic vector in $\mathcal{H}_1$ and $\mathcal{H}_2$.

5.4.3 THS

Hilbert space is $\mathcal{H} = \mathbb{C}_3 \oplus \mathbb{C}_3 \oplus \mathbb{C}_3$. We need here 9 operators as in all other three-state cases. The non-Hermitian Hamiltonian reads:

$$\hat{H}(t) = -\frac{\imath}{2}\Big((a(t) + b(t))|e\rangle\langle e| + (|\Delta_a(t)| + b(t))|a\rangle\langle a| \tag{5.59}$$

$$+(|\Delta_b(t)| + a(t))|b\rangle\langle b|\Big) \otimes \Big(|1\rangle\langle 1| + |2\rangle\langle 2|\Big). \tag{5.60}$$

Jump operators $J_{a0}(t),\ J_{a1}(t),\ J_{a2}(t),\ J_{a3}(t),\ J_{b0}(t),\ J_{b1}(t),\ J_{b2}(t),\ J_{b3}(t)$ are:

$$J_{a0}(t) = \sqrt{\frac{|\Delta_a(t)|}{2}}|a\rangle\langle e| \otimes \Big(|1\rangle\langle 1| + \mathrm{sgn}(\Delta_a(t))|2\rangle\langle 2|\Big), \tag{5.61}$$

$$J_{a1}(t) = \sqrt{\frac{|\Delta_a(t)|}{2}}|a\rangle\langle e| \otimes \Big(|2\rangle\langle 2| + \mathrm{sgn}(\Delta_a(t))|1\rangle\langle 1|\Big), \tag{5.62}$$

$$J_{a2}(t) = \Omega_a(t) \otimes |3\rangle\langle 1|, \qquad J_{a3}(t) = \Omega_a(t) \otimes |3\rangle\langle 2|, \tag{5.63}$$

$$J_{b0}(t) = \sqrt{\frac{|\Delta_b(t)|}{2}}|b\rangle\langle a| \otimes \Big(|1\rangle\langle 1| + \mathrm{sgn}(\Delta_b(t))|2\rangle\langle 2|\Big), \tag{5.64}$$

$$J_{b1}(t) = \sqrt{\frac{|\Delta_b(t)|}{2}}|b\rangle\langle a| \otimes \Big(|2\rangle\langle 2| + \mathrm{sgn}(\Delta_b(t))|1\rangle\langle 1|\Big), \tag{5.65}$$

$$J_{b2}(t) = \Omega_b(t) \otimes |3\rangle\langle 1|, \qquad J_{b3}(t) = \Omega_b(t) \otimes |3\rangle\langle 2|, \tag{5.66}$$

where $\Omega_a(t) = \sqrt{a(t)}\Big(|e\rangle\langle a| + |a\rangle\langle b|\Big)$, $\Omega_b(t) = \sqrt{b(t)}\Big(|b\rangle\langle e| + |a\rangle\langle b|\Big)$, $a(t) = |\Delta_a(t)| - \Delta_a(t)$ and $b(t) = |\Delta_b(t)| - \Delta_b(t)$. Graphical presentation of the action of the operators is in the Fig. 5.22. Again the definition of $\Omega_a(t)$ and $\Omega_b(t)$ is not unique.

6 Numerical comparison of NMQJ, DHS and THS methods

In this chapter we benchmark the NMQJ, DHS and THS methods. We are going to analyze the use of the CPU time, the accuracy of the methods and the memory usage of these methods. In the simulations we have different type of parameters. We have physical parameters describing the system and simulation parameters. The physical parameters are the initial state of the system ($|\psi_0\rangle$), the detuning of the transition frequency from the cavity resonance (δ_j), the coupling to the environment (α) and the spectral width (Γ). The simulation parameters are the length of the time step (δt) and the size of the ensemble (M). Units of time are $1/\Gamma$ and other units are thus scaled accordingly.

CPU time, accuracy and memory usage are linked together via the simulation parameters. Physical parameters can have mostly effect on the accuracy, because the CPU time and the memory usage depend on the size of the time step and size of the ensemble. Our plan is to take a fixed set of physical parameters (Table 6.1) and vary the simulation parameters to get quantitative numerical information about the properties of the three different methods.

CPU time is measured with `gprof` [16] which samples the code during the running time. This gives rise to a statistical error in CPU time measurements and it is eliminated by taking the average value of ten independent measurements. Standard deviation for `gprof` is approximately 0.01 seconds which is also the sampling interval. Another useful feature of `gprof` is that it creates a call graph which shows how many percent of the total time is spend on each function. Accuracy is measured by comparing absolute difference of simulated solution to the numerically integrated solution. We do this by finding the absolute value of the maximum deviation of the simulated solution from numerically integrated solution. Memory usage is measured

with `valgrind` and its `massif` tool [22],[27]. This measures heap allocation. Memory allocation methods are the same in each method and thus we assume that results are consistent.

	Two-state	Λ	V	Ladder
$\|\psi_0\rangle$	$\frac{3\|e\rangle+2\|b\rangle}{\sqrt{13}}$	$\frac{4\|e\rangle+2\|a\rangle+\|b\rangle}{\sqrt{21}}$	$\frac{\|a\rangle+\|b\rangle+\|g\rangle}{\sqrt{3}}$	$\frac{4\|e\rangle+2\|a\rangle+\|b\rangle}{\sqrt{21}}$
α	$\sqrt{5}$	$\sqrt{2}$	$\sqrt{2}$	$\sqrt{2}$
δ_a [Γ]	5	3	3	3
δ_b [Γ]	-	5	5	5

Table 6.1: Physical parameters used in simulations when comparing different methods.

6.1 Error vs. ensemble size and time step size

We compare the numerically integrated solution to the solutions calculated with the NMQJ, DHS and THS methods. $\rho_N(t)$ is the numerically integrated density matrix and $\rho_S(t)$ is the simulated density matrix. For each method we calculate

$$\mu_{M,\delta t} = \max_{|k\rangle\in\mathcal{I},t\in T} |\langle k|\rho_N(t)|k\rangle - \langle k|\rho_S(t))|k\rangle|, \tag{6.1}$$

where the states $|k\rangle$ are the states of the system. For example for the two state system, $\mathcal{I} = \{|e\rangle, |g\rangle\}$, the excited and the ground state. $T = [0, 10\,\Gamma^{-1}]$, the time interval in which we study the system. $\mu_{M,\delta t}$ tells us the deviation of the simulated solution from the numerically integrated solution and we can straightforwardly compare how accurate the different methods are. We are only interested in the solutions for the populations for simplicity. This number clearly depends on the values of M and δt. The values of M and δt used in the simulations are in the Table 6.2. We found that the state $|k\rangle$ which gives the maximum absolute error was the same in

δt	0.01	0.03	0.05	0.08	0.1	-	-
M	$1 \cdot 10^5$	$7.5 \cdot 10^4$	$5 \cdot 10^4$	$2.5 \cdot 10^4$	$1 \cdot 10^4$	$5 \cdot 10^3$	$1 \cdot 10^3$

Table 6.2: Values of δt and M used in the simulations.

a given system for all the methods. We have calculated the populations for each system and for all simulation parameters only once with each method. Considering the probabilistic nature of Monte Carlo methods we have statistical uncertainties in values of $\mu_{M,\delta t}$ which could be eliminated with further simulations, but this would require CPU time beyond our current resources. As mentioned in the introduction the errors involved in Monte Carlo methods are characterised by the standard deviation which is $\propto 1/\sqrt{M}$. We have calculated these values for the ensemble sizes used. They are in the Table 6.3. For each method we present two graphical presentations

M	10^5	$7.5 \cdot 10^4$	$5 \cdot 10^4$	$2.5 \cdot 10^4$	10^4	$5 \cdot 10^3$	10^3
$1/\sqrt{M}$	0.0032	0.0037	0.0045	0.0063	0.01	0.014	0.034

Table 6.3: Approximate values of $1/\sqrt{M}$ which gives the order of magnitude of the standard deviation for all three non-Markovian Monte Carlo methods studied.

of $\mu_{M,\delta t}$. In the Appendix (A.1) we give the values of $\mu_{M,\delta t}$ in a tabular form. We consider the following two aspects of the error

i) We expect that the error becomes smaller as we increase the ensemble size and make the time steps smaller. Deviations from this trend are due to the statistical fluctuations which this scheme is unable to eliminate.

ii) We can study the effect of different δt and M values if we study the relations $\mu_{M,\delta t} \approx \mu_{M,\delta t'}$ and $\mu_{M,\delta t} \approx \mu_{M',\delta t}$. If we have for a given ensemble/step size a

situation where two different time steps/ensemble sizes produce a similar error, then there is some region of δt or M values which we can use without affecting the magnitude of the error.

In the next paragraphs we present the results obtained for different systems and methods and in the final paragraph we explain the results and conclude.

Two state system In this system we found that the NMQJ is the most accurate method. It was the only method that had $\mu_{M,\delta t} < 0.003$ for some parameter values, Fig. 6.1. For all the values of δt and M used $\mu_{M,\delta t}$ for the NMQJ is less than 0.03. The smallest value is $\mu^{\mathrm{NMQJ}}_{100000,0.01} \approx 0.0017$ (see Appendix A.1). Considering the Fig. 6.5 we see that $\mu_{M,\delta t} \neq \mu_{M,\delta t'}$. For $M < 10000$ we see that in NMQJ the behavior of $\mu_{M,\delta t}$ changes. Statistical fluctuations become larger and this is reasonable because we have small statistical ensemble.

The DHS method in the two state system has the smallest value of $\mu^{\mathrm{DHS}}_{100000,0.01} \approx 0.0048$ (see the Appendix A.1). All the values of $\mu_{M,\delta t}$ were smaller than 0.06, Fig. 6.1 and the Appendix A.1. In the Fig. 6.1, the large value of $\mu_{25000,0.03}$ is caused by the statistical fluctuations. From the Fig. 6.5 we see that as in the NMQJ case $\mu_{M,\delta t} \neq \mu_{M,\delta t'}$. This effect is larger for DHS than NMQJ. For ensemble sizes $M < 10000$ we see that the behavior of $\mu_{M,\delta t}$ changes but not as much as in NMQJ.

For the THS the smallest $\mu_{M,\delta t}$ obtained was $\mu^{\mathrm{THS}}_{100000,0.01} \approx 0.0040$ and $\mu_{M,\delta t}$ is less than 0.05 for all the parameter values used (see Appendix A.1). In the Fig. 6.1, in the THS case, the values $\mu_{10000,0.01}$ and $\mu_{5000,0.01}$ are larger than expected and this is due the statistical fluctuations. Behavior of the $\mu^{\mathrm{THS}}_{M,\delta t}$ is similar to the DHS case.

V-system The smallest value of $\mu_{M,\delta t}$ for the NMQJ is $\mu^{\mathrm{NMQJ}}_{100000,0.01} \approx 0.0022$ and all the values of $\mu_{M,\delta t} < 0.029$ (see the Appendix A.1). In the Fig. 6.2 we see large statistical fluctuation in the values of $\mu_{25000,0.01}$ and $\mu_{10000,0.01}$. Otherwise the values of $\mu_{M,\delta t}$ behave as expected. We also see that the NMQJ has the largest region

of parameter values for which $\mu_{M,\delta t} < 0.04$. From the Fig. 6.6 we see that the $\mu_{M,0.01} \approx \mu_{M,0.03}$. This is something that did not happen for the two state system. For other values of δt behavior of $\mu_{M,\delta t}$ is similar than two state system.

Smallest value for the DHS is $\mu^{\text{DHS}}_{100000,0.01} \approx 0.0034$ and all the values of $\mu_{M,\delta t} < 0.023$. (see the Appendix A.1). From the Fig. 6.6 we see that the $\mu_{M,0.01} \approx \mu_{M,0.03}$. For the other values of δt the behavior of the $\mu_{M,\delta t}$ is similar as in the two state case. From the Fig. 6.2 we see that the $\mu_{M,\delta t}$ behaves as expected and the values of $\mu_{M,\delta t}$ grow as we get further away from the lower left corner and we also see that the DHS has smallest region of parameter values for which $\mu_{M,\delta t} < 0.04$.

THS has the smallest value of $\mu^{\text{THS}}_{100000,0.03} \approx 0.0020$ and all the values of $\mu_{m,\delta t} < 0.035$ (see the Appendix A.1). It obtained the smallest error with the time step size 0.03. As with the NMQJ and DHS method we see from the Fig. 6.6 that the $\mu_{M,0.03} \approx \mu_{M,0.01}$, except for $M = \{10000, 5000\}$. For the other values of δt behavior is as in the two state system. From the Fig. 6.2 we see statistical fluctuation in the values $\mu_{10000,0.01}$ and $\mu_{5000,0.01}$ and also that the THS has the second largest region of parameter values for which $\mu_{M,\delta t} < 0.04$.

Λ-system The smallest value for NMQJ is $\mu_{10^5,0.01} \approx 0.003$. For all the values of δt and M used $\mu_{M,\delta t} < 0.054$. From the Fig. 6.3 we see that the NMQJ has the largest parameter region for which $\mu_{M,\delta t} < 0.01$. From the Fig. 6.7 one sees that $\mu_{M,\delta t}$ behaves as in the two state system and $\mu_{M,\delta t} \neq \mu_{M,\delta t'}$. In the same figure we see that behavior of the $\mu_{M,0.01}$ does not change even for small M.

The smallest value for the DHS is $\mu_{10^5,0.01} \approx 0.003$. For all the simulation parameter values used $\mu_{M,\delta t} < 0.053$. From the Fig. 6.3 we see that there is same region of parameter values that give $\mu_{M,\delta t} < 0.01$ for the DHS and THS methods in this system. From the Fig. 6.7 we see that $\mu_{M,\delta}$ behaves as in the two state system and $\mu_{M,\delta t} \neq \mu_{M,\delta t'}$.

The smallest value for the THS is $\mu_{10^5,0.01} \approx 0.004$. For all the simulation

parameter values used $\mu_{M,\delta t} < 0.051$. From the Fig.6.3 we see that there is same region of parameter values that give $\mu_{M,\delta t} < 0.01$ for the THS than DHS methods in this system. From the Fig. 6.7 we see that $\mu_{M,\delta t}$ behaves as in two state system and that $\mu_{M,\delta t} \neq \mu_{M,\delta t'}$. In the same figure we see that the values of $\mu_{M,0.1}$ stays approximately constant even for small M.

Ladder-system The smallest value of error for the NMQJ is $\mu_{10^5,0.01} \approx 0.003$. For all the simulation parameter values used $\mu_{M,\delta t} < 0.035$ (see Appendix A.1). From the Fig. 6.4 we see that the NMQJ has the largest region of parameter values which give $\mu_{M,\delta t} < 0.01$. From the Fig. 6.8 we see that $\mu_{M,\delta t} \neq \mu_{M,\delta t'}$.

The smallest value of the error for the DHS is $\mu_{10^5,0.01} \approx 0.005$. For all the simulation parameter values used $\mu_{M,\delta t} < 0.049$ (see the Appendix A.1). From the Fig. 6.4 we see that DHS has second largest region of parameter values which give $\mu_{M,\delta t} < 0.01$. From the Fig. 6.8 we see that $\mu_{25000,0.01} \approx \mu_{25000,0.03}$ and $\mu_{M,0.01} > \mu_{M,0.03}$, when $M < 25000$.

The smallest value of the error for the THS is $\mu_{10^5,0.01} \approx 0.004$. For all the simulation parameter values used $\mu_{M,\delta t} < 0.051$ (see the Appendix A.1). From the Fig. 6.4 we see that the THS has the smallest region of parameter values which give $\mu_{M,\delta t} < 0.01$. From the Fig. 6.8 we see that when $M \leq 10^4$ the behavior of $\mu_{M,\delta t}$ changes for all the δt values.

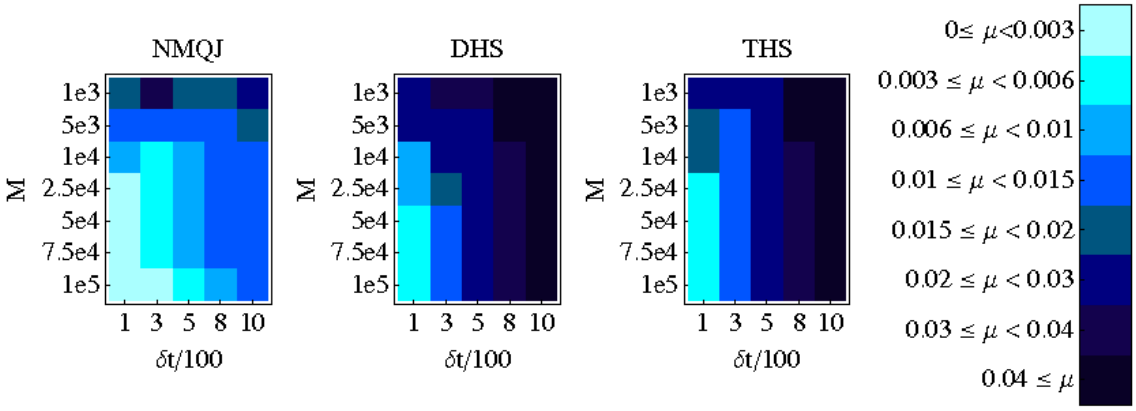

Figure 6.1: $\mu_{M,\delta t}$ for the NMQJ, DHS and THS methods in the two state system.

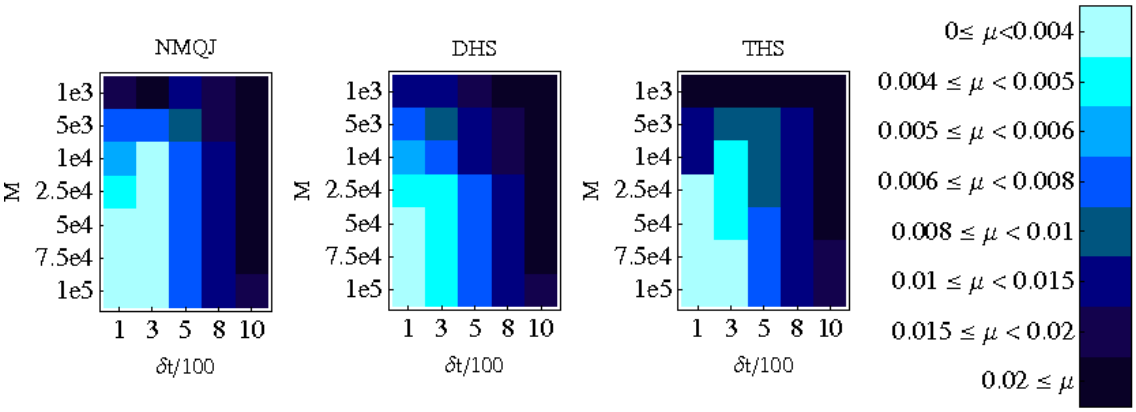

Figure 6.2: $\mu_{M,\delta t}$ for the NMQJ, DHS and THS methods in the V system.

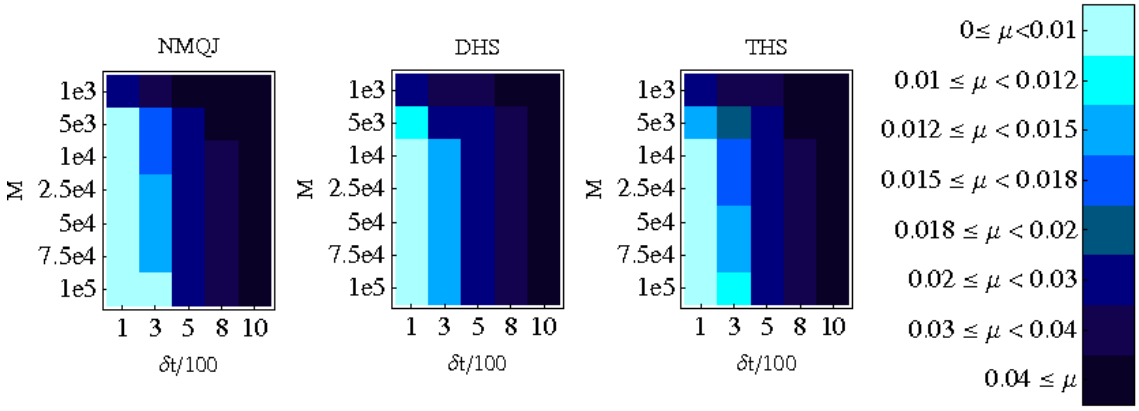

Figure 6.3: $\mu_{M,\delta t}$ for the NMQJ, DHS and THS methods in the Λ system.

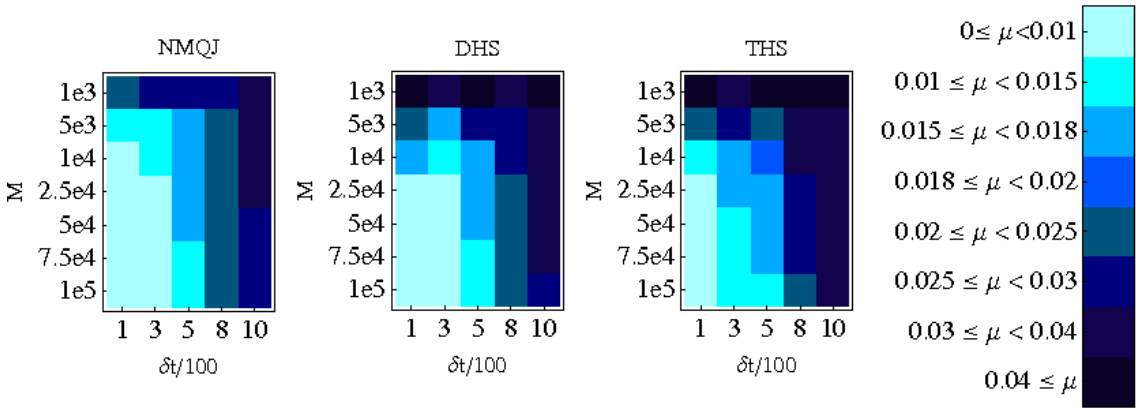

Figure 6.4: $\mu_{M,\delta t}$ for the NMQJ, DHS and THS methods in the Ladder system.

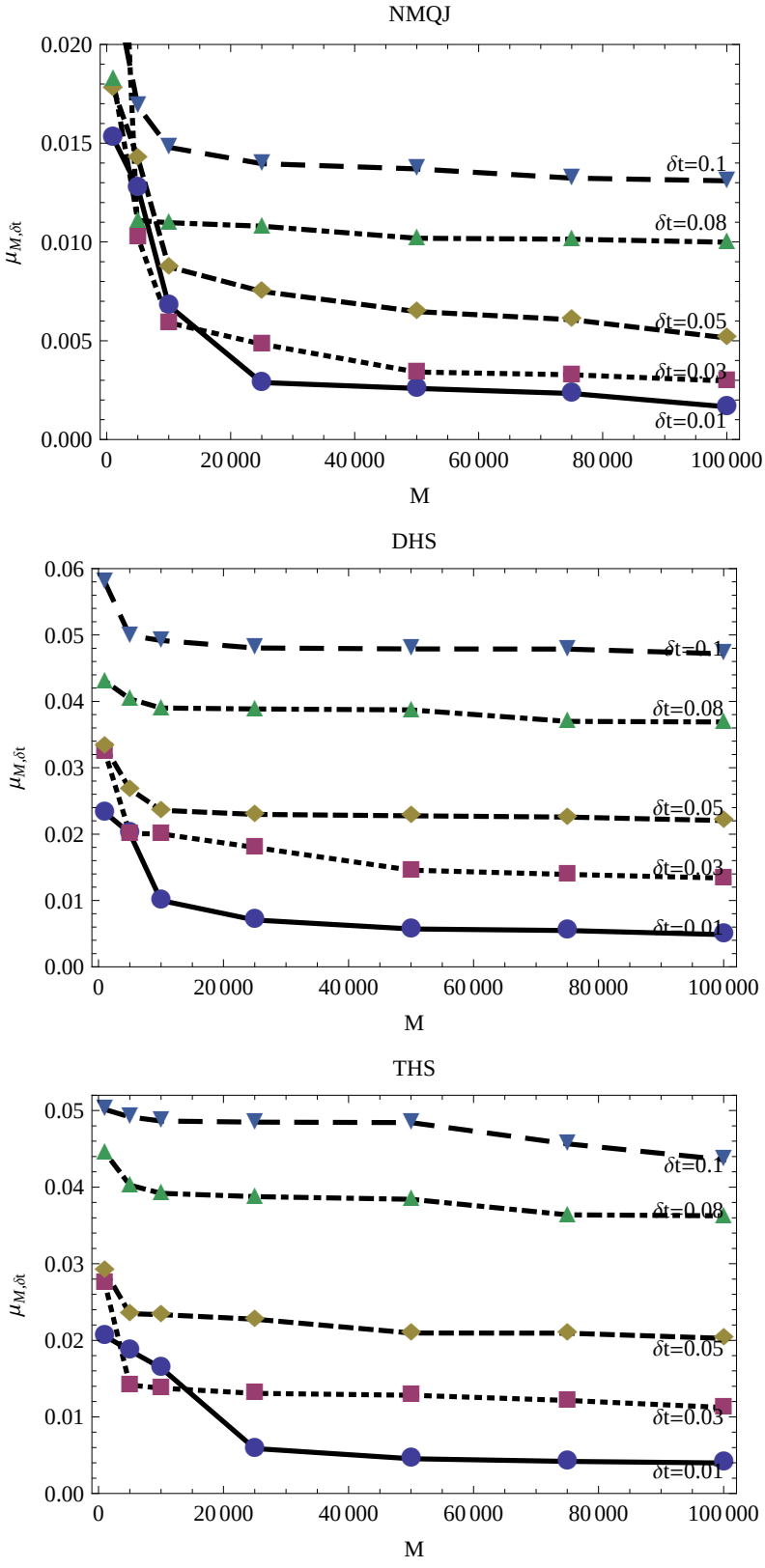

Figure 6.5: $\mu_{M,\delta t}$ for NMQJ, DHS, THS in the two state system with different parameter values.

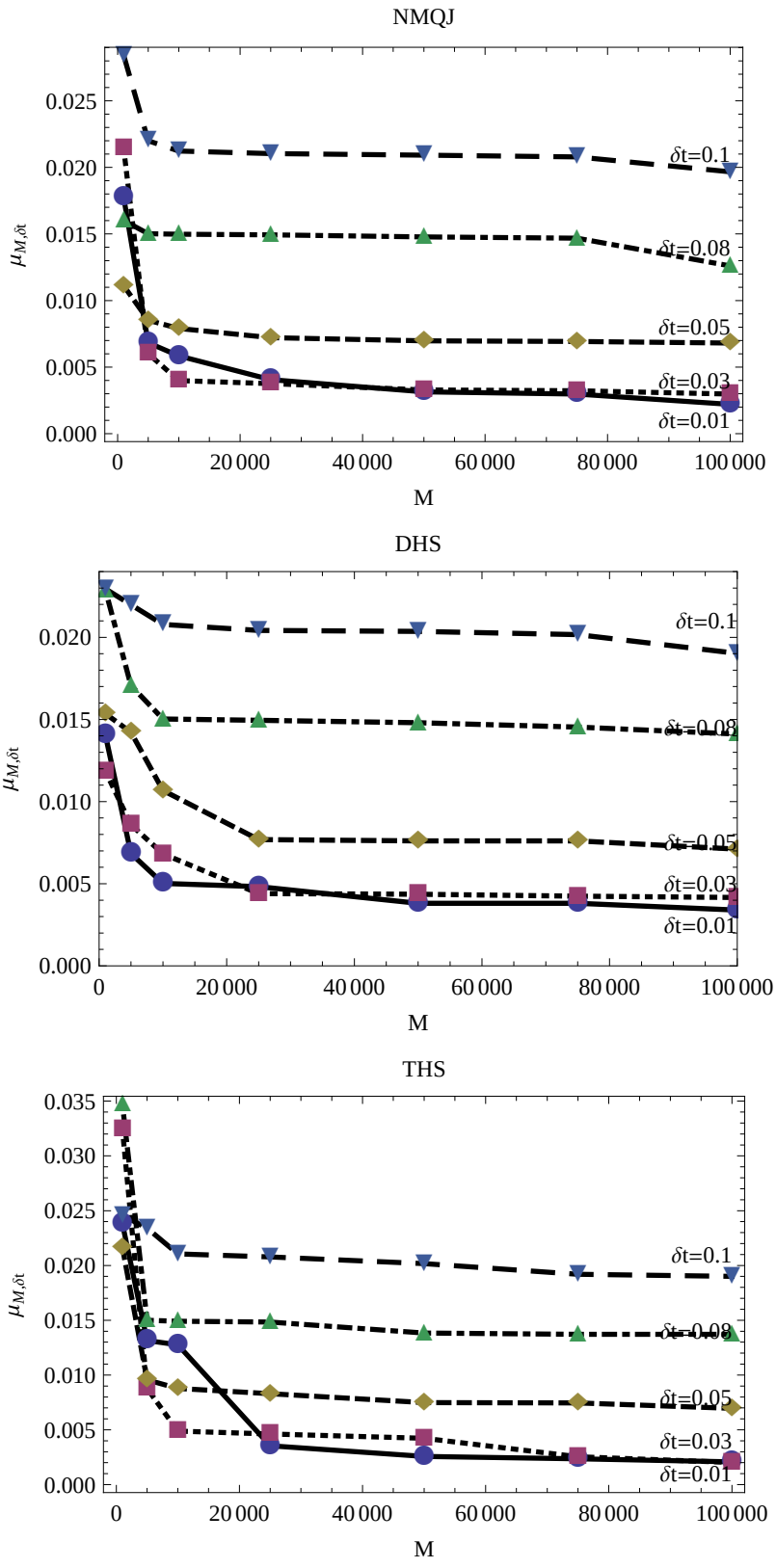

Figure 6.6: $\mu_{M,\delta t}$ for NMQJ, DHS, THS in the V system with different parameter values.

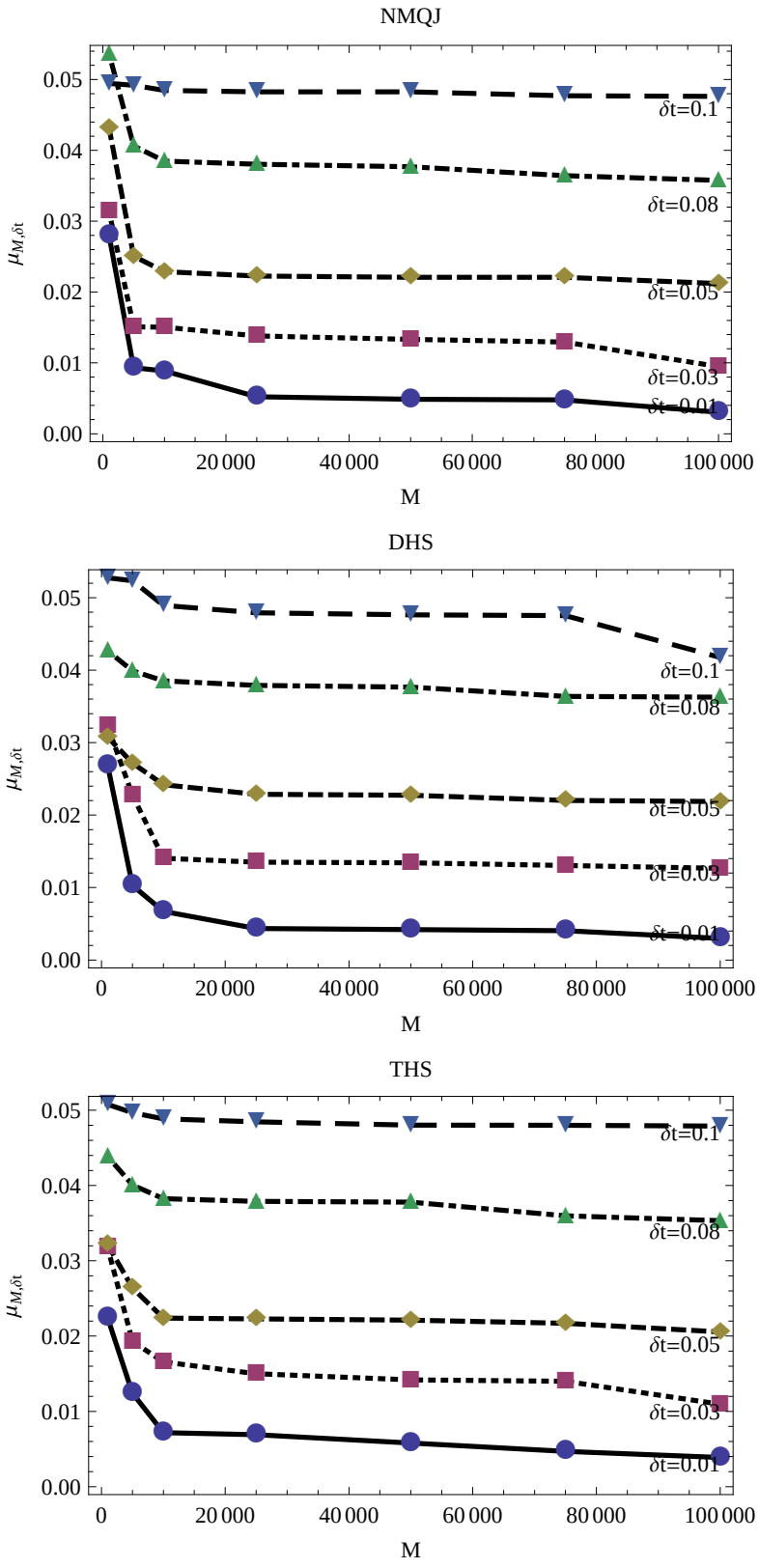

Figure 6.7: $\mu_{M,\delta t}$ for NMQJ, DHS, THS in Λ system with different parameter values.

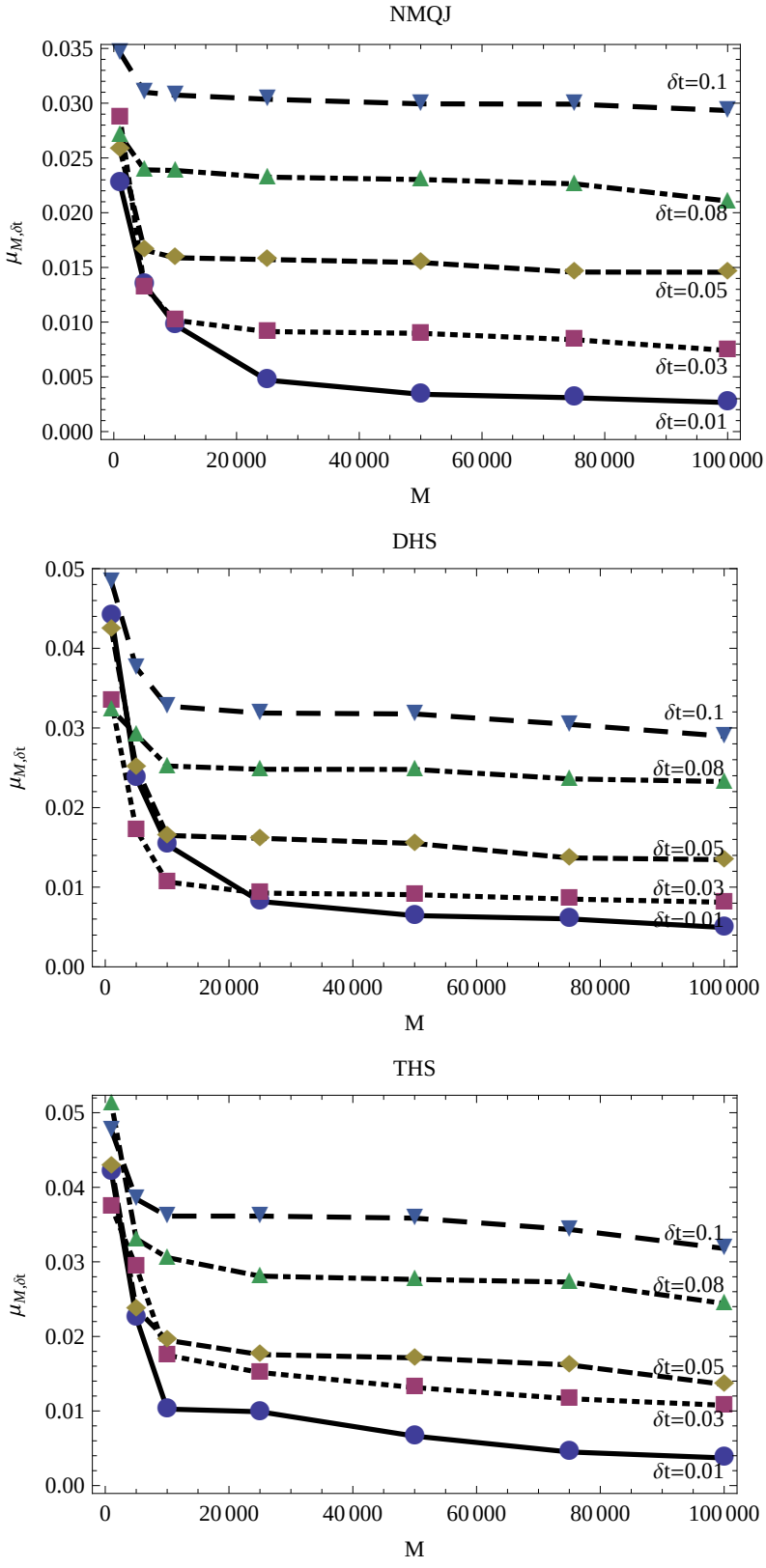

Figure 6.8: $\mu_{M,\delta t}$ for NMQJ, DHS, THS in the ladder system with different parameter values.

Conclusions We have seen two different kind of behavior for the $\mu_{M,\delta t}$. First one is that $\mu_{M,\delta t} \approx \mu_{M',\delta t}$. This means that we can save computational resources because larger ensemble size does not increase accuracy. We can say that in general when $M \geq 25 \cdot 10^3$ this behavior was detected in all systems and with all methods. For time steps 0.1 and 0.08 we have seen this behavior in THS method for two-state and Λ-systems for all M values used. Second type of behavior is that $\mu_{M,\delta t} \approx \mu_{M,\delta t'}$. This was seen in the V-system for all the methods with the time steps 0.01 and 0.03, when ensemble size $M \geq 25000$. This type of behavior also helps to save computational resources because we could increase the time step size without the loss of accuracy.

One reason for the different behavior in V-system is the strength of the coupling. We had $\alpha^2 = 2$ in the V-system. Level geometry in this system also couples the excited states and the ground state more weakly than in the other systems. We have studied this more with the following example. We considered the two state system with the parameter values $\alpha^2_{\text{two-state}} = 2$ and $\delta = 5$ and examined the initial state $|\psi_0\rangle = \sqrt{2/3}|g\rangle + \sqrt{1/3}|e\rangle$ and compared it to a case where $\alpha'^2_{\text{two-state}} = 5$. We found that with the smaller coupling the difference between $|\mu_{M,0.01} - \mu_{M,0.03}|$ was smaller, see the Fig. 6.9.

For the parameter values and the systems studied so far we see that all the methods behave similarly, but that the NMQJ has slightly better accuracy than THS and DHS. This can be seen for example if we consider the Figs. 6.5, 6.6, 6.7, 6.8 and calculate the number of such pairs of $(M, \delta t)$ values that $\mu_{M,\delta t}$ is in the smallest range in each figure. We see that the NMQJ has the largest number of pairs

$$\text{NMQJ} : 29,$$

$$\text{DHS} : 16,$$

$$\text{THS} : 15,$$

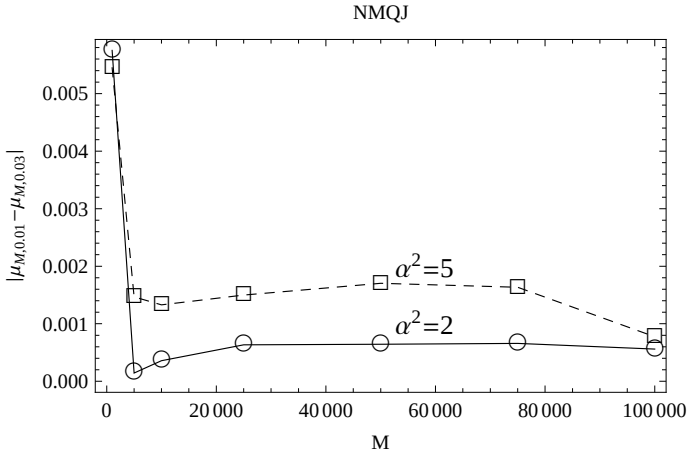

Figure 6.9: $|\mu_{M,0.01} - \mu_{M,0.03}|$ with $\alpha^2 = \{5, 2\}$ and with the initial state $|\psi_0\rangle = \sqrt{2/3}|g\rangle + \sqrt{1/3}|e\rangle$ in two state system.

which suggests that the NMQJ is more accurate than the DHS and THS methods. These results must be considered incomplete because of the lack of statistical aspect of the error analysis. NMQJ is more accurate than DHS and THS because:

- Jumps during the negative decay rate make the ensemble effectively smaller in THS. In NMQJ we simply "cancel" the earlier jumps during the negative decay rate and increase the population of the deterministic initial state. In THS we lose the state to $\mathcal{H}_3$ which does not contribute to the dynamics. This makes the ensemble size smaller because we have less states that contribute to the ensemble average.

- Number of the jumps in the negative decay rate has to match to the increase of the norm of the deterministically evolving state in DHS. This is a source of statistical error. One can study this by calculating $\mathrm{tr}[\rho_{\mathrm{S}}(t)]$, where S stands for the simulated density matrix. This is unity (in numerical sense) for the NMQJ and THS methods but not for the DHS method. See the Fig. 6.10.

- The deterministic evolution is solved from a linear differential equation in

NMQJ and from a non-linear differential equation in DHS. Error in the deterministic evolution causes error in the jump probabilities and that causes error in the number of jumps. Usually this error is smaller than statistical error coming from the Monte Carlo sampling.

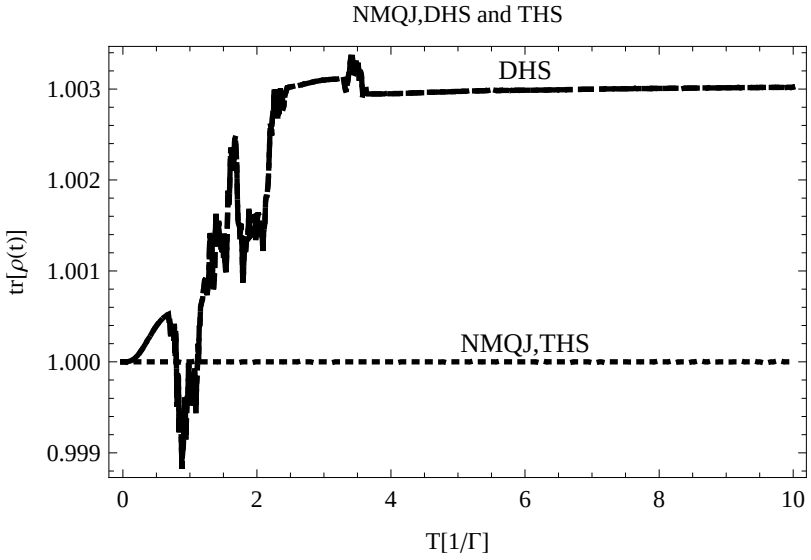

Figure 6.10: $\mathrm{tr}[\rho(t)]$ for the NMQJ, DHS and THS methods in the Λ -system. $\mathrm{tr}[\rho_{\mathrm{NMQJ}}(t)] = \mathrm{tr}[\rho_{\mathrm{THS}}(t)] = 1$. For DHS the trace of the density matrix does not stay constant. Noisy parts corresponds to times when one or both decay rates are negative. We see here that the number of the jumps does not match exactly to the increase of norm during negative decay rates. Norm differs from unity for the positive decay rates because of the error that emerges from solving the non-linear differential equation.

6.2 CPU time vs. ensemble size and time step size

Two state system NMQJ is faster than the DHS and THS methods with the parameter values used in the two state system. For the NMQJ method the running time of the code was so short that we could not get accurate measurements. See

Appendix A.2 for further explanation. Reason for that the NMQJ is so much faster than the DHS and THS is that in the NMQJ the ensemble consists effectively on two states only, the ground state and the deterministic initial state. This means that in the NMQJ we must evolve only the deterministic initial state over the interval $[0, T = 10/\Gamma]$ because the ground state is invariant. Only job that is left is to determine the jumps and generate the random numbers. In the DHS and THS methods in their standard form we must evolve all M ensemble members separately and the size of the Hilbert space is doubled and tripled respectively. Referring back to the Sec. 6.1 and choosing the parameters $(M, \delta t)$ in such way that $\mu_{M,\delta t} < 0.006$ we obtain the following minimum CPU times for each method:

$$\begin{aligned} \text{NMQJ:}\{M = 10000,\ \delta t = 0.03\} \quad & T_{\text{CPU}}^{\text{NMQJ}} = 0.011 \text{ s}, \\ \text{DHS:}\{M = 50000,\ \delta t = 0.01\} \quad & T_{\text{CPU}}^{\text{DHS}} = 13.339 \text{ s}, \\ \text{THS:}\{M = 25000,\ \delta t = 0.01\} \quad & T_{\text{CPU}}^{\text{THS}} = 6.799 \text{ s}. \end{aligned}$$

This shows that the NMQJ is more efficient than the DHS or THS with the parameter values used and that the THS is more efficient than DHS. Notice that $M^{\text{DHS}} = 5 \cdot M^{\text{NMQJ}}$, $M^{\text{THS}} = 2.5 \cdot M^{\text{NMQJ}}$ and $\delta t^{\text{DHS,THS}} = 3 \cdot \delta t^{\text{NMQJ}}$. This suggests that the NMQJ is also more accurate method than the DHS or THS because we can use larger time step and smaller ensemble size and still reach the same accuracy. In the Fig. 6.11 we have a graphical presentation of the behavior of the CPU time in this system. We see that it depends linearly on the ensemble size and the size of the time step defines its derivative. Slope of the line depends on δt because smaller time step increases the total number of time steps in the interval.

V system NMQJ method has advantage over DHS and THS because for this system $M_{\text{eff}} = 2$ and the dimension of Hilbert space is three. In DHS we must evolve M state vectors in six dimensional Hilbert space and in THS we must evolve

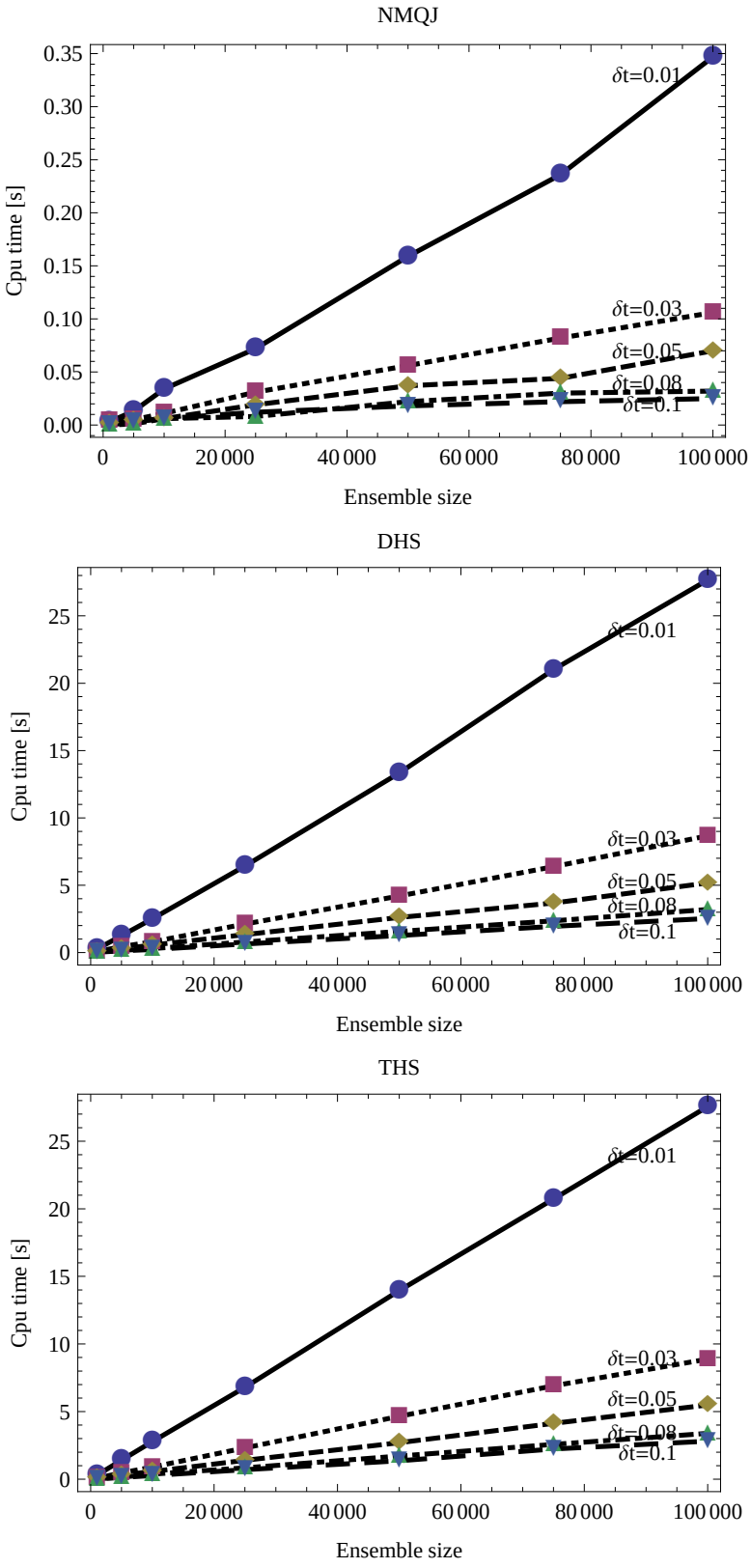

Figure 6.11: CPU times for different methods in the two state system.

M state vectors in nine dimensional Hilbert space. CPU time increases linearly with M for all methods, see Fig. 6.12. Referring back to the Sec. 6.1 and choosing the parameters $(M, \delta t)$ in such way that $\mu_{M,\delta t} < 0.004$, we obtain the following minimal CPU times for each method:

$$\begin{aligned} \text{NMQJ:}\{M = 10000,\ \delta t = 0.03\} \quad & T_{\text{CPU}}^{\text{NMQJ}} = 0.02 \text{ s}, \\ \text{DHS:}\{M = 50000,\ \delta t = 0.01\} \quad & T_{\text{CPU}}^{\text{DHS}} = 19.238 \text{ s}, \\ \text{THS:}\{M = 75000,\ \delta t = 0.03\} \quad & T_{\text{CPU}}^{\text{THS}} = 10.66 \text{ s}. \end{aligned}$$

Again NMQJ is faster compared to the DHS and THS methods. Difference between DHS and THS is larger than in the two state system case. Notice that in this case we have the same time step size for the NMQJ and THS methods, $\delta t^{\text{NMQJ,THS}} = 0.03$, but the NMQJ method uses much smaller ensemble size. The DHS method on the other hand uses smaller time step and larger ensemble size than NMQJ. The THS method uses the largest ensemble size.

Λ system In this system NMQJ has $M_{\text{eff}} = 3$. This is a more complex system than the two previous ones. Dimension of the Hilbert space is three for NMQJ. For DHS it is six and for THS nine. CPU time increases linearly with M for all the methods, as we can see from the Fig. 6.13. Referring back to the Sec. 6.1 and choosing the parameters $(M, \delta t)$ in such way that $\mu_{M,\delta t} < 0.01$ we obtain the following minimal CPU-times for each method:

$$\begin{aligned} \text{NMQJ:}\{M = 5000,\ \delta t = 0.01\} \quad & T_{\text{CPU}}^{\text{NMQJ}} = 0.019 \text{ s}, \\ \text{DHS:}\{M = 10000,\ \delta t = 0.01\} \quad & T_{\text{CPU}}^{\text{DHS}} = 4.641 \text{ s}, \\ \text{THS:}\{M = 10000,\ \delta t = 0.01\} \quad & T_{\text{CPU}}^{\text{THS}} = 4.319 \text{ s}. \end{aligned}$$

Once again NMQJ is much faster than DHS and THS. This time it seems that the DHS and THS are equal and we cannot say for sure which one is faster because of the fluctuations in the CPU time measurements. NMQJ can obtain the same accuracy as the DHS and THS methods but with smaller ensemble size.

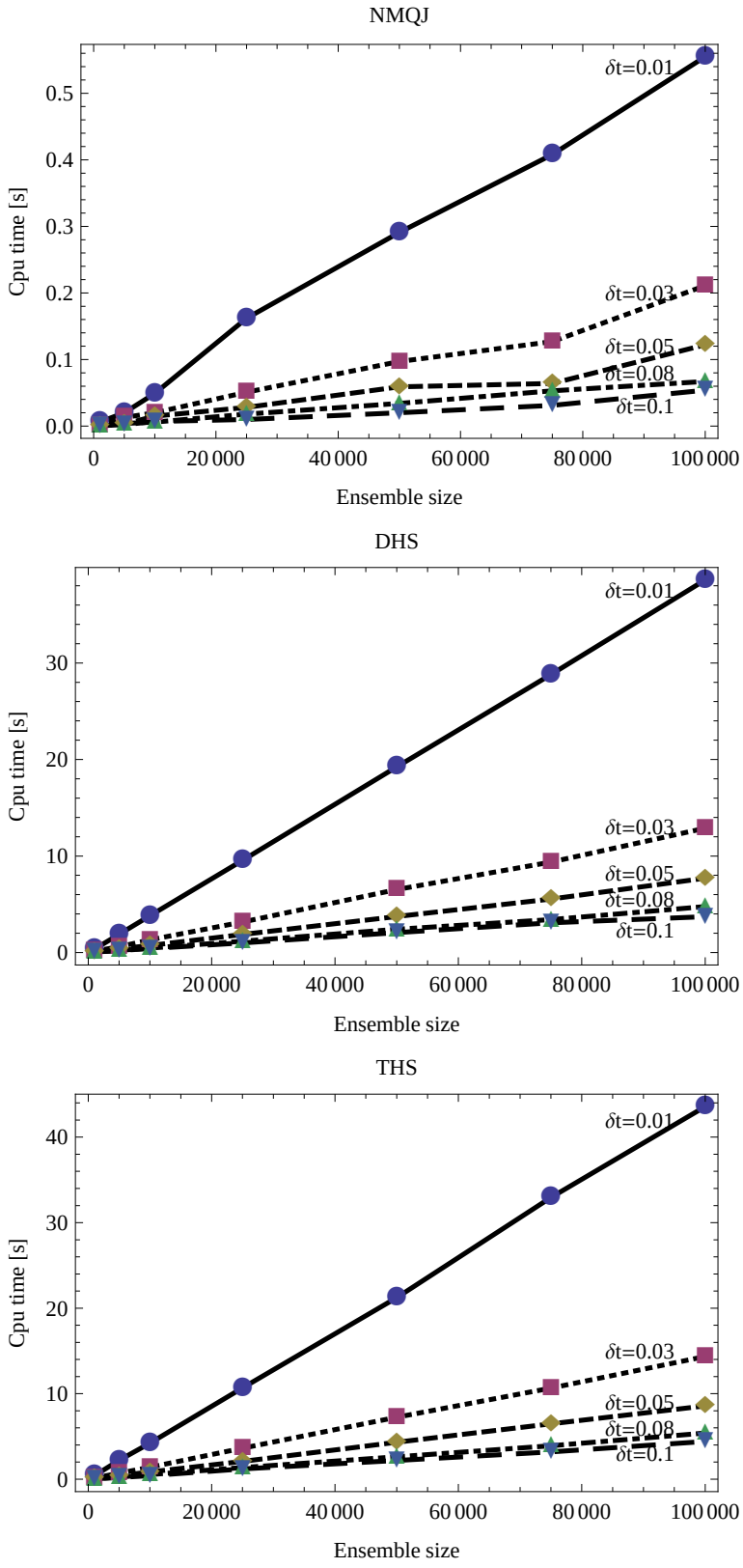

Figure 6.12: CPU times with different methods in the V system.

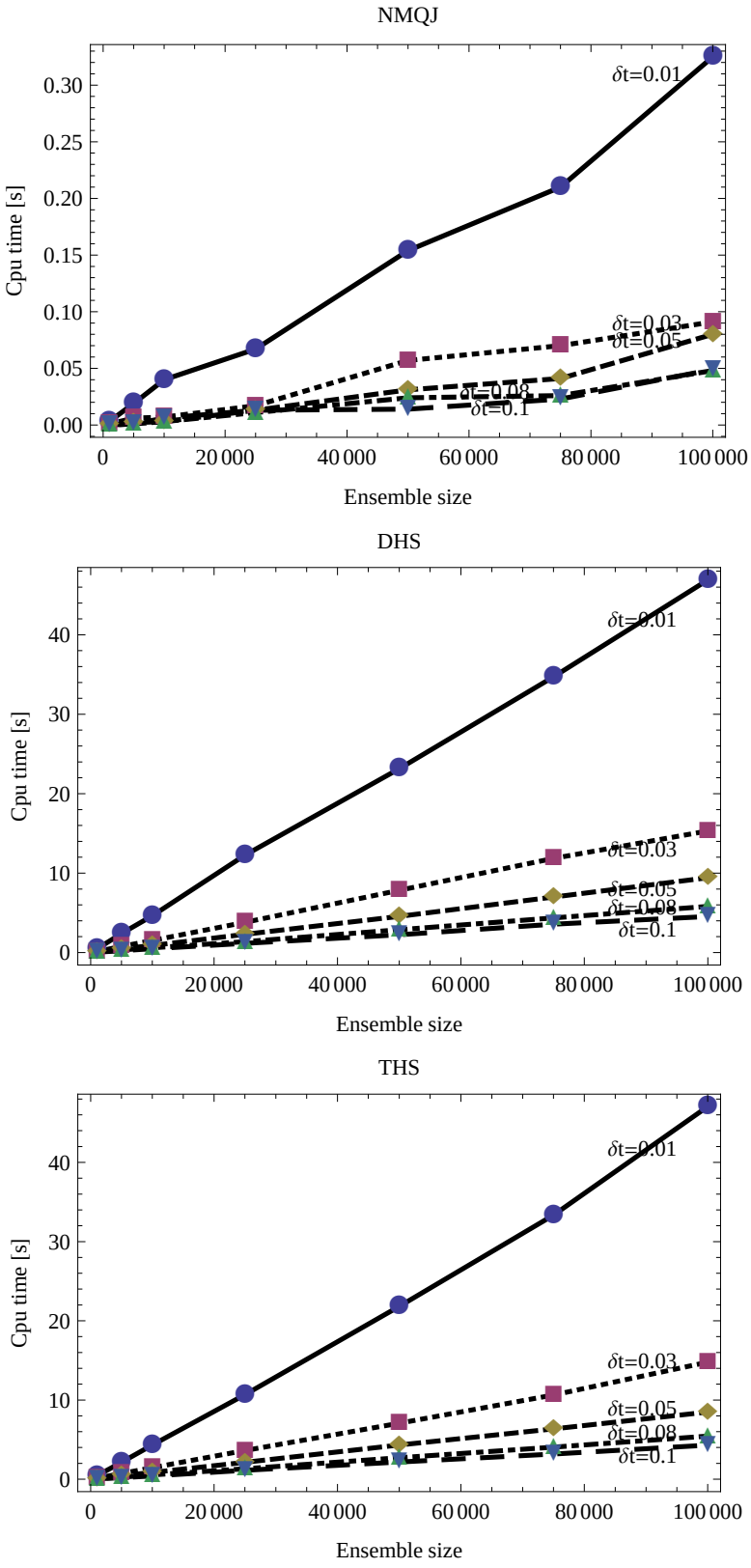

Figure 6.13: CPU times with different methods in the Λ system.

Ladder system In this system NMQJ has $M_{\text{eff}} = 3$. Dimension of the Hilbert space is three for NMQJ. For DHS it is six and for THS nine. CPU time increases linearly with M for all the methods as we see from the Fig. 6.14. Referring back to the Sec. 6.1 and choosing the parameters $(M, \delta t)$ in such way that $\mu_{M,\delta t} < 0.01$ we obtain the following minimal CPU-times for each method:

$$\begin{aligned} \text{NMQJ:}\{M = 25000,\ \delta t = 0.03\} \quad & T_{\text{CPU}}^{\text{NMQJ}} = 0.042 \text{ s}, \\ \text{DHS:}\{M = 25000,\ \delta t = 0.03\} \quad & T_{\text{CPU}}^{\text{DHS}} = 3.198 \text{ s}, \\ \text{THS:}\{M = 25000,\ \delta t = 0.01\} \quad & T_{\text{CPU}}^{\text{THS}} = 10.617 \text{ s}. \end{aligned}$$

In this case we see that NMQJ is much faster than DHS and THS and that DHS is significantly faster than THS. DHS is faster than THS in this case because we must use shorter time step in THS than in DHS in order to reach desired accuracy. If we consider the THS method with $\delta t = 0.03$ we have THS:$\{M = 25000,\ \delta t = 0.03\}$ $T_{\text{CPU}}^{\text{THS}} = 3.559$, which is consistent with the cases with the other systems.

Conclusions We have seen that the usage of CPU time increases linearly with the ensemble size. The following reasons for the performance differences are obtained from the call graph generated by `gprof`. For the DHS and THS methods we describe the operations that consume the most of the CPU time. Reasons why the NMQJ method is so fast:

- We do not have to evolve all M ensemble members separately. In these systems with the parameter values used we had to evolve only one state, the deterministic initial state.

- The most time consuming part is the determination of the jumps. This is done in a way where we do not necessarily have to go through the whole ensemble

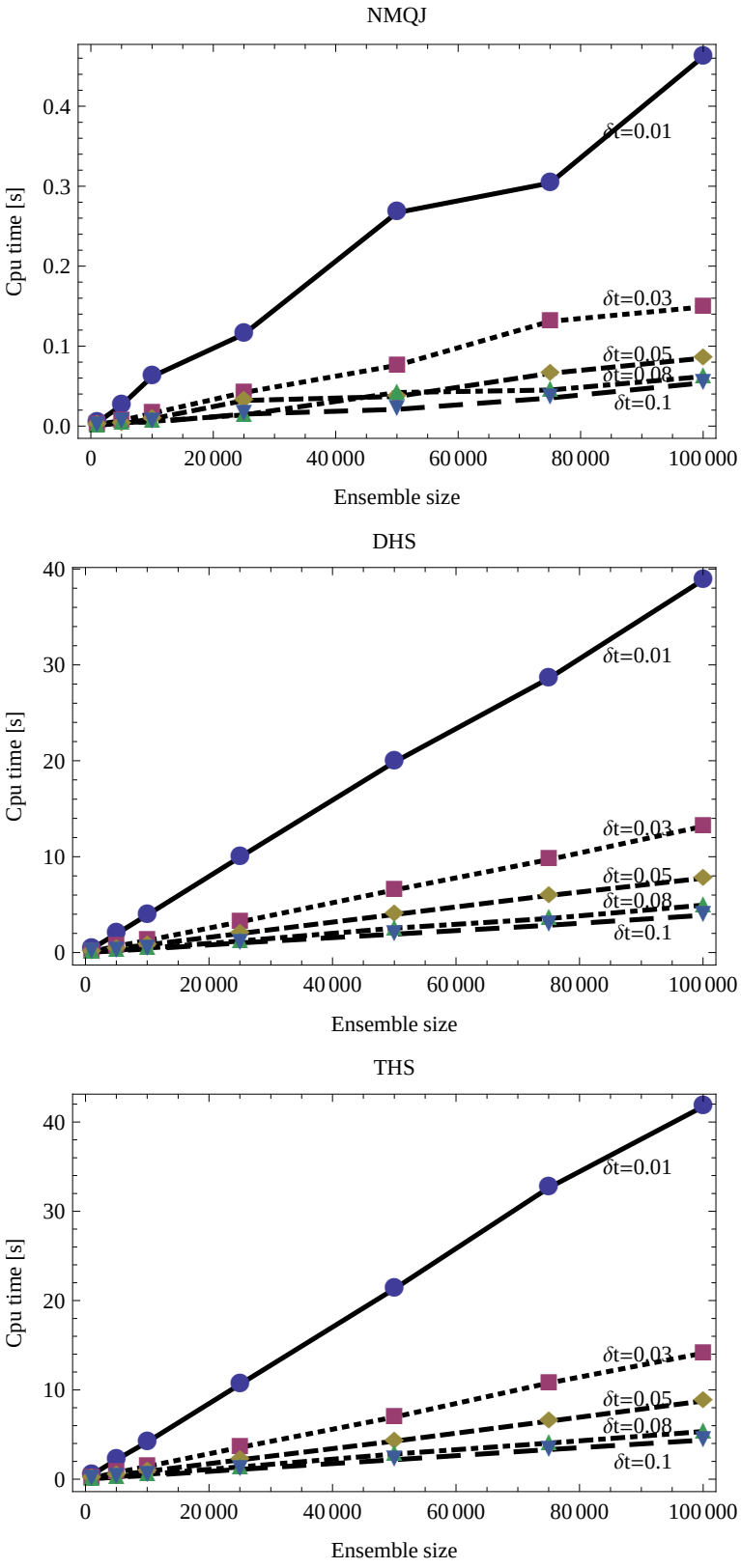

Figure 6.14: CPU times with different methods in the ladder system.

but only the part that can jump. This reduces the CPU time consumption in more complex systems.

Reasons why the DHS method is slower than the NMQJ method:

- We have to separately evolve all M ensemble members.
- In a j-level system, for every ensemble member $\theta_k(t_n) = \begin{pmatrix} \phi_k(t_n) & \psi_k(t_n) \end{pmatrix}^T$ at time t_n, we have to calculate one realization for the population of state $|a_j\rangle$ as $\rho_{aa,k}(t_n) = \langle a_j|\phi_k(t_n)\rangle\langle\psi_k(t_n)|a_j\rangle$, (see the Sec. (4.2)). This must be done j times to obtain the realizations for the populations of all j states. During the simulation this means $\propto M \cdot N \cdot j$ floating point operations (flops). Proportionality constant comes from the calculation of $\rho_{aa,k}(t_n)$ because we multiply two complex numbers.
- Because of the non-linearity of the generator of the deterministic evolution we have to calculate the total jump probability separately for every ensemble member using the jump operators

$$P_{\mathrm{tot},k}(t) = \sum_i \frac{J_i(t)\theta_k(t)}{||J_i(t)\theta_k(t)||}\delta t.$$

  This costs $\propto M \cdot N \cdot s$ flops. s is the number of jump channels. Proportionality constant comes from the linear algebra and the square root operation involved.

These operations consume approximately 50% of the CPU time of DHS method. Reasons why the THS method is slower than the NMQJ method:

- We have to separately evolve all the ensemble members.
- For every ensemble member $\Phi_k(t_n) = |\psi_{k,1}(t_n)\rangle \oplus |\psi_{k,2}(t_n)\rangle \oplus |\psi_{k,3}(t_n)\rangle$ in a j-level system at time t_n we have to calculate the population of states $|a\rangle$ as $\rho_{aa,k}(t) = \langle a|\psi_{k,1}(t)\rangle\langle\psi_{k,2}(t)|a\rangle$ and an inner product $C_k(t) = \langle\psi_{k,1}(t)|\psi_{k,2}(t)\rangle$ to see how many states are still in the subspace $\mathcal{H}_1 \oplus \mathcal{H}_2$ and thus achieve the

correct normalization. This costs the same $\propto M \cdot N \cdot j$ flops as in the DHS plus the additional cost of calculating $C_k(t_n)$.

- Estimation of populations of the states $|a\rangle$ at time t_n:

$$\hat{\rho}_{aa}(t_n) = \frac{E(|\psi_1\rangle\langle\psi_2|)}{E(\langle\psi_1|\psi_2\rangle)} = \frac{\sum_{k=0}^{M-1}\langle a|\psi_{k,1}(t_n)\rangle\langle\psi_{k,2}(t_n)|a\rangle}{\sum_{l=0}^{M-1} C_l(t_n)}.$$

  Here we have two summations of M real numbers. When the ensemble size becomes smaller the cost of this comes also smaller. For the j-level system the nominator has to be calculated j times but the denominator only once.

These operations consume approximately 50 % of CPU time of THS method. In the DHS method there is also the calculation of the ensemble average (as in THS) but without the division operation. It was not one of the most costly operations. NMQJ is superior compared to DHS and THS methods in their standard form. We see from the previous that even if we could optimize the THS and DHS methods in a way that we could eliminate 50 % of their CPU time consumption we could not achieve the same performance as with the NMQJ.

6.3 Memory consumption

In this section we measure how much computer memory each of the methods uses. In the measurements we use a tool called `massif` which is a part of the `valgrind`. It is clear that the NMQJ method needs the smallest amount of memory. Also its memory consumption depends only on the size of the time step δt, when the total time interval in which we observe our system is constant, and on the number M_{eff}. The THS and DHS methods depend on δt and M.

We have an ensemble size of M state vectors. The largest amount of memory is used on storing the M different realizations of the process. In these simulations where we want to calculate only the populations it means that in a j-level system we need to store jM `double` precision numbers in each time step to calculate the

ensemble averages in the DHS and THS methods. In the NMQJ method we have to store j `complex` numbers and M_{eff} `integer` numbers to calculate the ensemble average in each time step. Then there is some additional memory consumption which comes from storing all the operators needed and so on. We present the analysis method in detail with the two state system and only the results of the similar analysis made for the ladder system. Values of δt used in the NMQJ memory consumption measurements are in the Table 6.4. Values of δt and M used for the DHS and THS methods' memory consumption measurements are in the Table 6.5. We had to use smaller ensembles and larger time steps than with the NMQJ because the measurement slowed down the code so much.

δt $[\Gamma^{-1}]$	0.01	0.03	0.05	0.08	0.1

Table 6.4: Values of δt used for memory consumption measurements for NMQJ.

δt $[\Gamma^{-1}]$	0.03	0.05	0.06	0.08	0.1	-	-
M	$1 \cdot 10^3$	$5 \cdot 10^3$	$10 \cdot 10^3$	$15 \cdot 10^3$	$25 \cdot 10^3$	$35 \cdot 10^3$	$50 \cdot 10^3$

Table 6.5: Values of δt and M used for memory consumption measurements for DHS and THS.

NMQJ in the two state system The physical parameters used were the same as in the Sec. 6. Results are in the Table (6.6). Memory consumption seems to be $\propto \frac{1}{\delta t}$ which is verified by fitting a curve $a + \frac{b}{\delta t}$ to the data. We obtain the following parameter values $\{a \to 55.1098, b \to 0.88001\}$. A graphical presentation is in the Fig. 6.15.

δt [Γ^{-1}]	0.01	0.03	0.05	0.08	0.1
mem [kB]	143.116	84.420	72.716	66.116	63.916

Table 6.6: Memory used in the two state system with the NMQJ method.

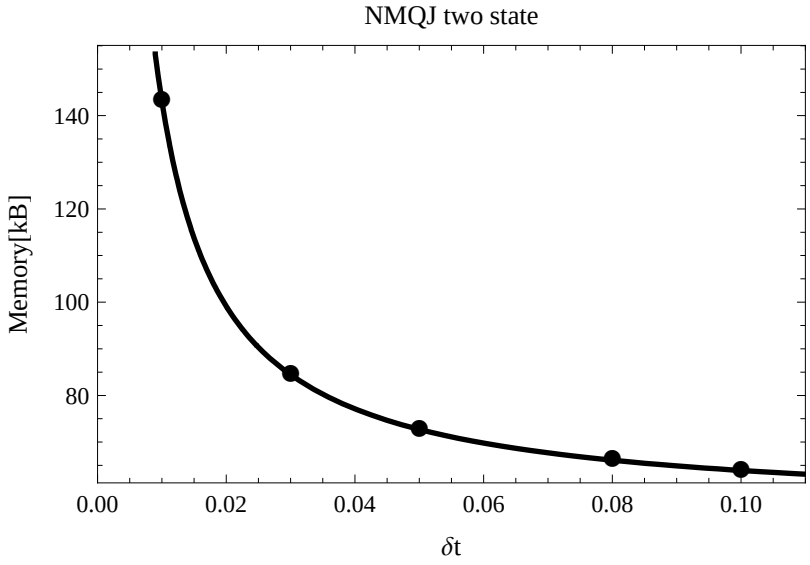

Figure 6.15: Memory consumption of the NMQJ method in the two state system.

DHS in the two state system We group the data according to the M value used and get data sets as a function of δt. We expect again that the dependence on δt is inversely proportional. We also expect that the different M values just scale the y-axis. We verify this by fitting a curve $x \to a_M + \frac{b_M}{x}$ to the data in the Table 6.7. The subscript M reminds us that we make this fit for each of the M values used separately. Values of b_M obtained from the fit are in the Table 6.8 for the different M values used. They are nearly identical. Their mean value is $\bar{b} = 0.237876$. Values of a_M are in the Table 6.9. To these values we fit the following $x \to c + dx$ curve. This is a function of the ensemble size M. We obtain the following values for the parameters $\{c \to 50.7357, d \to 0.0800004\}$. We have plotted the fit in the Fig. 6.16. Now we can extrapolate to other parameter values by using the following equation

$\delta t,\ M$	1e3	5e3	10e3	15e3	25e3	35e3	50e3
0.03	136.348	856.252	1256.25	2056.25	2856.25	456.348	4056.25
0.05	133.156	853.156	1253.06	2053.06	2853.16	453.06	4053.06
0.06	132.268	852.268	1252.27	2052.27	2852.36	452.268	4052.36
0.08	131.356	851.356	1251.26	2051.36	2851.26	451.356	4051.36
0.1	130.756	850.756	1250.76	2050.66	2850.66	450.756	4050.76

Table 6.7: Memory consumption of the DHS method in the two state system. Measured in kB.

M	1e3	5e3	10e3	15e3	25e3	35e3	50e3
b_M	0.240128	0.239697	0.235863	0.237157	0.237876	0.239505	0.234904

Table 6.8: Values of b_M for the DHS method in the two state system.

M	1e3	5e3	10e3	15e3	25e3	35e3	50e3
a_M	128.334	448.323	848.394	1248.33	2048.32	2848.31	4048.41

Table 6.9: Values of a_M for the DHS method in the two state system.

$$m^{\mathrm{TS}}_{\mathrm{DHS}}(M, \delta t) \approx 48.330635\,\mathrm{kB} + 0.080001 \cdot M\,\mathrm{kB} + \frac{0.237876\,\Gamma^{-1}}{\delta t}\,\mathrm{kB}. \tag{6.2}$$

We have studied graphically the quality of the extrapolation function in the Fig. 6.17. We see that it fits well to the data obtained from the opposite ends of M values used in the measurement.

THS in the two state system We use the same values of M and δt as with the DHS method. Memory consumption should be $\propto \frac{1}{\delta t}$ and $\propto M$. The measured results are in the Table 6.10. Fitting a curve $x \to a_M + \frac{b_M}{x}$ as a function of δt to the

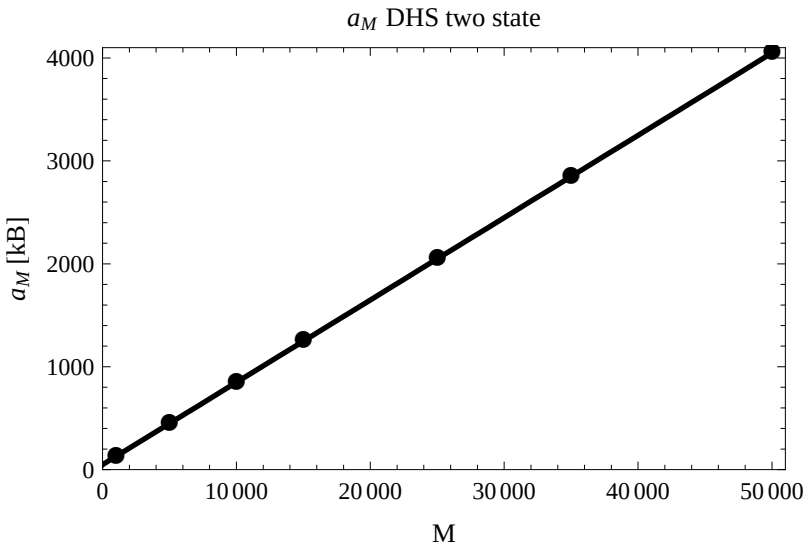

Figure 6.16: a_M values and fit. Fit is good.

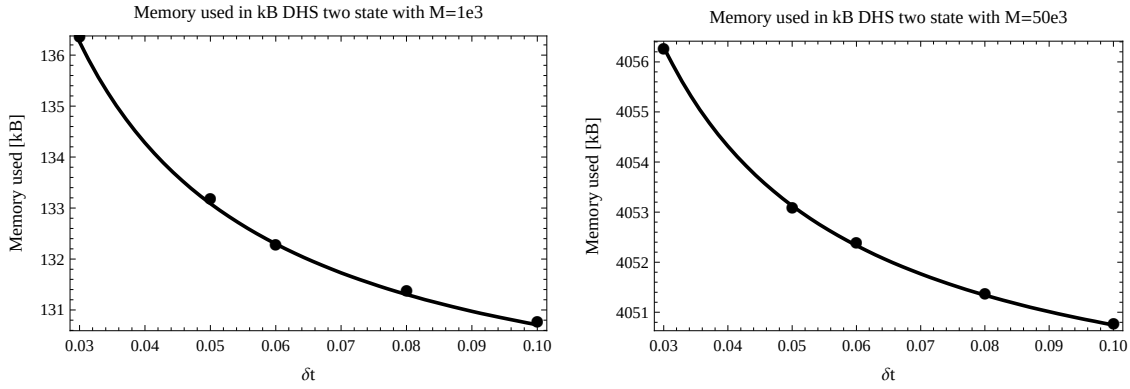

Figure 6.17: Extrapolating function fits nicely to the data from the opposite ends of the measured memory values.

data from the different M values used, we obtain that $b_M = 0.239601 \,\forall\, M$ and the different values of a_M are in the Table 6.11. Thus fitting a curve $x \to c + dx$ as an function of M to a_M values obtained we get the following values for the parameters $\{c \to 79.2514, d \to 0.12\}$. Fit is presented graphically in the Fig. 6.18. Now we can define an extrapolating function for the memory consumption of the THS method

$\delta t,\ M$	1e3	5e3	10e3	15e3	25e3	35e3	50e3
0.03	207.236	1287.24	1887.24	3087.24	4287.24	687.236	6087.24
0.05	204.044	1284.04	1884.04	3084.04	4284.04	684.044	6084.04
0.06	203.252	1283.25	1883.25	3083.25	4283.25	683.252	6083.25
0.08	202.244	1282.24	1882.24	3082.24	4282.24	682.244	6082.24
0.1	201.644	1281.64	1881.64	3081.64	4281.64	681.644	6081.64

Table 6.10: Memory consumption of the THS method in the two state system. Measured in kB.

M	1e3	5e3	10e3	15e3	25e3	35e3	50e3
a_M	199.251	679.251	1279.25	1879.25	3079.25	4279.25	6079.25

Table 6.11: Values of a_M for the THS method in the two state system.

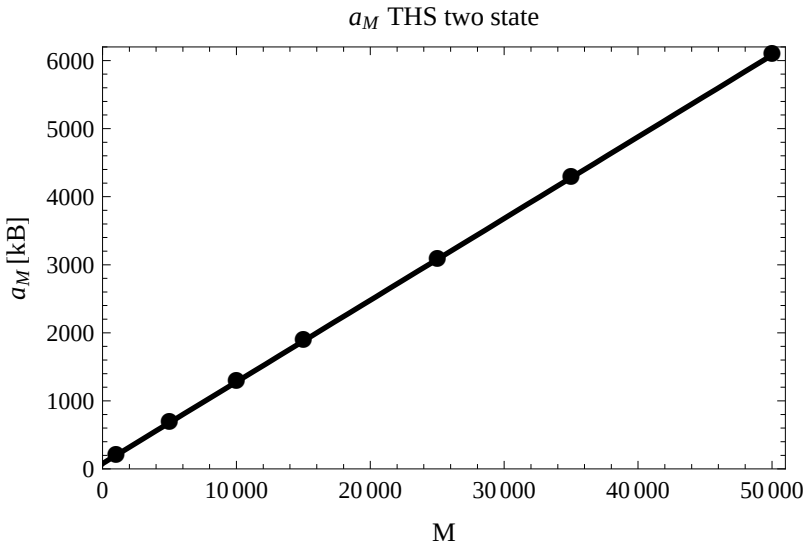

Figure 6.18: a_M values and fit. The fit is good.

in the two state system

$$m^{\mathrm{TS}}_{\mathrm{THS}}(M,\delta t) \approx 79.2514\,\mathrm{kB} + 0.12\cdot M\,\mathrm{kB} + \frac{0.239601\,\Gamma^{-1}}{\delta t}\,\mathrm{kB}. \tag{6.3}$$

We have studied the quality of the extrapolating function graphically in the Fig. 6.19 in the opposite ends of M values used in this measurement.

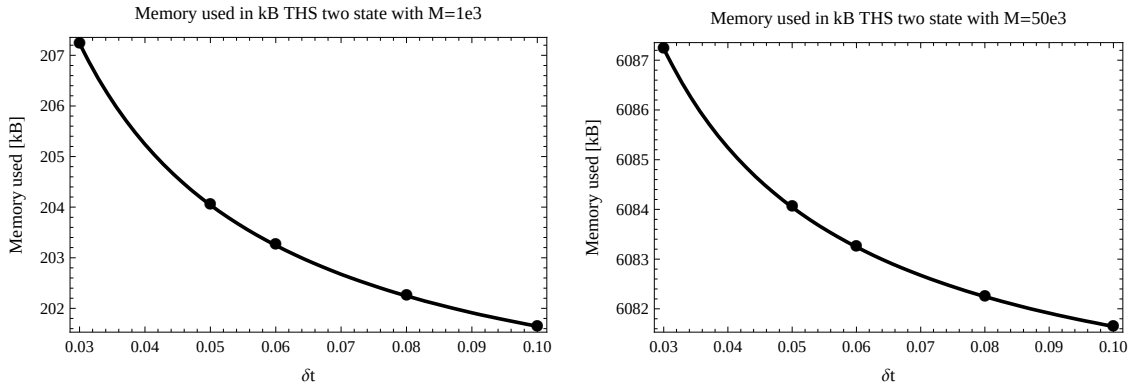

Figure 6.19: Extrapolating function is better in THS than in DHS in the opposite ends of the measured memory values.

Results We compare the memory consumption with the following parameter values $M = 10^5$ and $\delta t = 0.01$. We use the measured result for NMQJ and the extrapolated values for DHS and THS:

$$\begin{aligned}
\mathrm{Mem}^{\mathrm{TS}}_{\mathrm{NMQJ}} &= 143.116\,\mathrm{kB},\\
\mathrm{Mem}^{\mathrm{TS}}_{\mathrm{DHS}} &\approx 8072.19\,\mathrm{kB},\\
\mathrm{Mem}^{\mathrm{TS}}_{\mathrm{THS}} &\approx 12103.2\,\mathrm{kB}.
\end{aligned}$$

$\mathrm{Mem}^{\mathrm{TS}}_{\mathrm{DHS}} \approx \frac{2}{3}\mathrm{Mem}^{\mathrm{TS}}_{\mathrm{THS}}$. This reflects the different dimensionality of the Hilbert spaces $\dim\mathcal{H}_{\mathrm{DHS}} = \frac{2}{3}\dim\mathcal{H}_{\mathrm{THS}}$. We find also that $\mathrm{Mem}^{\mathrm{TS}}_{\mathrm{NMQJ}} \approx 0.018\,\mathrm{Mem}^{\mathrm{TS}}_{\mathrm{DHS}}$ and $\mathrm{Mem}^{\mathrm{TS}}_{\mathrm{NMQJ}} \approx 0.012\,\mathrm{Mem}^{\mathrm{TS}}_{\mathrm{THS}}$. Similar measurements and analysis for the ladder

system give

$$\mathrm{Mem}^{\mathrm{L}}_{\mathrm{NMQJ}} = 206.716\,\mathrm{kB},$$
$$\mathrm{Mem}^{\mathrm{L}}_{\mathrm{DHS}} \approx 12115.5\,\mathrm{kB},$$
$$\mathrm{Mem}^{\mathrm{L}}_{\mathrm{THS}} \approx 17778.1\,\mathrm{kB}.$$

Again $\mathrm{Mem}^{\mathrm{L}}_{\mathrm{DHS}} \approx \frac{2}{3}\mathrm{Mem}^{\mathrm{L}}_{\mathrm{THS}}$, $\mathrm{Mem}^{\mathrm{L}}_{\mathrm{NMQJ}} \approx 0.017\,\mathrm{Mem}^{\mathrm{L}}_{\mathrm{DHS}}$ and $\mathrm{Mem}^{\mathrm{L}}_{\mathrm{NMQJ}} \approx 0.012\,\mathrm{Mem}^{\mathrm{L}}_{\mathrm{THS}}$. This tells us that the NMQJ method needs approximately 80% less memory than the DHS method and 90 % less memory than the THS method.

6.4 Error analysis in two state system

A simple example with the two level system shows that the negative decay rates cause error in the estimates for the standard deviations of the ground state in the DHS and THS methods. Standard deviation for the ground state is $\sigma_{gg}(t)$ and for the excited state $\sigma_{ee}(t)$. The parameter values used are: $\alpha^2 = 5,\ \delta = 5\Gamma,\ \delta t = 0.01/\Gamma,\ M = 10^5,\ |\psi_0\rangle = \frac{3|e\rangle+2|g\rangle}{\sqrt{13}}$. The estimate for the $\sigma_{gg}(t)$ is calculated as [8]

$$\sigma_{gg}(t) = \sqrt{\frac{1}{M(M-1)}\sum_{j=0}^{M-1}(\rho_{gg,j}(t) - \hat{\rho}_{gg}(t))^2}, \tag{6.4}$$

where $\hat{\rho}_{gg}(t)$ is the estimated value of the ground state population. Similarly for the excited state. In this case the two state system decays towards the ground state. It means that most of the ensemble members jump to the ground state. Therefore the estimate for the standard deviations should become smaller as the terms $(\rho_{gg,j}(t) - \hat{\rho}_{gg}(t))$ are getting smaller. This is exactly what happens in NMQJ.

In DHS terms $(\rho_{gg,j}(t) - \hat{\rho}_{gg}(t))$ are not necessarily small. They are not small when the decay rate is negative and jump happens, because for the jumped ensemble member $\rho_{gg,j} = -||\theta_j(t)||^2$. During the negative decay rate the norm of the deterministically evolving ensemble members is larger than one.

In THS terms $(\rho_{gg,j}(t) - \hat{\rho}_{gg}(t))$ are not small when the decay rate is negative and an ensemble member jumps via channel J_0 or J_1 and does not jump at some

later time via channel J_2 or J_3 to $\mathcal{H}_3$. These members have $\rho_{gg,j} = -|\langle g|g\rangle|^2 = -1$. This leads to a large contribution to the estimate of the standard deviation for the ground state. In THS this effect is smaller than in DHS because part of the ensemble members that would give a negative contribution jump to $\mathcal{H}_3$, where they do not contribute to the estimate of the standard deviation. Behavior of the standard deviation can be verified from the Fig. 6.20. Note that the negative contribution to the ensemble average is essential in the THS and DHS methods in order to get the correct non-Markovian dynamics.

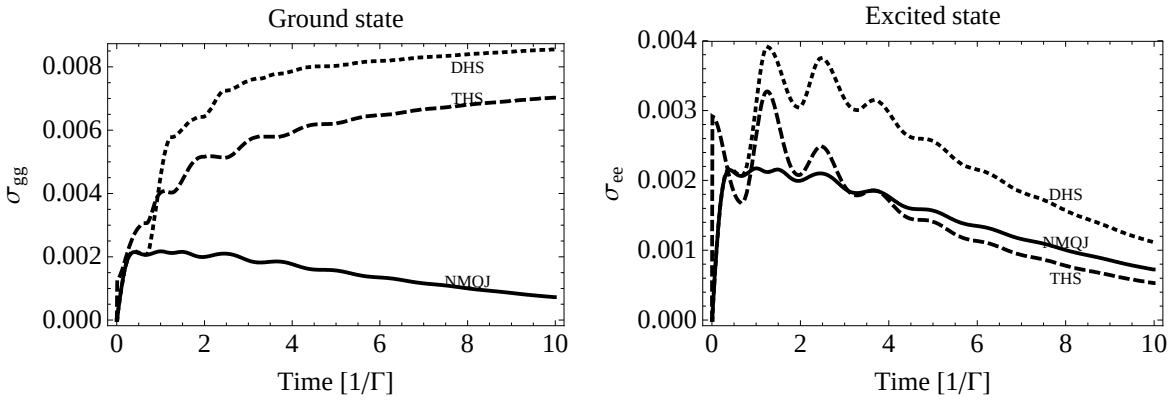

Figure 6.20: Standard deviations for the ground and the excited states of the two state system. NMQJ gives the same values for the both states. THS and DHS have a component in the ground state standard deviation that does not go towards zero even if all the members of the ensemble jump to the ground state if there has been transition(s) from the deterministic initial state to the ground state during the negative decay rate.

6.5 Conservation of positivity in ladder system

The local in time non-Markovian master equations used in this thesis were obtained by using the TCL2 approximation. This approximation does not guarantee that the obtained master equation conserves the positivity of the density matrix. Exact

form of the TCL method guarantees the positivity of the density matrix. In the Ref. [5] it is shown that a Stochastic Schrödinger Equation can be formulated for a non-Markovian process. This is very important result, because the density matrix generated by this SSE is positive. Simulation method for this SSE turns out to be NMQJ. Another important result of this paper is that by using this SSE we can identify the point where the positivity of the density matrix is lost. Jump probability for a non-Markovian jump in NMQJ is

$$P^{j_-}_{\beta\to\beta'}(t) = \frac{M_{\beta'}(t)}{M_\beta(t)}|\Delta_{j_-}(t)|\delta t\langle\psi_{\beta(t)'}|C^\dagger_{j_-}C_{j_-}|\psi_{\beta'}(t)\rangle. \tag{6.5}$$

The point where positivity is violated turns out to be the point where the Eq. (6.5) is not well defined. This happens when a negative jump channel is open but there is not any ensemble members on the source state of the non-Markovian jump.

Positivity of density matrix is violated when we study the ladder system with certain parameters. We define that $|e\rangle$ is the excited state, $|a\rangle$ is the intermediate state and $|g\rangle$ is the ground state. The parameters are the same as before except that the initial state is $|\psi_0(0)\rangle = |e\rangle$. At time $T_0 \approx 1\,\Gamma^{-1}$ the positivity is violated. We show here that the NMQJ method indeed identifies the point of the positivity violation, but the DHS and THS methods follow the master equation. After making some simulations and numerical integration we find that in the DHS, THS and numerically integrated solutions the population of the state $|g\rangle$ turns negative. This suggests us that the quantity of interest in the NMQJ simulation is $M_2(t)$, the number of the states that have jumped to the state $|g\rangle$. Initially $M_2(0) = 0$ and until the time τ it stays zero, thus $M_2(t) = 0$, $t < \tau$. Let us define T as the time when $M_2(t)$ reaches zero for the first time, when $t > \tau$. In the simulation we find that $\tau = 0.05\,\Gamma^{-1}$, $T = 1.01\,\Gamma^{-1}$, $M_2(T) = 0$, $M_1(T) = 54919$, $M_0(T) = 45081$, $\Delta_a(T) > 0$ and $\Delta_g(T) \approx -0.4$. Here $\Delta_i(t)$ is the decay rate of the channel i, $M_0(t)$ is the number of the deterministic ensemble members and $M_1(t)$ is the number of the states jumped to the state $|a\rangle$. These numbers tell us that NMQJ has successfully

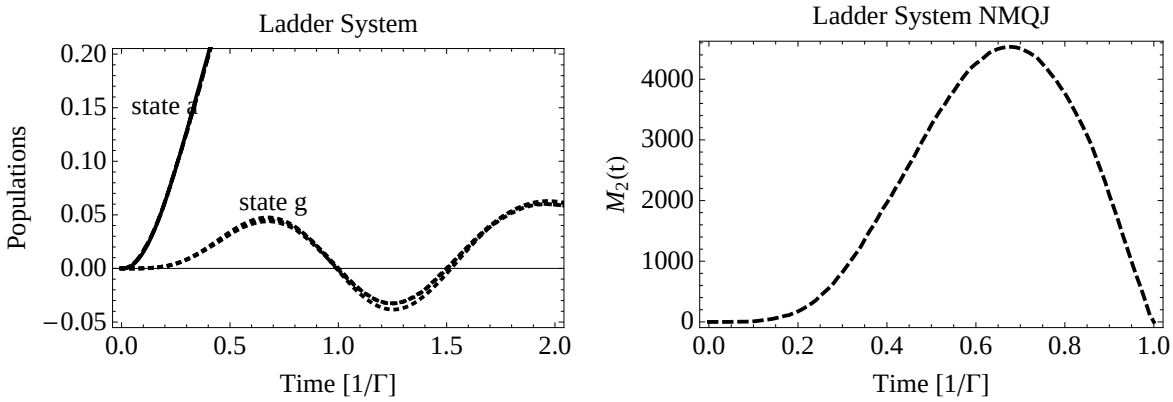

Figure 6.21: In the left figure we have the solutions with the numerical integration and DHS and THS methods. We see that when $T \approx 1\Gamma^{-1}$ the density matrix loses its positivity. That suggests us that the quantity of interest in the NMQJ simulation is $M_2(t)$ which tells us the number of ensemble members that have jumped to the ground state. We have plotted that in right hand side figure.

found the point where the positivity is lost and indeed the probability for the non-Markovian jump is not well defined. The fact that SSE in Ref. [5] generates positive density matrix leads us to conclusion that TCL2 approximation in this case fails to generate the correct master equation.

7 Conclusions

In this thesis we have studied the NMQJ, DHS and THS methods from different perspectives. We have measured their performance using various measures and also analyzed their physical properties. We have also gathered some knowledge about the difficulties of applying these methods. NMQJ is very optimized method. There is no need for Hilbert space extensions and the use of effective ensemble size uses efficiently statistical correlations between the ensemble members. These two things result in low CPU times and small memory consumption. In the DHS method we need to double the dimension of Hilbert space. We need to solve a non-linear differential equation for calculating the deterministic evolution of an ensemble member. We must also evaluate all the ensemble members separately. We see the cost of these operations in the consumption of the CPU time and memory. THS has similar down sides than DHS, but there is a linear differential equation which has to be solved and we can obtain the total jump probability directly from this solution. This has the effect that DHS and THS are quite close to each other when measured with the CPU time and memory consumption. This is somewhat surprising because in THS we have larger Hilbert space than in DHS.

All methods have intrinsic statistical errors involved. When using Monte Carlo methods this error can be estimated with the standard deviation. We chose not to follow this route. We instead measured absolute error compared to numerically integrated solution. From those results we cannot say that one method is clearly more accurate than other, but we can say that NMQJ had a larger range of parameter values, in all cases studied, for which some desired accuracy goal was reached. This then results in even more efficient simulations, because by tuning the ensemble size and time step size we can obtain smaller CPU times. These results are incomplete because in this thesis we did not analyze thoroughly the statistical aspect of these errors, but the coherence of results suggest that our conclusions are correct.

We noticed that the standard deviation of the DHS and THS methods behaves differently than in the NMQJ method. We obtained large estimates for the standard deviation with the DHS and THS methods because of the negative contribution to the ensemble average. This might become a problem if one applies these methods to a system where the analytical solution is unknown and direct numerical integration is impossible.

The NMQJ method offers in many ways much more physical insight in the non-Markovian systems than DHS and THS. We can clearly see how the memory effects come in to play and we can obtain information about the validity of the local in time non-Markovian master equation that we simulate. The first point is harder to catch with DHS and THS and the second is not possible with the DHS and THS methods.

For further studies, it would be interesting to find some optimization methods for DHS and THS and to see how well they match NMQJ after that. Also it would be interesting to study the limits of NMQJ and how easily it can be applied to more complex systems. One interesting aspect to study is the statistical nature of the error in the NMQJ. We know that the realizations of the NMQJ process are dependent of each other and therefore Central Limit Theorem is not valid. This then leads to a question that what is the limiting distribution of the error?

M \ δt	0.01	0.03	0.05	0.08	0.1
1e3	0.0152729	0.0378712	0.0177804	0.0182449	0.0233189
5e3	0.0127485	0.0102386	0.0142621	0.0110894	0.0168706
1e4	0.00678478	0.00591652	0.00874541	0.0109764	0.0147922
2.5e4	0.00288442	0.00482781	0.00749664	0.0108018	0.0139636
5e4	0.00258261	0.00341658	0.00647941	0.0101864	0.0136966
7.5e4	0.00232764	0.00327791	0.00606591	0.0101424	0.0132316
1e5	0.00165544	0.00296327	0.00514491	0.00998942	0.0131006

Table A.1: Values of $\mu_{\mathrm{M},\delta t}$ for the two state system and the NMQJ method.

A Numerical results

A.1 Values of $\mu_{M,\delta t}$

We present the numerical values $\mu_{M,\delta t}$ in a tabular form. Parameters are as in the Sec. 6.1. Exceptions are mentioned separately. $\mu_{M,\delta t}$ is defined as

$$\mu_{M,\delta t} = \max_{|k\rangle\in\mathcal{I},t\in T}|\langle k|\rho_S(t)|k\rangle - \langle k|\rho_N(t)|k\rangle|,$$

where $\mathcal{I}$ is a set indexing the energy eigenstates of the system, T is the time interval in which we observe the system, $\rho_S(t)$ is the simulated density matrix and $\rho_N(t)$ is the numerically integrated density matrix.

M \ δt	0.01	0.03	0.05	0.08	0.1
1e3	0.0232818	0.0324422	0.0332032	0.0430833	0.0579547
5e3	0.0201279	0.02009	0.0267804	0.0403658	0.0499236
1e4	0.00999203	0.0200391	0.0235808	0.0390008	0.0491836
2.5e4	0.00706744	0.018011	0.0229688	0.0388564	0.0480396
5e4	0.00570227	0.0145777	0.0227656	0.0387118	0.0478916
7.5e4	0.00546838	0.0139377	0.0225734	0.0369878	0.0478736
1e5	0.00484779	0.0133738	0.0220366	0.0369008	0.0471646

Table A.2: Values of $\mu_{\mathrm{M},\delta t}$ for the two state system and the DHS method.

M \ δt	0.01	0.03	0.05	0.08	0.1
1e3	0.0205619	0.0274932	0.0291272	0.0445638	0.0501585
5e3	0.0186722	0.0141638	0.0234856	0.0402708	0.0491636
1e4	0.0164061	0.0137547	0.0233518	0.0391968	0.0486386
2.5e4	0.00586379	0.0130727	0.0227678	0.0387718	0.0484846
5e4	0.00454474	0.0128327	0.0209486	0.0384118	0.0484236
7.5e4	0.00418468	0.0121487	0.0209395	0.0363828	0.0456686
1e5	0.00399497	0.0112315	0.0202597	0.0362658	0.0435856

Table A.3: Values of $\mu_{\mathrm{M},\delta t}$ for the two state system and the THS method.

δt \ M	1e3	5e3	1e4	2.5e4	5e4	7.5e4	1e5
0.01	0.004256	0.002505	0.002418	0.001212	0.0009156	0.0008766	0.0007348
0.03	0.01000	0.002649	0.002059	0.001845	0.001559	0.001535	0.001294

Table A.4: $\mu_{M,\delta t}$ for the NMQJ method in the two state system with the parameter values as in the Sec. 5.1 except that $\alpha^2 = 2$ and $|\psi_0\rangle = \sqrt{2/3}|g\rangle + \sqrt{1/3}|e\rangle$. We see that $\mu_{M,0.01}$ is closer to $\mu_{M,0.03}$ than in the case when $\alpha^2 = 5$.

δt \ M	1e3	5e3	1e4	2.5e4	5e4	7.5e4	1e5
0.01	0.003596	0.003219	0.002802	0.002534	0.002150	0.001910	0.001830
0.03	0.009043	0.004686	0.004130	0.004032	0.003854	0.003545	0.002604

Table A.5: $\mu_{M,\delta t}$ for the NMQJ method in the two state system with the parameter values as in the Sec. 5.1 except that $\alpha^2 = 5$ and $|\psi_0\rangle = \sqrt{2/3}|g\rangle + \sqrt{1/3}|e\rangle$. See also the previous table.

M \ δt	0.01	0.03	0.05	0.08	0.1
1e3	0.0177632	0.0214303	0.0111133	0.0160159	0.0284297
5e3	0.00683306	0.00600766	0.00851672	0.0150219	0.0219997
1e4	0.00584605	0.00398863	0.00789687	0.0149839	0.0212287
2.5e4	0.00405425	0.00376541	0.00721352	0.0149329	0.0210357
5e4	0.00314448	0.00328273	0.00697552	0.0147839	0.0209197
7.5e4	0.00297472	0.00323095	0.00692154	0.0146839	0.0207907
1e5	0.00220495	0.00297428	0.00680772	0.0126067	0.0196677

Table A.6: Values of $\mu_{M,\delta t}$ for the NMQJ in the V system.

M \ δt	0.01	0.03	0.05	0.08	0.1
1e3	0.014055	0.0118477	0.0153498	0.0228782	0.0229457
5e3	0.00683514	0.00858594	0.0142219	0.0170657	0.0219798
1e4	0.00501673	0.00681705	0.0106812	0.0150279	0.0207847
2.5e4	0.00481989	0.00439977	0.00768752	0.0149519	0.0204177
5e4	0.00380904	0.00435731	0.00760654	0.0147979	0.0203597
7.5e4	0.00380781	0.0042375	0.00760472	0.0145347	0.0201587
1e5	0.00339105	0.00416497	0.00710272	0.0141124	0.0190217

Table A.7: Values of $\mu_{M,\delta t}$ for the DHS in the V system.

M \ δt	0.01	0.03	0.05	0.08	0.1
1e3	0.0238176	0.0324752	0.0216487	0.0347176	0.0245717
5e3	0.0131497	0.00877709	0.00956654	0.0149969	0.0234147
1e4	0.012762	0.0048868	0.00877172	0.0149139	0.0210567
2.5e4	0.00355218	0.00462395	0.00829822	0.0148439	0.0207777
5e4	0.00256858	0.00423398	0.0074816	0.0138369	0.0201677
7.5e4	0.00234989	0.00254468	0.00746172	0.0137229	0.0191967
1e5	0.00207458	0.00202068	0.00696072	0.0137229	0.0190012

Table A.8: Values of $\mu_{M,\delta t}$ for THS in V-system.

M \ δt	0.01	0.03	0.05	0.08	0.1
1e3	0.0280346	0.0314376	0.043204	0.0536947	0.0494457
5e3	0.0093341	0.0150867	0.0250527	0.0406214	0.0491857
1e4	0.00885414	0.0150324	0.0228879	0.0384903	0.0484647
2.5e4	0.00523028	0.0138163	0.0222489	0.0380443	0.0482627
5e4	0.0048786	0.0133158	0.0220939	0.0376794	0.0482627
7.5e4	0.00477135	0.0129518	0.0220897	0.0364313	0.0477147
1e5	0.0030451	0.00948871	0.0212057	0.0357683	0.0476137

Table A.9: Values of $\mu_{\mathrm{M},\delta t}$ for the Λ system and the NMQJ method.

M \ δt	0.01	0.03	0.05	0.08	0.1
1e3	0.0268556	0.0322786	0.0307642	0.0426633	0.0527584
5e3	0.0102817	0.0227367	0.0271769	0.0399075	0.0523287
1e4	0.00670369	0.0140368	0.0241879	0.0385233	0.0489267
2.5e4	0.00435456	0.0135057	0.0228609	0.0378893	0.0479187
5e4	0.00418731	0.0134117	0.0227427	0.0376543	0.0476387
7.5e4	0.00403669	0.0130517	0.0220289	0.0363863	0.0475227
1e5	0.00297582	0.0126483	0.0218637	0.0362693	0.0417627

Table A.10: Values of $\mu_{\mathrm{M},\delta t}$ for the Λ system and the DHS method.

M \ δt	0.01	0.03	0.05	0.08	0.1
1e3	0.0224047	0.031773	0.0321433	0.0438636	0.0507867
5e3	0.012406	0.0192913	0.0264057	0.0400643	0.0496767
1e4	0.0071808	0.0165658	0.0223849	0.0382553	0.0488687
2.5e4	0.00690547	0.0150081	0.0222879	0.0379023	0.0484644
5e4	0.00579979	0.0141788	0.0221177	0.0377913	0.0480154
7.5e4	0.00469462	0.0140058	0.0216929	0.0359743	0.0480107
1e5	0.00387428	0.0109508	0.0205499	0.0353273	0.0479027

Table A.11: Values of $\mu_{\mathrm{M},\delta t}$ for the Λ system and the THS method.

M \ δt	0.01	0.03	0.05	0.08	0.1
1e3	0.022679	0.0287479	0.0258162	0.027109	0.0346479
5e3	0.0134423	0.0131764	0.0165891	0.023916	0.0309994
1e4	0.00975707	0.0101604	0.0158809	0.023858	0.0307509
2.5e4	0.00470171	0.00913845	0.0157219	0.023248	0.0303714
5e4	0.00340589	0.00897343	0.0154466	0.023033	0.0299409
7.5e4	0.00308366	0.00839272	0.0145776	0.02264	0.0299109
1e5	0.00265199	0.00740843	0.0145594	0.02107	0.0293424

Table A.12: Values of $\mu_{\mathrm{M},\delta t}$ for the ladder system and the NMQJ method.

M \ δt	0.01	0.03	0.05	0.08	0.1
1e3	0.044135	0.0333735	0.042369	0.0323289	0.0483658
5e3	0.0237125	0.0172191	0.0250461	0.0291829	0.0375609
1e4	0.0153294	0.010664	0.0164926	0.0252129	0.0327309
2.5e4	0.00821014	0.00925543	0.0161364	0.024815	0.0318609
5e4	0.00644541	0.00905189	0.0154879	0.0247879	0.0317559
7.5e4	0.0060151	0.00851643	0.0136744	0.023607	0.0304499
1e5	0.00494492	0.00811043	0.0134691	0.023274	0.0289664

Table A.13: Values of$\mu_{\mathrm{M},\delta t}$ for the ladder system and the DHS method.

M \ δt	0.01	0.03	0.05	0.08	0.1
1e3	0.0420277	0.0373895	0.042874	0.0512795	0.0476791
5e3	0.0224935	0.0293352	0.0236997	0.0330759	0.0384355
1e4	0.0102633	0.0174565	0.0194858	0.0305643	0.0361469
2.5e4	0.00988712	0.0151641	0.0175775	0.0280883	0.0361305
5e4	0.00663405	0.0131521	0.0171357	0.0276393	0.0358695
7.5e4	0.00450906	0.0116381	0.0161765	0.0272783	0.0343515
1e5	0.00370745	0.0107706	0.0135581	0.0244113	0.0317999

Table A.14: Values of $\mu_{\mathrm{M},\delta t}$ for the ladder system and the THS method.

δt / M	0.01	0.03	0.05	0.08	0.1
1000	0.003	0.004	0.001	0	0
5000	0.013	0.005	0.004	0.001	0.003
10000	0.034	0.011	0.006	0.006	0.006
25000	0.072	0.031	0.019	0.008	0.012
50000	0.159	0.056	0.037	0.022	0.018
75000	0.236	0.082	0.044	0.03	0.022
100000	0.347	0.106	0.07	0.032	0.025

Table A.15: CPU times for the NMQJ method in the two state system.

A.2 Values of CPU time

Zeros in the measurement records tell that `gprof` could not measure CPU time because the running time of the simulation was too short. `gprof` measures the CPU time by sampling the code during running. The shorter the running time the larger are statistical errors that rise from the measurement of CPU time. The sampling interval is 0.01 s and this number also characterises the standard deviation of measurement process. The benefit of using `gprof` is that it generates also a call graph from the execution of the program which tells directly the amount of CPU time consumed by different functions. Zeros in the results occur only with the NMQJ method and this tells us that run time for the NMQJ method is much shorter than for the THS or DHS methods.

M \ δt	0.01	0.03	0.05	0.08	0.1
1000	0.25	0.07	0.048	0.028	0.022
5000	1.256	0.443	0.276	0.161	0.124
10000	2.502	0.793	0.553	0.297	0.232
25000	6.417	2.114	1.327	0.782	0.637
50000	13.339	4.207	2.605	1.567	1.267
75000	21.005	6.379	3.681	2.355	1.947
100000	27.673	8.668	5.165	3.2	2.525

Table A.16: CPU times for the DHS method in the two state system.

M \ δt	0.01	0.03	0.05	0.08	0.1
1000	0.281	0.079	0.049	0.023	0.036
5000	1.412	0.462	0.304	0.144	0.13
10000	2.776	0.898	0.568	0.37	0.271
25000	6.799	2.316	1.391	0.841	0.699
50000	13.946	4.654	2.701	1.716	1.356
75000	20.724	6.912	4.134	2.579	2.238
100000	27.564	8.886	5.491	3.389	2.814

Table A.17: CPU times for the THS method in the two state system.

M \ δt	0.01	0.03	0.05	0.08	0.1
1e3	0.006	0.	0.	0.	0.001
5e3	0.02	0.013	0.003	0.004	0.002
1e4	0.049	0.02	0.015	0.006	0.007
2.5e4	0.162	0.051	0.028	0.018	0.01
5e4	0.291	0.097	0.059	0.034	0.02
7.5e4	0.408	0.127	0.064	0.053	0.031
1e5	0.555	0.211	0.122	0.067	0.054

Table A.18: CPU times for the NMQJ method in the V system. `gprof` could not measure the CPU time (all ten runs gave zero) for values of $M = 1000$, $\delta t = \{0.03, 0.05, 0.08\}$, but it has been able to measure it for $M = 1000$, $\delta t = 0.01$.

M \ δt	0.01	0.03	0.05	0.08	0.1
1e3	0.352	0.137	0.09	0.039	0.052
5e3	1.884	0.606	0.384	0.224	0.214
1e4	3.819	1.321	0.732	0.462	0.415
2.5e4	9.552	3.157	1.878	1.181	0.994
5e4	19.238	6.534	3.738	2.411	2.065
7.5e4	28.796	9.373	5.544	3.423	3.078
1e5	38.61	12.886	7.712	4.77	3.711

Table A.19: CPU times for the DHS method in the V system.

M \ δt	0.01	0.03	0.05	0.08	0.1
1e3	0.418	0.139	0.08	0.046	0.043
5e3	2.208	0.699	0.406	0.255	0.206
1e4	4.209	1.402	0.834	0.535	0.412
2.5e4	10.673	3.626	2.078	1.363	1.199
5e4	21.223	7.244	4.314	2.617	2.187
7.5e4	32.934	10.66	6.481	3.918	3.198
1e5	43.582	14.354	8.563	5.402	4.417

Table A.20: CPU times for the THS method in the V system.

M \ δt	0.01	0.03	0.05	0.08	0.1
1e3	0.003	0.001	0.	0.	0.
5e3	0.019	0.006	0.002	0.001	0.001
1e4	0.04	0.007	0.003	0.003	0.006
2.5e4	0.067	0.017	0.013	0.011	0.013
5e4	0.154	0.057	0.031	0.024	0.014
7.5e4	0.21	0.07	0.041	0.026	0.023
1e5	0.325	0.091	0.08	0.048	0.049

Table A.21: CPU times for the NMQJ method in the Λ system. `gprof` could not measure the CPU time for the parameter values $M = 1000,\ \delta t = \{0.05, 0.08, 0.1\}$.

δt / M	0.01	0.03	0.05	0.08	0.1
1e3	0.448	0.137	0.082	0.08	0.045
5e3	2.395	0.766	0.483	0.329	0.232
1e4	4.641	1.519	0.887	0.591	0.48
2.5e4	12.255	3.799	2.291	1.365	1.158
5e4	23.143	7.838	4.561	2.871	2.231
7.5e4	34.715	11.855	6.988	4.364	3.568
1e5	46.914	15.3	9.412	5.812	4.538

Table A.22: CPU times for the DHS method in the Λ system.

δt / M	0.01	0.03	0.05	0.08	0.1
1e3	0.424	0.131	0.08	0.051	0.041
5e3	2.133	0.72	0.451	0.243	0.201
1e4	4.319	1.445	0.851	0.542	0.416
2.5e4	10.669	3.614	2.139	1.314	1.119
5e4	21.814	7.061	4.325	2.702	2.174
7.5e4	33.349	10.634	6.343	4.04	3.171
1e5	47.055	14.766	8.472	5.432	4.293

Table A.23: CPU times for the DHS method in the Λ system.

M \ δt	0.01	0.03	0.05	0.08	0.1
1e3	0.004	0.002	0.002	0.001	0.
5e3	0.026	0.007	0.003	0.004	0.005
1e4	0.062	0.016	0.009	0.006	0.005
2.5e4	0.115	0.042	0.032	0.014	0.015
5e4	0.267	0.076	0.037	0.042	0.021
7.5e4	0.304	0.131	0.066	0.045	0.035
1e5	0.462	0.149	0.085	0.062	0.054

Table A.24: CPU times for the NMQJ method in the ladder system.

M \ δt	0.01	0.03	0.05	0.08	0.1
1e3	0.382	0.113	0.095	0.055	0.038
5e3	1.938	0.655	0.418	0.249	0.194
1e4	3.924	1.271	0.804	0.47	0.365
2.5e4	9.94	3.198	1.987	1.197	1.009
5e4	19.865	6.52	3.969	2.538	1.927
7.5e4	28.579	9.691	5.954	3.551	2.853
1e5	38.867	13.161	7.753	4.948	3.891

Table A.25: CPU times for the DHS method in the ladder system.

δt / M	0.01	0.03	0.05	0.08	0.1
1e3	0.456	0.139	0.106	0.058	0.044
5e3	2.181	0.744	0.451	0.273	0.223
1e4	4.156	1.43	0.88	0.547	0.419
2.5e4	10.617	3.559	2.165	1.37	1.092
5e4	21.307	6.963	4.256	2.811	2.183
7.5e4	32.619	10.77	6.483	4.035	3.314
1e5	41.735	14.118	8.756	5.343	4.372

Table A.26: CPU times for the THS method in the ladder system.

References

[1] L. E. Ballentine. *Quantum Mechanics - A Modern Development*. World Scientific, 2006.

[2] H.-P. Breuer. *Phys. Rev. A*, 70:012106, 2004.

[3] H.-P. Breuer, B. Kappler, and F. Petruccione. *Phys. Rev. A*, 59:1633–1643, 1999.

[4] H.-P. Breuer and F. Petruccione. *Theory of Open Quantum Systems*. Oxford University Press, 2007.

[5] H.-P. Breuer and J. Piilo. *EPL*, 85:50004, 2009.

[6] H. J. Carmichael. *Statistical methods in Quantum Optics*. Springer-Verlag, 2008.

[7] R. Dum, P. Zoller, and H. Ritsch. *Phys. Rev. A*, 45:4879–4887, 1992.

[8] W. Feller. *An Introduction to Probability Theory and Its Applications I*. John Wiley & Sons, 1968.

[9] A. M Ferrenberg, D. P. Landau, and K. Binder. *J. Stat. Phys.*, 63:867–882, 1991.

[10] M. Galassi et al. *Gnu Scientific Library - Reference Manual*, 1.12 edition, 2008.

[11] J. Gambetta and H. M. Wiseman. *Phys. Rev. A*, 66:012108, 2002.

[12] J. Gambetta and H. M. Wiseman. *Phys. Rev. A*, 68:062104, 2003.

[13] C. C. Gerry and P. L. Knight. *Introductory Quantum Optics*. Cambridge University Press, 2005.

[14] N. Gisin and I. C. Percival. *J. Phys. A: Math. Gen.*, 25:5677–5691, 1992.

[15] V. Gorini, A. Kossakowski, and E.C.G Sudarshan. *J. Math. Phys.*, 17:821–825, 1976.

[16] B. J. Gough. *An Introduction to GCC - for the GNU compilers gcc and g++.* Network Theory Ltd, 2005.

[17] P. Lambropoulos and D. Petrosyan. *Fundamentals of Quantum Optics and Quantum Information.* Springer, 2007.

[18] G. Lindblad. *Comm. Math. Phys.*, 48:119–130, 1976.

[19] K. Mølmer and Y. Castin. *Quantum Semiclass. Opt.*, 8:49–72, 1996.

[20] K. Mølmer, Y. Castin, and J. Dalibard. *J. Opt. Soc. Am. B*, 10:524–538, 1993.

[21] Klaus Mølmer. Density matrices and the quantum monte-carlo method in quantum optics. Lectures presented at the Winter School on Quantum Optics, International Centre of Theoretical Physics, Trieste, Italy, Feb. 1994.

[22] N. Nethercote, R. Walsh, and J. Fitzhardinge. Building workload characterization tools with valgrind. In *IEEE International Symposium on Workload Characterization (IISWC 2006)*, 2006.

[23] J. Piilo, K. Härkönen, S. Maniscalco, and K.-A. Suominen. *Phys. Rev. A*, 79:062112, 2009.

[24] J. Piilo, S. Maniscalco, K. Härkönen, and K.-A. Suominen. *Phys. Rev. Lett.*, 100:180402, 2008.

[25] M. B. Plenio and P. L. Knight. *Rev. Mod. Phys.*, 70:101–144, 1998.

[26] M. Reed and B. Simon. *Methods of Modern Mathematical Physics, vol. II.* Academic Press Inc., 1975.

[27] J. Seward and et al. *Valgrind User Manual*. `http://valgrind.org/docs/manual/manual.html`.

[28] F. Shibata, Y. Takahashi, and N. Hashitsume. *J. Stat. Phys.*, 17:171, 1977.

[29] M. H. Stone. *Ann. Math.*, 33:643–648, 1932.

[30] R. C. Whaley and A. Petitet. *Software: Practice and Experience*, 35:101–121, 2005. `http://www.cs.utsa.edu/~whaley/papers/spercw04.ps`.

[31] E. P. Wigner. *Group Theory*. Academic Press Inc., New York, 1959.

[32] H. M. Wiseman and G. J. Milburn. *Phys. Rev. A*, 47:1652–1666, 1993.

[33] P. Zoller, M. Marte, and D. F. Walls. *Phys. Rev. A*, 35:198–207, 1987.